Assembly of an Ionic-Complementary Peptide on Surfaces and its Potential Applications

by

Hong Yang

A thesis
presented to the University of Waterloo
in fulfillment of the
thesis requirement for the degree of
Doctor of Philosophy
in
Chemical Engineering

Waterloo, Ontario, Canada, 2007

AUTHOR'S DECLARATION

I hereby declare that I am the sole author of this thesis. This is a true copy of the thesis, including any required final revisions, as accepted by my examiners.

I understand that my thesis may be made electronically available to the public.

Abstract

Self-assembling peptides have emerged as new nanobiomaterials and received considerable attention in the areas of nanoscience and biomedical engineering. In this category are ionic-complementary peptides, which contain a repeating charge distribution and alternating hydrophobic and hydrophilic residues in the amino acid sequence, leading to the unusual combination of amphiphilicity and ionic complementarity. Although their self-assembled nanostructures have been successfully applied as scaffoldings for tissue engineering, novel materials for regenerative medicine and nanocarriers for drug and gene/siRNA delivery, aspects of the assembly process remain unclear. Since many of these applications involve peptide-modified interfaces and surfaces, a better understanding and control of the peptide assembly on a surface are very crucial for future development of peptide-based applications in nano-biotechnology.

This thesis contains two major parts: (i) fundamental study of the assembly of a model ionic-complementary peptide EAK16-II on surfaces and (ii) potential applications of such a peptide in surface modification and nanofabrication.

In the fundamental study, EAK16-II assembly on negatively charged mica was first investigated via *in-situ* Atomic Force Microscopy (AFM). It was found that EAK16-II nanofiber growth on mica is surface-assisted and follows a nucleation and growth mechanism involving two steps: (i) adsorption of nanofibers and fiber clusters (from the bulk solution) on the surface to serve as the seeds and (ii) fiber elongation from the active ends of the seeds. Such a process can be controlled by adjusting the solution pH since it modulates the adsorption of the seeds and the growth rates. Unlike what is observed on mica, EAK16-II formed well-ordered nanofiber patterns with preferential orientations at angles of 60° or 120° to each other on hydrophobic highly ordered pyrolytic graphite (HOPG) surfaces, resembling the crystallographic structure of the graphite. Nanofiber formation on

HOPG is also surface-assisted and adopts a nucleation and growth mechanism that can be affected by solution pH. The pH-dependent adsorption of peptides to HOPG is attributed to the resulting changes in peptide hydrophobicity.

It was also found that EAK16-II assembly can be induced by the mechanical force of a tapping AFM tip. It occurs when the tip cuts the adsorbed EAK16-II nanofibers into segments that then serve as seeds for new nanofiber growth. This finding allows one to locally grow nanofibers at specific regions of the surface. The tip cutting has been combined with the effect that solution pH has on peptide assembly to develop a new AFM lithography method to fabricate local patterned peptide nanostructures on HOPG.

To study the use of EAK16-II for surface modification applications, the wettability and stability of the peptide-modified surfaces were characterized. EAK16-II-modified mica becomes slightly hydrophobic as the water contact angle increases from <10° to 20.3 ± 2.9°. However, the hydrophobicity of the HOPG surface is significantly reduced, as reflected in a contact angle change from 71.2 ± 11.1° to 39.4 ± 4.3°. The EAK16-II-modified mica surface is stable in acidic solution, while the modified HOPG surface is stable in both acidic and alkaline solutions. The peptide-modified HOPG shows potential as a biocompatible electrode for (bio)molecular sensing.

The ability of EAK16-II to form nanofibers on surfaces has also promoted research on peptide-based metallic nanowire fabrication. Our approach is to provide EAK16-II with metal ion binding ability by adding a GGH motif to the C-terminus. This new peptide EAK16(II)GGH has been found to form one-dimensional nanofibers while binding to Cu^{2+} ions. The dimensions of the nanofibers were significantly affected by the nature of the anions (SO_4^{2-}, Cl^- and NO_3^-) in the copper salt solution. This work demonstrates the potential usage of EAK16-II for nanowire fabrication.

Acknowledgements

First of all, I would like to express my deepest gratitude to my supervisors, Professor Pu Chen and Professor Mark Pritzker, who have provided me unlimited support and critical guidance during my PhD study in Waterloo. Their guidance has helped me go through difficulties I met in the research and give me confidence and energy to continue pursuing my career in nano-bioengineering. In addition, their scientific vision, keen attitude and charisma toward research also provide me lively models for my future life and career. I also appreciate them for providing me this invaluable research opportunity to do innovative research. I did enjoy this cut-edge research for the last four years.

I also would like to thank Professor E.M. Meiering for allowing me to use the Zetasizer Nano ZS instrument in her lab and giving advice on NMR experiment, Professors J.G. Gillemette and C.P. Chou for training and letting me use their circular dichroism instruments, Professor S. Mikkelsen and Dr. W. Sun for collaboration on the biosensor project, Professor N. McManus for kind help on my research, Professor G.A. Scholz for help with the TEM experiment, Professer D. Ban from Electrical Engineering for collaboration on electrical conductance measurement of peptide nanofibers. I also thank Janet Venne for help with NMR experimental work.

I also want to extend my special thanks to our group members, Shan-Yu Fung, Yooseong Hong, Bobby Dhadwar, Hyuk Sang Park, Andrew Prpch, Yuebiao Sheng, Maggie Law, Nasim Hyder, Pinghai Shao and Elias Biswas for their helpful suggestions, advice and support during my study in Waterloo.

During my PhD study, I also have received great help from undergraduate research assistants working in our group: Stephen, Om, Ted, Sandeep, Edi, Anterjot and Stephane. I appreciate their support and help. I would also like to thank my friends Gongpu Zhao, Yunzhi Gao, Junping Bao and Peng Gao for their encouragement and support.

Lastly, but most importantly, I would like to thank my lovely husband, parents, parents-in-law, and relatives in China, who have supported me all the time. Without their unlimited love, understanding and support, none of my achievement would be possible.

This thesis, a product of my four year PhD study, is dedicated to all of them.

Table of Contents

List of Figures

List of Tables

Chapter 1
Introduction

1.1 Overview

A historic address entitled "There is plenty of room at the bottom", given by physicist Richard Feynman in 1959, predicted the potential of atomic/molecular engineering. Two decades later, numerous research activities in nanotechnology had been initiated. Nowadays, nanotechnology is entering into all aspects of science and technology including, but not limited to, biology, bioengineering, materials, medicine, electronics, agriculture, aerospace, military science and technology. It is mainly based on "bottom-up" atomic/molecular manufacturing for building chemically and physically stable nanostructures or supramolecules. The key component of this "bottom-up" approach is molecular self-assembly. This remarkable engineering route is habitually adopted in nature, permitting the formation of supramolecules such as DNA, ribosomes, collagen and biological membranes.[1] In engineering, self-assembly has emerged as a novel approach to design and fabricate supramolecules with novel functionalities from single and simple molecules. One major achievement has been the evolution of microelectronics toward molecular-scale electronic devices and machines through the development of nanowires, nanoarrays and molecular chips.[2-5] This has allowed modern-day electronic devices to be scaled down considerably and achieve higher operational efficiency.

Molecular self-assembly is, by definition, the spontaneous organization of molecules under near thermodynamic equilibrium conditions into structurally well-defined and stable arrangements through noncovalent interactions.[1,6] Such interactions typically include hydrogen bonding, electrostatic attraction, hydrophobic force and van der Waals interactions.[7] Frequently, molecular self-assembly relies on chemical complementarity and structural compatibility.[1,8] These features are

critical to the design of molecular building blocks for the fabrication of artificial functional macrostructures that are commercially required to produce micro/nano-electronics.

In both nature and engineering, the control of the self-assembly process is crucial. The failure to exert control over protein assembly is most exemplified by the *in vivo* formation of protein insoluble aggregates which are associated with numerous conformational diseases such as Alzheimer's and prion diseases.[9-12] On the other hand, proper control over DNA self-assembly allows the formation of assemblies with various shapes (such as X, Y and T-shapes),[13,14] two-dimensional lattices,[15] triangular and hexagonal patterns.[16,17] Such molecular-level control benefits the development of DNA-based bionanomachines, devices and sensors. For example, DNA "tweezers", "nanoactuators" and "scissors" have been constructed with rigid and flexible fragments in the assemblies through control of the degree of hybridization.[18,19] In addition, the two- and three-dimensional nanoarchitectures of DNA have been used to organize other functional components such as inorganic nanoparticles, carbon nanotubes and biomolecules (proteins and nucleic acids) into patterns.[20] The integration of functional entities to DNA supramolecules can be applied to build hybrid (bio)sensing devices.

Among the many self-assembly systems (DNA, protein/peptide, lipid and surfactant), peptides have drawn much attention in nanoscience and nanotechnology due to their desirable chemical/physical properties and biological functionalities. First, peptides can be easily engineered to form a variety of stable nanostructures such as fibers,[21,22] rod,[23] tubes,[24] nanovesicles,[25] globules[26,27] and so on. Second, the peptide sequence can be designed to incorporate natural binding motifs with affinity to inorganic materials,[22,28,29] oligonucleotides (e.g. anti-senses),[30,31] si-RNA and hydrophobic anti-cancer drugs.[32] Third, they possess the natural propensities for cell penetration and targeting.[33,34] With such features, self-assembling peptides have a wide range of potential applications in nano-biotechnology such as templates for nano-fabrication,[35] scaffolds for tissue engineering,[36,37] and

protection coatings for nano-medicines.[32] Since peptides are fragments of proteins, they can serve as simple models to study the process of protein aggregation. A better understanding of protein aggregation could be crucial to understanding the onset of conformational diseases such as Alzheimer's and prion diseases and discovering inhibitors and treatments for their prevention or alleviation.

Most of these applications involve an interface between peptides and other entities. Therefore, it is necessary to understand and control peptide assembly on a surface. For example, cell membranes have been found to facilitate fibrillization of β-amyloid peptides upon their binding to the membrane surface.[38,39] In addition, the fibrillization of α-synuclein, a protein associated with Parkinson's disease, has been found to depend on the nature of the micelle surface in incubation solutions.[40] A better understanding of peptide behaviour on a cell membrane surface will help develop inhibitors for conformational diseases. Furthermore, surface-directed assembly has been explored to construct a variety of nanosystems. For example, self-assembly on a hydrophobic graphite surface can lead to peptides being organized into patterned structures.[41-43] These nanostructures can be used to construct nanoscopic devices such as (bio)sensors, information storage units, optical computers and solar cells.[44-47] Dipeptide FF has been applied to modify electronic conductive materials such as gold and graphite to accelerate the electrochemical reaction of enzymes for amperometric biosensor applications.[48,49] Optimization of the performance of these peptide-based devices requires a better understanding and manipulation of peptide assembly on surfaces.

In this research, the ionic-complementary peptide EAK16-II is used as a model peptide to investigate the effect of surfaces on its assembly and potential applications. This peptide is a good choice for several reasons. First, it has a simple sequence and unique structure for the study of peptide assembly. It contains 16 amino acids in sequence, but is made of only three different amino acids: glutamic acid (E), lysine (K) and alanine (A). These three amino acids are arranged in a special

manner with hydrophobic (●, A) and hydrophilic residues (○, K or E) alternating in the sequence (●○●○●○●○●○●○●○●○) that renders the peptide amphiphilic. EAK16-II also contains a unique charge distribution with two negative and two positive charges alternating in the sequence (- - + + - - + +), giving it ionic complementarity. Second, this peptide has been found to form a β-sheet-rich secondary structure in aqueous solutions.[50] In a β-sheet arrangement, all the hydrophilic residues of the peptide are arranged on one side and hydrophobic resides on the other side. This unusual amphiphilic property allows the peptide to interact with both hydrophilic and hydrophobic surfaces. Third, the unique molecular structure of EAK16-II enables various interactions (hydrogen bonding, electrostatic and hydrophobic interactions) for peptide assembly to be possible; these interactions also occur in protein folding/aggregation and other biomolecular assembly systems. Therefore, the study of such a molecule assembly will help in the understanding of other more complicated systems. Fourth, fundamental aspects and applications of this peptide have been explored by our group for several years. Previous studies have shown that many factors such as peptide sequence[26,27] and concentration,[21,51] salt type and concentration,[22,51,52] and solution pH[26] affect the self-assembled micro-/nanostructures of the peptide and their derivatives. In addition, these peptides can be utilized as nanocarriers for anticancer drug and gene delivery. The combination of the simple structure, unique properties and our previous knowledge of EAK16-II provides a good basis to further investigate the surface effect on peptide assembly and to more fully control this process.

This research project consists of two major parts: i) fundamental studies of EAK16-II assembly on surfaces, and ii) potential applications of such a peptide in surface engineering and nanofabrication. EAK16-II assembly on two different surfaces (hydrophilic mica and hydrophobic highly ordered pyrolytic graphite, HOPG) was systematically investigated to study the surface effect on biomolecular assembly and the underlying mechanisms. This further allowed us to develop methods to possibly control peptide assembly on surfaces. Strategies to fabricate patterned peptide

nanostructures at desired locations were then developed and applied. Potential applications of such a system include a model of protein aggregation at interfaces implicated in conformational diseases, formation of different patterns of peptide nanofibers on the surface and modification of surfaces to obtain desired properties such as wettability, biocompatibility and enzyme immobilization for (bio)molecular sensing. In addition, since EAK16-II can form nanofibers on surfaces, these nanofibers may serve as templates to fabricate one-dimensional metallic nanowires. For such a purpose, a metal ion binding motif was introduced into the peptide sequence. The self-assembled nanostructure and metal ion binding ability of this newly designed peptide has been characterized in detail.

1.2 Research Objectives

The overall objectives of this thesis are to:

1. investigate the assembly of peptide on particular surfaces using a model ionic-complementary peptide EAK16-II.

2. study and propose mechanisms for peptide assembly on surfaces and, if possible, relate them to amyloid fibrillogenesis to help understand conformational diseases.

3. understand and develop approaches to manipulate peptide assembly and pattern peptide nanostructures on surfaces.

4. develop new applications of self-assembling peptides in surface modification and (bio) molecular sensing as well as in nanowire fabrication.

1.3 Outline of the Thesis

This thesis consists of seven chapters. The scope of each chapter is listed as follows:

Chapter 1 gives an introduction to the thesis, including an overview of self-assembling peptides, their applications and the significance of the study and control of peptide assembly on surfaces. The hypothesis, objectives and the scope of the thesis are also given in this chapter.

Chapter 2 reviews the previous progress on understanding peptide self-assembly and its potential applications in nano-biotechnology. The roles that surfaces play in nanotechnology and biological systems are also reviewed.

Chapter 3 presents the effect of a mica surface on the assembly of EAK16-II. EAK16-II nanofiber growth on mica surface is directly monitored by *in-situ* AFM. Of particular interest is the effect of solution pH on peptide assembly on the surface.

Chapter 4 describes the effect of surface properties, such as hydrophobicity, on peptide assembly using two model surfaces (hydrophilic mica and hydrophobic HOPG) and their potential application in surface modification and (bio)molecular sensing.

Chapter 5 investigates the use of a mechanical force to induce peptide assembly at liquid-solid interfaces. A new AFM lithography technique that combines the effects of AFM probe tapping and solution chemistry is developed to fabricate patterned EAK16-II nanostructures on surfaces.

Chapter 6 describes the design, characterization and a potential application of a functional self-assembling peptide molecule with metal ion binding capability for nanowire fabrication. The effects of the type of anion present in solution on the self-assembly of the peptide and the binding of the metal ion to the peptide self-assembly are also investigated.

Chapter 7 presents the conclusions of this study, contributions of this research and recommendations for future work.

Chapter 2
Literature Review

2.1 Self-Assembling Peptides

The last decade has witnessed an explosion in the use and design of short peptide sequences capable of forming nano/microstructures for various applications in nanoscience, surface engineering and biotechnology.[8,53-56] These self-assembling peptides are either fragments of naturally existing proteins or derived by *de novo* biomolecular design. They share a common capability of self-association in aqueous solutions. Short fragments of natural proteins, such as amyloid peptides and prion peptides, have been found to self-assemble into fibril structures in various environments.[57-59] Different from naturally existing protein fragments, synthetic peptides can be easily engineered to self-associate by taking advantage of the intrinsic property of amino acids. For example, designed amphiphilic peptides (i.e. containing hydrophobic and hydrophilic regions in the sequence) can spontaneously associate to form nano/microstructures. Such synthetic peptides have been used to build functional supramolecules.[22,60-62] Several classes of synthetic self-assembling peptides are reviewed in the following paragraphs.

Peptide-amphiphiles (PAs) are an attractive class of bioactive molecules consisting of a hydrophilic, bioactive peptide sequence covalently linked to a hydrophobic moiety such as an alkyl chain.[63] For example, Hartgerink *et al.* synthesized a PA with five different functional regions shown in Figure 2.1.[64] Region 1 is a 16-carbon alkyl tail that imparts hydrophobic character to the molecule, resembling the hydrophobic tails in traditional surfactants. Region 2 is a string of four cysteines to stabilize the assembled structures through the formation of disulfide bonds between individual PAs. Region 3 is composed of three glycine residues providing a flexible linkage. Region 4 is a single phosphorylated serine to interact with calcium ions for the purpose of biomineralization. Finally,

region 5 is a cell adhesion group–RGD. The cysteine, phosphorylated serine and RGD group give the PA its special bioactive characteristics. The assembly of this PA can be triggered by pH. At pH 4, it can form nanofiber networks with the fiber dimension of ~7 nm in diameter and several microns in length. These nanofibers can direct the growth of hydroxyapatite crystals, mimicking the function of collagen fibers in bone tissue.

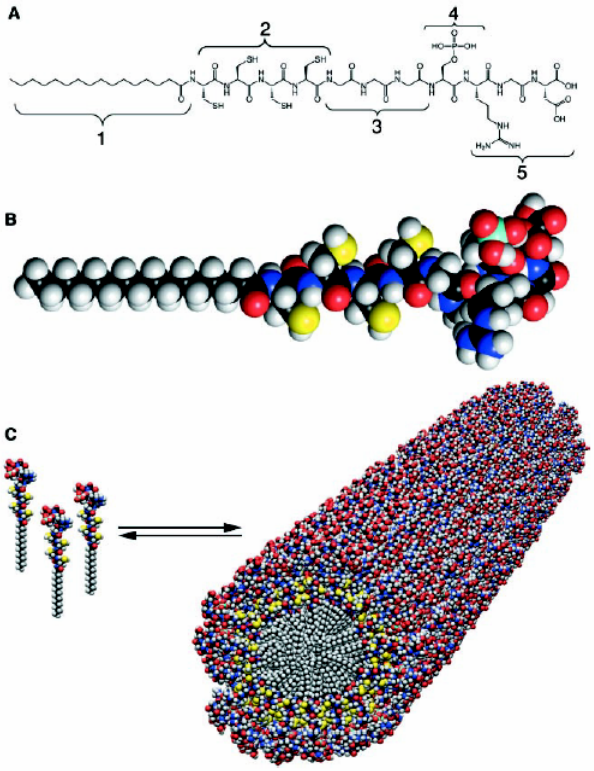

Figure 2.1 (a) Chemical structure of the peptide amphiphile, highlighting five key structural features. (b) Molecular model of the PA. (c) Schematic showing the self-assembly of PA molecules into a cylindrical micelle.[64]

Extensive studies have been carried out to understand the self-assembly of PAs; the ultimate goal is to control their assembly for a number of biomedical applications. First, modification of the amino acids in the peptide region and the alkyl tails has shown no significant effect on the formation of one-dimensional PA nanofibers. The assembly can be induced by three different methods: drying on surfaces, addition of divalent ions such as calcium and increase of PA concentrations.[7] Recently, Niece *et al*. reported that two oppositely charged PA molecules can form nanofibers via electrostatic attraction,[65] which indicates the importance of this type of interaction. Furthermore, the chemical and mechanical properties of PA nanofibers can be modulated through the addition of phospholipids into the assemblies.[63] The self-assembled nanostructures of PAs have shown promising usage in artificial bone synthesis, tissue engineering and regenerative medicine.[66]

(a) (b)

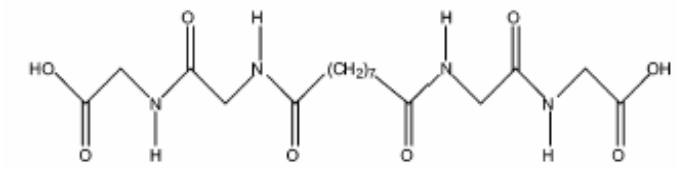

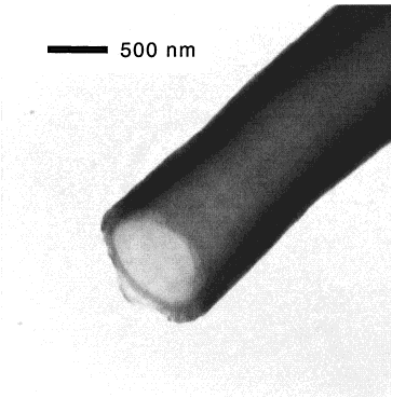

Figure 2.2 Chemical structure of a peptide bolaamphiphile, bis(N-α-amido-glycylglycine)-1,7-heptane dicarboxylate (a) and transmission electron micrograph of Ni-coated bolaamphiphile nanotube (b).[24,67]

Bolaamphiphiles are the derivatives of amphiphilic peptides that contain two hydrophilic ends linked by a hydrophobic alkylene chain with variable length. The two hydrophilic ends are made of the same number of amino acids in a symmetric fashion. Figure 2.2a shows an example of the chemical structure of a bolaamphiphile with two glycine amino acid residues on each end. It has been found that bolaamphiphiles can form microtubes and helical ribbons depending on the chain length of the hydrophobic portion, terminal amino acid and solution pH.[68,69] An interesting property of these self-assembled bolaamphiphile nanotubes is that they contain free amide and carboxylic groups which can intercalate with other functional peptides or capture metal ions such as Pt, Pd, Cu, and Ni.[67] Matsui and his group showed that bolaamphiphile nanotubes can serve as templates for Au, Ni, Pt and Cu metallic nanowire fabrication.[70-73] (Figure 2.2b) The ability of peptides to interact with metals or even semiconductors enables 'bottom-up' fabrication of bioelectronic and photonic devices and nanoscale chemical sensors.[74]

Cyclic peptides consist of six or eight amino acids with alternating D- and L- enantiomers. By means of elegant structural design, they can stack into nanotubes.[75-78] Ghadiri and colleagues have shown that cyclic hexa- and octa-D,L-α-peptides can stack in an anti-parallel fashion to form uniform nanotubes.[76-79] (Figure 2.3) The stacking of the peptides is pH-dependent according to their amino acid sequences. The researchers were able to control the stacking by selective protonation of the amino acid residues on each cyclic peptide disk at different pH values.[79] This peptide system has several important applications in nanobiotechnology. First, assembled nanotubes could be used as an antibacterial agent since they act preferentially on bacterial membranes to increase membrane permeability and collapse transmembrane ion potentials. In combination, these actions lead to cell death.[78] Second, the physical properties of the nanotube interiors can be modified by introducing heterocyclic alterations allowing for the passive transportation of small molecules.[80] Amorin *et al*. also reported a newly designed cyclic peptide which adopts a flat, ring-shaped conformation.[81] These

peptides stack into nanotubes through an anti-parallel β-sheet through hydrogen bonding, creating a partially hydrophobic cavity and, thereby, facilitating passive diffusion of hydrophobic molecules.

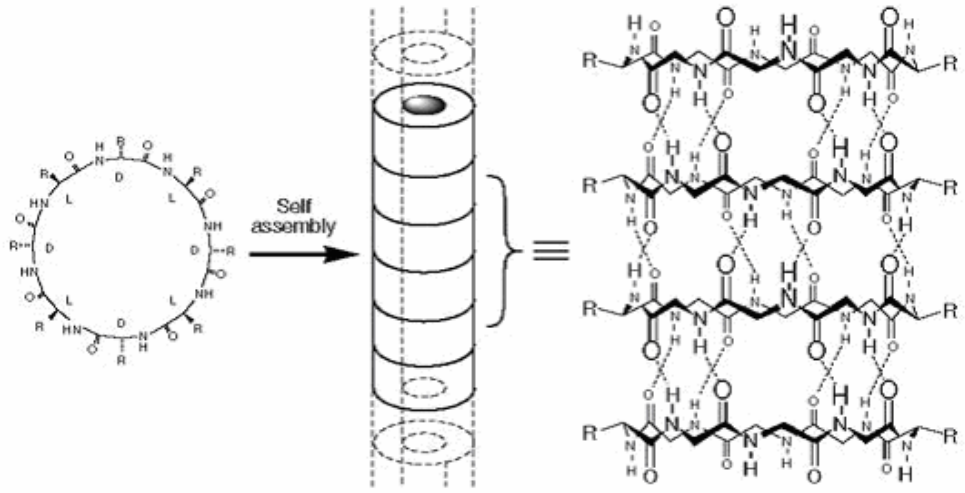

Figure 2.3 Self-assembly of eight-residue cyclic D,L-α-peptides into nanotubes. The self-assembly of the eight residue cyclic D,L-α-peptides with a flat and ring-shaped conformation is directed by backbone-backbone hydrogen bonding to give β-sheet-like tubular supramolecular structures. These nanotubes are open-ended and hollow.[78]

Surfactant-like peptides are also of interest to materials scientists in nanobiotechnology. They are basically a molecular mimicry of membrane phospholipids and detergents. Using the varied nature of different amino acids, these peptides are constructed with a hydrophilic head (hydrophilic amino acid residue) and a hydrophobic tail (hydrophobic amino acid residue) and can self-assemble into well-defined nanostructures.[82] With the appropriate molecular design, nanotubes and nanovesicles can be formed (Figure 2.4).[54,56,62,83] Vauthey *et al.* synthesized a peptide monomer with

7 to 8 residues, containing a hydrophilic head of aspartic acid and a hydrophobic tail of alanine, valine or leucine.[62] These peptide monomers self-assemble into nanotubes and nanovesicles with an average diameter of 30-50 nm at a pH level of 7 in aqueous solution. They later reported similar results with modified surfactant-like peptides. In this instance, either the hydrophobic tail was replaced with variable lengths of glycine residues[25] or the hydrophilic head was replaced with positively charged lysine or histidine.[84] This newly designed peptide system has the potential for use in drug and gene delivery, the study of prebiotic molecular evolution and tissue engineering.[54]

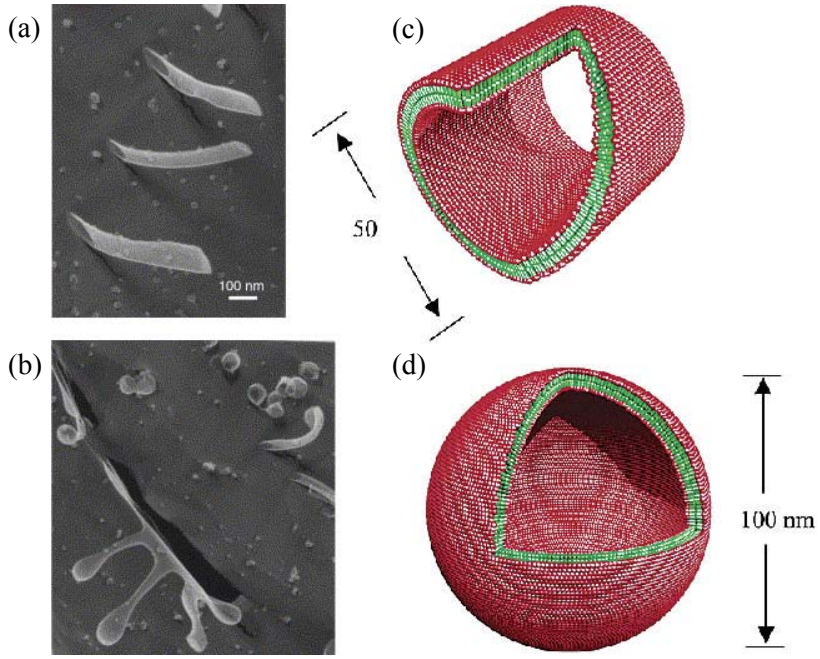

Figure 2.4 The TEM images of nanotubes (a) and nanovesicles (b) from a surfactant-like peptide – V_6D;[56] molecular modeling of cut-away structures of nanotubes (c) and nanovesicles (d) formed from surfactant-like peptides.[25]

Along with the development of peptide amphiphiles and surfactant-like peptides, ionic-complementary peptides have emerged as promising materials for many biomedical applications. A novel class of ionic-complementary peptides was derived from a fragment (EAK16-II) of the Z-DNA

binding protein zoutin in yeast in 1993 by Zhang *et al.*[85,86] These peptides have a systematic arrangement of amino acids in sequence made of alternating hydrophobic and hydrophilic residues, leading to an unusual amphiphilic property. In addition, they contain a repetitive charge distribution in the amino acid sequence, resulting in a unique property of ionic complementarity. These peptides can form an unusually stable β-sheet-rich secondary structure and self-assemble into nanofibers and membranes.[86] With relatively good biocompatibility and biodegradability, this class of peptides is a promising group of materials for nanobiotechnology; in particular, they have been used as scaffolds for tissue engineering and 3-D cell cultures, nanocarriers for therapeutic agents and novel materials for regenerative medicine.[55,56,87] As a result, ionic-complementary peptides have attracted a great deal of interest in nanomaterial science. Detailed information of their physical and biochemical properties, self-assembly process and factors influencing the assembly will be reviewed in the following section.

2.2 Ionic-Complementary Peptides

2.2.1 Molecular Structure

Ionic-complementary peptides are characterized by an alternating arrangement of negatively and positively charged residues. In order to have ionic complementarity, the distribution of the charges should follow certain patterns. The most simple and widely studied types of charge distribution are type I $(-+)$, type II $(--++)$ and type IV $(----++++)$. Such ordered charge distribution results in unique electrostatic interactions which promote molecular self-assembly apart from the more usual hydrogen bonding and hydrophobic interactions.

Table 2.1 The family of ionic-complementary peptides[55,88,89]

Name	Sequence (n → c)	Charge Distribution	Type	Structure
P_{11}-I	n- QQRQQQQQEQQ -c	+ −	I	α/β
P_{11}-II	n- QQRFQWQFEQQ -c	+ −	I	α/β
P_6-1	n- KTVIIE -c	+ −	I	β/r.c.
P_6-6	n- KTVLIE -c	+ −	I	β/r.c.
P_6-7	n- KTVIVE -c	+ −	I	β/r.c.
P_6-8	n- KTVIYE -c	+ −	I	r.c.
$A\beta_{16-22}$	n- KLVFFAE -c	+ −	I	α/β/r.c.
KADA8-I	n- KADAKADA -c	+ − + −	I	r.c.
KFE8-I^T	n- KFEFKFEF -c	+ − + −	I	β
KFE8-I	n- FKFEFKFE -c	+ − + −	I	β
RADA8-I	n- RADARADA -c	+ − + −	I	r.c.
RAEA8-I	n- RAEARAEA -c	+ − + −	I	r.c.
EFK8-I	n- FEFKFEFK -c	− + − +	I	β
EAKA8-I	n- AEAKAEAK -c	− + − +	I	r.c.
KFE12-I	n- FKFEFKFEFKFE -c	+ − + − + −	I	β
KIE12-I	n- IKIEIKIEIKIE -c	+ − + − + −	I	β
KVE12-I	n- VKVEVKVEVKVE -c	+ − + − + −	I	β
KLD12-I	n- KLDLKLDLKLDL -c	+ − + − + −	I	β
KLE12-I	n- KLELKLELKLEL -c	+ − + − + −	I	β
EFK12-I	n- FEFKFEFKFEFK -c	− + − + − +	I	β
RADA16-I	n- RADARADARADARADA -c	+ − + − + − + −	I	β
RGDA16-I	n- RADARGDARADARGDA -c	+ − + − + − + −	I	r.c.
RAEA16-I	n- RAEARAEARAEARAEA -c	+−+−+−+−	I	β
KADA16-I	n- KADAKADAKADAKADA -c	+ − + − + − + −	I	β
KFE16-I	n- FKFEFKFEFKFEFKFE -c	+ − + − + − + −	I	β

EAKA16-I	n- AEAKAEAKAEAKAEAK -c	− + − + − + − +	I	β
RAD8-II	n- RARADADA -c	+ + − −	II	r.c.
EAH8-II	n- AEAEAHAH -c	− − + +	II	r.c.
ELK8-II	n- LELELKLK -c	− − + +	II	β.
EAK8-II	n- AEAEAKAK -c	− − + +	II	r.c.
EAK12-a	n- AKAKAEAEAKAK –c	+ + − − + +	II	r.c.
RAD16-II	n- RARADADARARADADA -c	+ + − − + + − −	II	β
EAH16-II	n- AEAEAHAHAEAEAHAH -c	− − + + − − + +	II	β
EFK16-II	n- FEFEFKFKFEFEFKFK -c	− − + + − − + +	II	β
ELK16-II	n- LELELKLKLELELKLK -c	− − + + − − + +	II	β
EAK16-II	n- AEAEAKAKAEAEAKAK -c	− − + + − − + +	II	β
KAE16-IV	n- KAKAKAKAEAEAEAEA-c	+ + + + − − − −	IV	β
RAD16-IV	n- RARARARADADADADA -c	+ + + + − − − −	IV	β
EAK16-IV	n- AEAEAEAEAKAKAKAK -c	− − − − + + + +	IV	β
DAR16-IV	n- ADADADADARARARAR -c	− − − − + + + +	IV	α/β
DAR16-IV^{T}	n- DADADADARARARARA -c	− − − − + + + +	IV	α/β
DAR32-IV	n- (ADADADADARARARAR)$_2$ -c	− − − − + + + +	IV	α/β
EAK12-b	n- AKASAEAEAKAK -c	+ − − + +	N/A	r.c.
EAK12-c	n- AKAEAEAEAKAK -c	+ − − − + +	N/A	r.c.
EAK12-d	n- AEAEAEAEAKAK -c	− − − − + +	IV/II	α/β

Note: β: β-sheet; α: α-helix; r.c.: random coil; N/A not applicable.

Table 2.1 lists a number of ionic-complementary peptides that have been studied. These peptides are either fragments of naturally existing proteins or rationally designed to mimic natural proteins and help study protein folding. Aggeli *et al* designed a series of ionic-complementary peptides with 11 amino acids in sequence and a type I charge distribution + − (P_{11}-I and P_{11}-II in Table 2.1).[60] These peptides contain glutamine (Gln) residues with side chains that presumably interact strongly in water via hydrophobic interaction and complementary hydrogen bonding.

Arginine (Arg) and glutamic acid (Glu) residues have been located in positions 3 and 9 to allow molecular recognition between adjacent anti-parallel β-strands in fibril aggregates. These favourable intermolecular side-chain interactions and the intermolecular hydrogen bonding between the peptide backbones promote the formation of β-sheets. As expected, these peptides were found to form anti-parallel β-sheet rich fibrils as revealed by FTIR and electron microscopy studies.[60] Another class of ionic-complementary peptides with a type I charge distribution has been designed with only 6 amino acids in their sequences (P_6-1, P_6-6, P_6-7 and P_6-8, Table 2.1).[90] Among these hexapeptides, P_6-1, P_6-6 and P_6-7 have been found by CD spectroscopy to form predominantly β-sheet structures. However, only P_6-1 was found to form amyloid fibrils. The substitution of the Ile residues (e.g. Ile-4 → Leu from P_6-1 to P_6-6; Ile-5 → Val from P_6-1 to P_6-7) completely prevents fibril growth from preformed β-sheets. These results highlight the importance of the specific side-chain interactions.

The majority of the review hereafter focuses on a new class of ionic-complementary peptides designed by Zhang *et al.* (Table 2.1).[8,50,55,86] The first ionic-complementary peptide of its kind is EAK16-II, a 16-amino-acid peptide segment originating from a Z-DNA binding protein.[85,86] Derivatives such as EAK16-I and EAK16-IV have different charge distributions. Their molecular structures are shown in Figure 2.5. The repetitive arrangement of hydrophilic and hydrophobic amino acids imparts an amphiphilic property to the peptide. Zhang *et al.*[86] have demonstrated that this peptide can self-assemble into β-sheet-rich fibril structures. The supramolecular structure formation of such peptides may be due to the combination of electrostatic and hydrophobic interactions from the ionic-complementary residues and hydrophobic side, respectively. The molecular structure of EAK16-II forms a basis to construct other similar self-assembling ionic-complementary peptides with different functionalities. For example, RADA16-I was designed to enhance the biocompatibility and cell adhesion for tissue scaffoldings.[91]

(A)

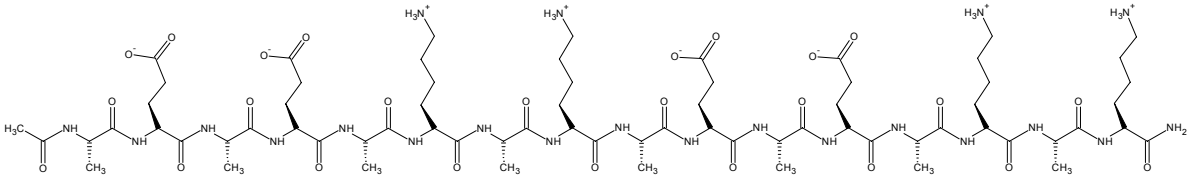

(B)

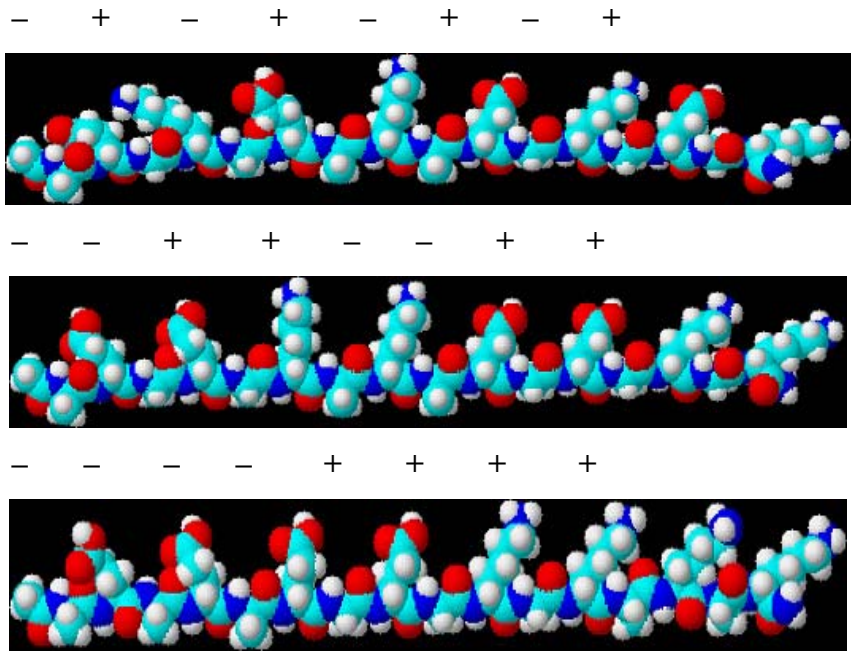

Figure 2.5 (a) Chemical structure of the ionic-complementary peptide EAK16-II. It contains alternating hydrophobic (alanine, A) and hydrophilic (glutamic acid, E and lysine, K) residues, producing amphiphilic structure that is hydrophobic on one side and hydrophilic on the other. The charged residues are arranged as type II, $--++--++$, where pairs of negatively (E) and positively (K) charged residues alternate. (b) Three-dimensional molecular model of EAK16s. The top, middle and bottom schemes represent the EAK16-I, EAK16II and EAK16-IV structures with charge distribution of $-+-+-+-+$, $--++--++$ and $----++++$, respectively.[89]

Ionic-complementary peptides have several important features. First, their charge distribution can be altered through simple molecular design, resulting in several peptide types, such as I, II and IV, as noted previously. For example, the sequence design based on the same components (E, A, and K) can generate three peptide sequences of EAK16-I, EAK16-II and EAK16-IV. The design of the charge distribution may determine the peptide secondary structure and influence peptide self-assembly.

A second feature, particular to the ionic-complementary peptides first studied by Zhang *et al*, is the specific peptide chain lengths required to exhibit ionic complementarity. The length of these peptides varies from eight to thirty-two amino acids in sequence due to the alternating hydrophobic and hydrophilic residues in the peptide sequence. (Table 2.1) The minimum number of amino acids required to build type I peptides is four, while the creation of type II and type IV peptides require eight and sixteen amino acids, respectively. The sequence of these short peptides can also be utilized for the design of polypeptides such as poly-EAK.[92]

A third feature is that the ionic-complementary peptide family can be easily expanded with the same charge distribution by using different amino acids. For example, DAR can be derived from EAK by replacing the residues glutamic acid (E) and lysine (K) with aspartic acid (D) and arginine (R), respectively. Similarly, the replacement of the hydrophobic residue alanine (A) of EAK with phenylalanine (F) or leucine (L) will generate two other ionic-complementary peptides EFK and ELK, respectively. Such simple replacement maintains the intrinsic properties of ionic-complementarity and self-assembly. This can also strengthen their propensity to form the desired supramolecules (e.g., the introduction of more hydrophobic residues). The increase in the hydrophobicity of the hydrophobic residues also reduces the shortest peptide length that can form a β-sheet secondary structure. For example, EAK requires a minimum of sixteen amino acids to form a

predominant β-sheet secondary structure, whereas EFK requires a minimum of only eight amino acids.

2.2.2 Physical/Biochemical Properties

Unusually stable β-sheet formation

An important characteristic of ionic-complementary peptides is the formation of unusually stable β-sheets in aqueous solution.[50,55,93] Once the β-sheets are formed, they remain unchanged under a broad range of physicochemical conditions (extreme pH, high temperature and dilution) and are even impervious to denaturing agents.[50] The β-sheet character can be clearly seen from the maximum absorbance in the CD spectra of EAK16-II at 218 nm and minimum absorbance at 195 nm, respectively, even at the very low peptide concentration of 0.612 μM.[50] In addition, the CD spectra of EAK16-II show that β-sheets remain stable up to 90 °C. Compared to most proteins that are denatured above 65 °C, β-sheets formed by EAK16-II are much more stable at higher temperature. Also, only a small change in the CD spectra at 218 nm was observed when the peptide solution pH was varied from 1.5 to 11, indicating that the β-sheets remain stable over this range. Unlike normal proteins that denature when the concentration of denaturation agents (e.g., guanidine-HCl and urea) is above 4 M, β-sheet structures of EAK16-II remained stable even in 7 M guanidine-HCl and 8 M urea. Such high stability was also found in 0.1% sodium dodecylsulphate (SDS) solution.

The analysis of the molecular structures and interactions in ionic-complementary peptides may explain the formation of such unusually stable β-sheet structures. The β-sheet formation is mainly caused by the hydrogen bonding between individual peptide backbones, which is evidently found in protein folding and aggregation. In addition, charged residues can also interact to stabilize the β-

sheets by means of electrostatic interactions and hydrogen bonding. Similarly, the hydrophobic interactions from the nonpolar residues also play a role in stabilizing the structure.

α-β structural transition

While some ionic-complementary peptides have very stable β-sheet structures, others can undergo structural transitions between α-helices and β-sheets. This conformational change is caused primarily by environmental factors, including solvent type, pH, salt and peptide concentration. For example, pH and the presence of salts can trigger or inhibit the α-β structural transitions of peptides such as EAK12-d and DAR16-IV.[86,94,95] Peptide sequence also affects this process, as indicated by the observation that α-β transitions occur with DAR16-IV but not RADI6-IV and EAK16-IV.[94] Other ionic-complementary peptides can undergo structural transition, as indicated in Table 2.1. Considerable effort has been made to design peptides for such a purpose. Not only could such a peptide be used to model the self-assembly of the peptides in conformational diseases, but it could also be useful in the development of nanomaterials that respond to changes in the environment. Such peptides could serve as a molecular switches for nanoscale devices and (bio)molecular sensors.

Stable and biocompatible supramolecular structure

Although small, ionic-complementary peptides can readily self-assemble into nano/microstructures, and interestingly some of the formed structures seem to be stable under various physiological conditions.[50,86] Several of these self-assembled structures have been shown to resist degradation by acidic or alkaline environments ranging from pH 1.5-11,[86] sodium dodecyl sulfate (SDS)/urea and a number of proteolytic enzymes including trypsin, protease K and pronase.[50,86] In addition, ionic-complementary peptides have been shown to be biocompatible when injected into rabbits, rats and goats.[86,96] The unusual stability of the peptides in serum, combined with their high resistance to

proteolytic digestion, simple composition and apparent lack of cytotoxicity,[36,50,86,96,97] make them attractive for many biomedical applications.

2.2.3 Understanding and Controlling Supramolecular Structure Formation

Ionic-complementary peptides are promising molecules for material fabrication because they can form stable nano/microstructures.[8,55,56] In order to regulate its nano/microstructure formation, the understanding and precise control of peptide self-assembly is always a big challenge for material scientists. For such a purpose, studies have focused on the internal and external factors that influence peptide self-assembly. These factors include (a) amino acid sequence, (b) molecular size, (c) peptide concentration, (d) solution pH, (e) ionic strength, (f) medium components such as solvent or substrate, (g) presence of denaturation agents, such as SDS and urea, (h) temperature and (i) time. The effects of amino acid sequence, peptide concentration, salt, pH and time effects on peptide nanostructure formation have been studied in particular.[21,51,98-100] Each factor is discussed below.

Effect of amino acid sequence

Peptide sequence serves as an internal factor that tunes peptide self-assembly. The type, number and arrangement of amino acids in the sequence play important roles in determining the secondary structures and self-assembled nanostructures of the peptides. For example, EFK8-I, containing eight amino acids in the sequence, forms β-sheet secondary structure in aqueous solution. However, when phenylalanine (F) is replaced with alanine (A), while maintaining the same charge distribution, the resulting peptide EAKA8-I forms random coils instead although it remains the same charge distribution. The reason for this phenomenon is still not clear. A possible explanation could be that the steric hindrance of the hydrophobic phenylalanine may help form β-sheets.

In addition to the type of amino acid, the length of the peptide sequence has significant impact on nano/macrostructure formation.[50,86,92,99] EAK16-II (16 amino acids) spontaneously associates to

form a macroscopic membrane when dissolved in a salt solution such as phosphate-buffered saline (PBS). EAK12 (12 amino acids) can also form membranes, but to a much lesser degree (<50%). In contrast, EAK8-II (8 amino acids) does not form membranes under the same condition. This might be due to the fact that peptides with a shorter chain length have fewer ionic-complementary pairs and less electrostatic interactions when peptides self-assemble into macroscopic structures.

The difference in charge distribution due to the arrangement of amino acids also influences the nano/microstructures formed by ionic-complementary peptides. For instance, EAK16-I and EAK16-II form fibril-like nanostructures, while EAK16-IV forms globular aggregates at neutral pH (Figure 2.6).[26] Furthermore the globular EAK16-IV assemblies have lower surface tension, indicating a higher hydrophobicity than the fibrillar EAK16-II assemblies. This could be due to the bending of EAK16-IV via strong intramolecular electrostatic attraction to form β-turns, exposing hydrophobic residues to the solution and lowering the surface tension. On the other hand, EAK16-II prefers a stretched β-strand, resulting in linear fibrils. This speculation is supported by Monte Carlo simulations.[27]

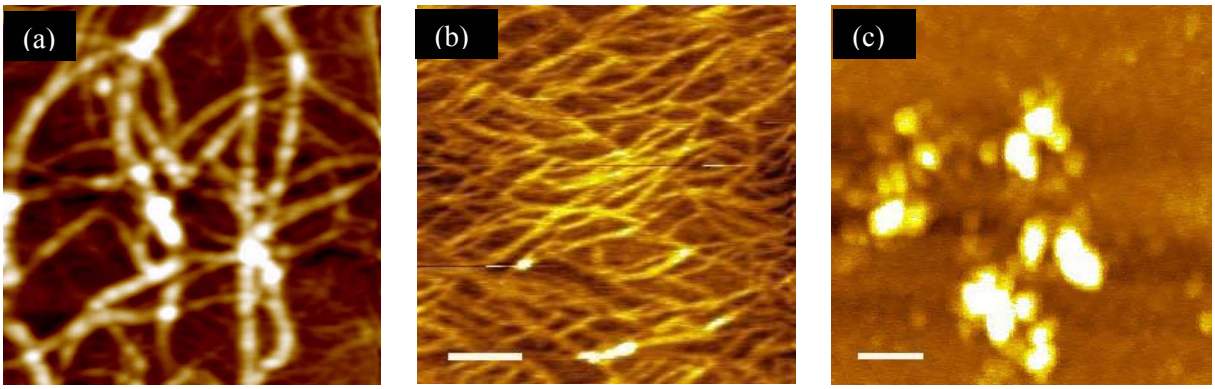

Figure 2.6 AFM images of EAK16-I (a), EAK16-II (b) and EAK16-IV (c) self-assembled nanostructures.[51,98]

Effect of peptide concentration

Another factor that triggers peptide self-assembly and further controls the nanostructure formation is the peptide concentration. Since the ionic-complementary peptides have an amphiphilic structure similar to surfactants, one would expect the concentration dependence of peptide self-assembly to be similar to that of surfactants. In analogy to the micelle formation of surfactants, having a critical micelle concentration (CMC), ionic-complementary peptides would have a critical aggregation concentration (CAC). This expectation is reasonable since the CAC has been reported for many proteins and amphiphilic peptides.[101-105] The ionic-complementary peptide P_{11}-I with 11 amino acids in sequence and a type I $+-$ charge distribution exhibits several critical concentrations corresponding to the formation of different nanostructures. It self-assembles into β-sheet tapes when the peptide concentration is larger than 0.01 mM.[60] When the peptide concentration reaches 1 mM, loose ribbons are formed. Fibrils are not observed at concentrations up to 25 mM. If the concentration continues to increase, a gel is eventually formed. Similar behaviour was found with its derivative P_{11}-II.

In comparison with other self-assembling peptide systems, EAK16-II was found to have a CAC of ~0.1 mg/ml (60 μM) by surface tension measurements.[21] AFM studies of the nanostructure of EAK16-II revealed that nanofiber networks are formed when the peptide concentrations exceed the CAC, while isolated filaments and globules are observed at concentrations below the CAC.[21] In addition, the fibril size and network density were found to depend on the peptide concentration as well. Similarly, another peptide EAK16-I was reported to have a critical concentration of 0.3 mg/ml (180 μM).[51] Unlike EAK16-II, EAK16-I assembly has been shown from AFM studies to undergo two nanostructure transitions.[51] The first transition from globules to fibril morphology occurs when the peptide concentration is about 0.05 mg/ml (30 μM). The second transition involves dramatic increase in the fibril size as the concentration rises above 0.3 mg/ml (180 μM).

Effect of pH and salt

In biological systems, the solution pH and salt content are two important environmental factors affecting protein and peptide structures. A pH change will influence the ionic state of the charged residues as well as the net charge of peptides/proteins. This will further influence the self-assembly behavior of the peptide and protein folding/aggregation. On the other hand, the presence of salts can affect the conformation and properties of many biological molecules, including their stability, solubility and biological activity.[106,107] A well known example is that of DNA which takes on a random coil conformation when placed in a phosphate buffer solution, but is condensed in the presence of multivalent cations.[108]

Interestingly, the assemblies of ionic-complementary peptides respond to the solution pH differently according to the peptide charge distribution. EAK16-IV with a type IV charge distribution has been found to undergo nanostructural transition depending on pH.[98] It forms globular nanostructures at pH ranging from pH 6.5 to pH 7.5, while nanofiber networks appear at other pHs. In contrast, EAK16-II formed fibrillar nanostructures throughout the pH range from 4 to 11. These findings suggest that the charge distribution in sequence plays an important role in determining the self-assembled peptide nanostructures. With a type IV charge distribution, strong intramolecular electrostatic attractions occur at neutral pH, which may cause molecular bending and the formation of globular nanostructures. At extreme pHs such as pH 4 and 11, either glutamic acid or lysine residues are neutralized, resulting in weakened intramolecular electrostatic interaction and smaller tendency for the peptide to bind and form a β-turn structure. Thus, nanofiber formation would be predominant.

The stability and conformation of the peptide assemblies are influenced by the presence of salts that can screen the charged residues and further reduce intermolecular electrostatic attractions. On the other hand, charge screening may also increase the hydrophobicity of the peptide which may promote peptide aggregation. In addition, the peptide may become less soluble in aqueous solution. It has been

found that the addition of salts induces the formation of EAK16-I fibrils at very low peptide concentration (below 0.05 mg/ml), which otherwise does not occur in the absence of salts.[51] On the other hand, the critical peptide concentration for the secondary nanostructure transition from small fibrils to large fibers increases from 0.3 mg/ml (180 μM) to 0.8 mg/ml (480 μM) in the presence of 20 mM NaCl. The reason for this phenomenon is still not clear.

Effect of time

Molecular self-assembly is a time-dependent, dynamic process. Hence, the self-assembled nanostructures of ionic-complementary peptide may evolve with time. The evolution of the peptide KFE8 (type I) assembly was monitored by AFM.[109] From the AFM images, left-handed helical ribbons were clearly visualized in the early stages, but gradually disappeared and replaced by fibril networks. It was believed that the disappearance of the helical ribbons was due to their subsequent assembly into fibril bundles. The time-dependence of the self-assembly of EAK16-II was studied with static light scattering and shown to be affected by the peptide concentration.[21] Above the CAC (~0.1 mg/ml), the intensity of scattered light increased sharply with time over the first 6 hours and then slowly approached a plateau. This indicates that the peptide self-assembles into large aggregates faster at peptide concentrations above the CAC. However, below the CAC, the intensities did not change much with time initially and increased slightly only after 100 hours. This suggests that the peptide formed smaller and/or fewer aggregates that was not easily detected by this technique initially at very low peptide concentrations. Although kinetic effects may not be as important as those of concentration in the early stages of self-assembly, it becomes an essential component in later stages.

In summary, the formation of peptide nanostructures can be controlled by peptide sequence design, peptide concentration, solution pH, the addition of salts and time. The controllable nanostructures coupled with biocompatibility and biodegradability make ionic-complementary

peptides promising biomaterials for use in nano-biotechnology. Some examples of such applications are described in the following sections.

2.3 Applications of Self-Assembling Peptides

2.3.1 Nanofabrication

Certain self-assembling peptides have shown promise in nanofabrication, in particular, of nanowires since they are able to self-assemble into well-defined nanostructures (e.g., nanofibers and nanotubes) and can easily bind with a range of inorganic compounds according to their natural biomineralization properties. As listed in Table 2.2, the affinity of several peptide sequences to gold, copper, silver, platinum, nickel and some conductive polymers has been studied. These peptide motifs can be used in conjunction with self-assembling peptides to fabricate metallic nanowires. One well-known example is the application of bolaamphiphiles as nanotube templates to construct Ni, Cu, Au and Pt nanowires.[70-73] The surface of the bolaamphiphile nanotubes can be further modified with histidine-rich peptide motifs for specific metallic binding; such modification can also control the size and growth of the metallic nanocrystals on the peptide template.[24,69-71,110-112]

Table 2.2 Peptide sequences exhibiting affinity for various metal ions

Metal ion	Peptide	Size (number of amino acids)	Charge
Au	AHHAHHAAD[72,113]	9	-1
Pt	HPGAH[73]	5	0
Ag	NPSSLFRYLPSD[111]	12	0
Cu	HGGGHGHGGGHG[67,71]	12	0
	Bis(N-α-amido-glycylglycine)-1,7-heptane dicarboxylate[67]	N/A	N/A
Ni	HGGGHGHGGGHG[70]	12	0
	Bis(N-α-amido-glycylglycine)-1,7-heptane dicarboxylate[24,67]	N/A	N/A

Another example is the use of the aromatic dipeptide FF (Phe-Phe), the shortest peptide possible, to form a template for Ag nanowire fabrication.[29] This peptide can self-assemble into well-ordered, discrete and stiff nanotubes in suitable organic solvents and serve as the templates. Silver ions can then enter the nanotubes and be reduced to metallic silver in the lumen of the tube, as shown in Figure 2.7. The peptide template can then be removed by enzymatic degradation, leaving an Ag nanowire with 20 nm in diameter. This method may have applications in molecular electronics since such small nanowires cannot be made by conventional top-down methods such as photolithography.

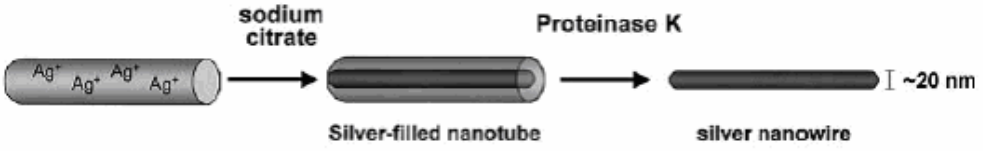

Figure 2.7 Casting of silver nanowires inside peptide nanotubes.[29]

In addition, Linquist *et al.*[35] have reported another peptide candidate, the N-terminal and middle region (NM) of yeast *Saccharomyces cerevisiae* Sup35p to function as a template for metallic nanowire fabrication. NM self-assembles into β-sheet-rich amyloid fibers with size and shape suitable for nanocircuits. The fibers have diameters of 9-11 nm and lengths from 60nm to several hundred micrometeres. NM can be engineered to incorporate more cysteine residues to interact with Au nanoparticles. The immobilized Au nanoparticles then serve as catalysts for the chemical reduction of Au ions in solution to fabricate nanowires.

2.3.2 (Bio)Molecular Sensing

Biosensors are analytical devices that combine a biologically sensitive element (bio-receptor) with a physical or chemical transducer to selectively detect and measure the amount of specific compounds in a given external environment. The biological sensitive elements are usually enzymes, microorganisms, cells, antibodies, tissues or DNAs. The transducer is used to convert the biological recognition reaction or eventually the biocatalytic process into a measurable electronic signal. For example, in an electrochemical enzyme biosensor, an electrical conductor such as graphite and noble metals can act as a transducer to convert enzyme catalysis reaction rates to electrical signals such as current or potential. Rapid and reliable detection of specific nucleic acid sequences, proteins, antibodies, antigens, cell-surface markers and pathogens is essential in the diagnosis of diseases, high-throughput assays, drug discovery as well as unraveling the complexities of cellular chemical networks. Therefore, intense research efforts have been made to fabricate novel biosensing devices that are highly efficient, reliable, portable, easy to use and inexpensive to operate. With fast developing nanotechnology, materials scientists and chemists are now focusing on using various nanoscale assemblies for these purposes. Some recent advances using self-assembling peptides in this field are reviewed below.

The self-assembled nanotubes of the peptide diphenylalanine (FF) have shown potential for biosensor applications.[49] In terms of morphology and aspect ratio (length to thickness), these peptide nanotubes are similar to carbon nanotubes (CNTs) that have been found to be advantageous in sensing applications due to their small size, high aspect ratio and electrical conductance.[114,115] Additional properties such as biocompatibility and good water solubility make peptide nanotubes particularly attractive for electrochemical sensing. Early work involved a graphite electrode modified with peptide nanotubes through direct deposition on the electrode surface. The electrochemical characteristics of the nanotube-modified and unmodified electrodes were examined from cyclic voltammetry scans for the $Fe(CN)_6^{4-}$/ $Fe(CN)_6^{3-}$ redox couple. The use of the modified electrode produced well-defined, reversible anodic and cathodic peaks and an improved electrochemical reactivity over that observed with the unmodified electrode. Meanwhile, the difference in anodic and cathodic peak potentials (ΔEp) decreased from 0.14 V for the bare electrode to 0.07 V for the nanotube modified electrode. This result demonstrated that the presence of peptide nanotubes improves the reversibility of this couple and can significantly improve the electrochemical fingerprint of the electrode. One possible reason for this phenomenon is that the electron transfer between spatially aligned aromatic systems of the dipeptide (FF) assemblies can enhance the conductivity and electrochemical activity of the modified electrode.

Apart from improving electrochemical parameters of graphite electrodes, peptide nanotubes can also modify Au electrodes for use in electroanalytical devices.[48] In order to link the peptide nanotubes to the Au surface, researchers have incorporated thiol groups into the nanotubes using Traut's reagent. The thiol-modified peptide nanotubes were then directly deposited on the Au electrode. This modified electrode demonstrated a direct and unmediated response to hydrogen peroxide and NADH. The successive additions of hydrogen peroxide and NADH at a potential of 0.4 V (vs. a SCE reference electrode) produced rapid responses of the peptide nanotube-based Au

electrode so that steady-state currents were obtained within 5 s, indicating that the modified electrode showed high electrocatalytic activity toward hydrogen peroxide and NADH oxidation. On the other hand, the unmodified electrode showed virtually no response. To detect the glucose level, glucose oxidase, the enzyme widely used in glucose biosensors, was immobilized to the peptide nanotubes. This modified electrode also exhibited unmediated rapid responses to the successive addition of glucose. These studies illustrate successful examples of using self-assembled peptide nanostructures as an electrochemical sensing platform for highly sensitive detection and measurement of biological analytes.

2.3.3 Model for Studying Amyloid Fibrillogenesis in Protein Conformational Diseases

A common cause of many conformational diseases is amyloid fibril formation, in which a normally soluble protein undergoes a conformational transition to initiate aggressive protein aggregation into abnormal, insoluble, macroscopic plaques. These extracellular deposits may block cell-to-cell communications, damage neuronal pathways and cause neuron death. A partial list of conformational diseases includes Alzheimer's diseases, bovine spongiform encephalopathy (BSE), Type II diabetes, Creutzfeldt-Jakob disease and various unrelated amyloidosis diseases. In spite of the significant clinical importance of amyloid formation, the mechanism of fibrillization is still not fully understood and a successful treatment not yet discovered.

A notable common property of amyloid protein deposits is that fibrils of different origins show similar biophysical and ultrastructural characteristics, including three major structural criteria.[116] First, amyloid fibrils are straight, unbranched and highly ordered fibrous assemblies with a diameter of 7-10 nm. Second, fibrils stained with Congo red dye show green birefringence under cross-polarized light. Third, by X-ray fiber diffraction, they exhibit a unique cross-β diffraction pattern in which the β-

strand is perpendicular to the fibril axis. This diffraction pattern arises from the underlying repeating core structure of predominant β-sheets.

Many self-assembling protein/peptide systems that can assemble into amyloid-like structures have been investigated to better understand molecular self-assembly. A notable example is the amyloid-β (Aβ) peptide containing 40-42 amino acid residues, which is the major constituent of the abnormal extracellular amyloid plaque found in the brains of Alzheimer's patients. The Aβ (1-42) and Aβ(1-40) peptides are full length amyloid peptides which form β-sheet rich amyloid fibrils. Solid-state NMR studies on the molecular structures within amyloid fibrils have shown that Aβ(1-40) fibrils are made of parallel β-structures; each contains a turn at residues 25-30, separating two β-strands (12-24) and (30-40).[116,117] The turn structure enables the two β strands to form intermolecular β-sheets that are in contact via their side chains. This arrangement results in a parallel, in-register, cross-β structure with a hydrophobic core and one hydrophobic face. Aβ(1-42) fibrils show similar parallel β-sheet arrangement.

It is widely accepted that amyloid fibrillogenesis in most cases occurs by a nucleation and growth mechanism.[118-120] Lomakin *et al*.[105] have proposed that the Aβ fibrillogenesis begins with the formation of nuclei in the Aβ solution. The nuclei are generated by either seeding or micellization, depending on whether the concentration of Aβ is below or above the critical micelle concentration (CMC). These nuclei provide a core for Aβ molecules to rearrange themselves into fibrils. Fibril elongation occurs by irreversible binding of the Aβ monomers to the fibril ends.

Although the study of full length native proteins involved in conformational diseases is the best way to obtain structural information and elucidate the aggregation mechanism, a number of difficulties are encountered with this approach. First, determining the basis of molecular recognition

and assembly process from the full length protein is remarkably challenging.[121] Second, the synthesis of large peptides, especially aggregative peptides is expensive and difficult. Third, but not the least, long and complicated protein/peptide sequences are not feasible for theoretical modeling with current computing capabilities. Therefore, efforts to understand amyloid formation focus on the study of short peptides, which are either fragments of disease-related proteins or synthetic self-assembling peptides.

The use of peptide fragments corresponding to specific regions of Aβ has enabled the formation of highly ordered amyloid fibrils, more amenable to structural analysis. For example, Aβ (11-25) located in a central region of Aβ is thought to be essential for fibril formation. Although the β-sheets of Aβ (11-25) fibrils are anti-parallel rather than parallel as is the case of full length Aβ peptides,[117] these fibrils are more rigid with a highly ordered arrangement of β-sheets than those of the full length Aβ peptides as revealed from their diffraction patterns.[116] Such highly repeating structures in a single fiber can be directly visualized with electron microscopy.[116] Apart from providing detailed structural information at a molecular-level, peptide fragments are short enough that they (and various analogues) can be easily synthesized by simple solid-phase chemistry. Moreover, the comprehensive study of a peptide fragment and its analogues should help determine the role of individual amino acids in amyloid fibril formation.[121] Through isotropic labeling in solid-state NMR experiments, it has been found that the intermolecular hydrogen bonds in the hydrophobic segments of Aβ (11-25) vary with solution pH. F19 forms intermolecular backbone hydrogen bonds with V18 at pH 7.4, whereas the intermolecular backbone hydrogen bonds formed between F19 and F20 at pH 2.3.[117]

Since conformational transitions of amyloid peptides have been found to be critical to the formation of amyloid fibrils, the study of synthetic peptides that can undergo structural transitions to form amyloid fibrils would help us to understand and hopefully mitigate amyloid fibrillogenesis.[122]

Mihara *et al.* have formulated a class of ionic-complementary peptides that undergo α-helix-to-β-sheet transitions.[123-126] This class of peptides consists of two amphiphilic α-helix segments which are linked by a disulfide bond between cysteine residues at the C-termini. The N-termini are attached by hydrophobic amino acids or 1-adamantanecarbonyl (Ad). The peptides initially form α-helix structures, but gradually change to β-structures in neutral aqueous solution. This transition is found to depend on many factors including the peptide concentration, temperature, pH, salt type and solvent type. An increase in peptide concentration and temperature enhances the transition from α-helices to β-sheets (i.e., more β-sheets are formed). However, the presence of organic solvents and salts can retard and even inhibit the transition.[127] The following mechanism for this transition has been proposed: monomeric α-helices first assemble into α-helix oligomers; when the concentration of α-helix oligomers increases above a critical point, they begin to form large aggregates and undergo conformational transition to β-sheets.[124] The hydrophobicity of the peptide has been found to affect the stability of these α-helix oligomers and thereby affect the α-β transition.[124] In addition, ionic complementarity has also been found to be important for amyloid fibril formation from investigations of the effect of charge distribution (e.g., periodicity of E and K in the sequence) on such peptides.[125,128]

Understanding the self-assembly of ionic-complementary peptides may provide insights into amyloid fibrillogenesis due to many similarities between ionic-complementary peptides and amyloid peptides.[60,90,129] First, the self-assembled nanostructures of ionic-complementary peptides and amyloid peptides both contain protofibrils and fibrils made of stable β-sheets.[50,117] Second, both self-assembly processes follow a nucleation and growth mechanism. This mechanism is peptide/protein concentration dependent. Above a critical concentration, nuclei form via monomeric assembly, which further induces peptide/protein aggregation into fibrils; below the critical concentration, nuclei form

only through seeding (i.e., from impurities or additives).[21,130] Third, the intermediates such as nuclei or protofibrils play an important role in both self-assembly processes. Although the intermediates may have different structures, they all aggregate into fibrils. The similarities with amyloid peptides and the simplicity in the molecular structures of ionic-complementary peptides could make them good model systems for studying amyloid fibrillogenesis.

2.3.4 Tissue Engineering

Tissue engineering is an interdisciplinary field that applies the principles of engineering and the life sciences to the development of biological substitutes that restore, maintain or improve tissue function.[131] It requires temporary scaffold materials for cells to control/maintain their bioactivity and physical properties. An ideal biologically compatible scaffold should meet several criteria: (i) structures resemblance to biological extracellular matrices; (ii) derived from biological sources; (iii) easy design and modification for specific needs; (iv) biodegradability; (v) non-cytotoxic with minimal immune responses and inflammation; (vi) ability to undergo good cell-substrate interactions; (vii) simple material production, purification and processing; (viii) readily transportable; and (ix) chemically compatible with aqueous solutions and physiological conditions.[132] Developments in material chemistry offer synthetic strategies for biomimetic materials to meet the challenges of designing artificial extracellular matrices. The use of self-assembly to generate hierarchical supramolecular structures is a biomimetic strategy and is now receiving growing attention in the field of biomaterials.[133-135]

Self-assembled peptide fibrous networks have shown potential for use in tissue engineering.[55] For example, ionic-complementary peptides EAK16-II and RAD16-II can self-assemble into well-ordered nanofibers and porous membranes, with fiber width of 10 nm and pore size ranging from 5 to 200 nm.[86,97] Their three-dimensional nanofiber structures are similar to natural extracelluar matrices

such as collagen. These peptides have been used to study cell attachment, survival and proliferation.[36,97,136] The cells were observed to spread out in a flat manner as they attached to the EAK16-II-coated substrate, similar to the behaviour of the cells attached to a fibronectin-coated substrate. In contrast, the same cells retained a round shape and did not spread on the malleable RAD16-II membranes. Malleable peptide membranes, unlike rigid substrates, can yield to cytoskeletal tensions, resulting in rounded cells. These peptide membranes provided sufficient attachment for endothelium cells even after the membrane was transferred to fresh culture wells.

RAD16-I has been intensively studied for its potential in tissue engineering due to its similarity to the ubiquitous integrin receptor-binding site RGD.[137] It has been used to culture liver-derived stem cells in three-dimensional systems that subsequently differentiated into functional hepatocyte-like cells.[37] Another example is the ability of three-dimensional RAD16-I peptide nanofiber scaffolds to entrap migrating hippocampal neural cells.[138] When hippocampal slices are cultured on such a nanofiber layer (~500 μm thick), a more extended interface between each tissue slice and the scaffold is formed. This simple method may not only allow the development of technology for neural progenitor cell isolation and enrichment *in vitro*, but also to expand the use of cell-based therapies of regenerative medicine. Apart from the 3D culture of liver-derived stem cells, RAD16-I matrices have been found to support neuronal cell attachment, differentiation and extensive neurite outgrowth.[96] The nanofibrous RAD16-I scaffolds create an environment amenable for functional synapse formation between the attached neurons. Importantly, these peptides do not elicit a measurable immune response or tissue inflammation when introduced into rats, rabbits and goats.[96,97]

Many other ionic-complementary peptides have also been found to be good candidates for tissue scaffolds. KFE8-I can form a matrix with an elastic modulus that compares favorably with that of soft tissues such as young male thigh and forearm skin and collagen sponge.[139] KLD12-I can form 3-D hydrogels that have shown potential for cartilage tissue repair.[36]

Superior scaffolds have been designed by coupling ionic-complementary peptides with specific functional motifs. These new scaffolds not only self-assemble into nanofiber networks that can create a fine-tuned microenvironment for 3D tissue cell cultures, but also enhance cell-materials interactions, cell proliferation, migration, differentiation and biological functions.[140] For example, RADA16-I can be functionalized with three short motifs: osteogenic growth peptide OGP (ALKRQGRTLYGFGG), osteopontin cell adhesion motif (DGRGDSVAYG) and a designed 2-unit RGD binding sequence (PRGDSGYRGDS).[141] The new peptides are synthesized by adding these three motifs to the C-termini of RADA16-I. These functionalized self-assembling peptide scaffolds significantly increase mouse preosteoblast MC3T3-E1 proliferation and differentiation towards bone formation in comparison to unfunctionalized RADA16-I. In addition, inclusion of bone marrow homing motifs (BMHP1, SKPPGTSS and BMHP2, PFSSTKT) in RADA16-I remarkably enhances adult mouse neural stem cell survival, proliferation and differentiation into neurons and glial cells.[140]

In summary, ionic-complementary peptides have great potential as scaffolding materials in tissue engineering applications such as neurite outgrowth, cartilage repair, osteoblast and neural stem cell proliferation, differentiation and 3-D migration. Not only are they highly biocompatible and biodegradable, they also have suitable mechanical properties and possess diverse biological functionality. Ease of molecular design and the ability to self-assemble will make these small peptide building blocks important tools in future tissue engineering. The application of ionic-complementary peptides in tissue engineering involves the interfaces between the peptide scaffold and the underlying supporting material and between the peptide scaffold and supported cells. Thus, control of the peptide nanostructures at interfaces is crucial for obtaining biocompatible matrices for cells.

2.3.5 Drug Delivery

The very slow progress in the efficacy of treating severe diseases such as cancer has suggested a growing need for novel approaches to the delivery of therapeutics to the targets regions in tissues. Accordingly, drug delivery systems are emerging as new strategies to control pharmacokinetics, pharmacodynamics, non-specific toxicity, immunogenecity, biorecognition, and drug efficacy.[142] In order to develop novel drug delivery systems for clinical use, the design and/or discovery of effective delivery vehicles play important roles.

Peptides have shown much potential for drug delivery. The most attractive aspect of peptide-mediated drug delivery is the natural propensities of many peptides for cell penetration and targeting.[143,144] Peptide-based delivery systems have shown the potential to deliver therapeutic proteins, bioactive peptides, small molecules and nucleic acids.[143-145]

Ionic-complementary peptides may be a new and promising material as carriers for drug delivery. Their unique amphiphilic structure and ability to self-assemble allow them to encapsulate both hydrophobic chemotherapeutics and hydrophilic gene therapeutics. Moreover, no detectable immune response is observed when these peptides were introduced into animals.[86,96,97] These peptides can spontaneously organize themselves into nano/micro structures that may provide a protected and stable environment for drug/gene molecules. Another advantage of using peptide-based carriers is the ease of sequence modification and design for cell penetration and targeting.

Ionic-complementary peptides have been shown to readily encapsulate hydrophobic materials and increase their solubility in aqueous environments. Recent work using pyrene as a model hydrophobic compound has demonstrated the potential of ionic-complementary peptides in the delivery of hydrophobic anticancer drugs.[146] The use of EAK16-II was shown to stabilize pyrene microcrystals in an aqueous solution at concentration up to a ten-thousand fold increase beyond its solubility in water of 7.0×10^{-7} M. Since the encapsulated pyrene is in a crystalline form so that more

pyrene molecules are encapsulated per peptide, the loading efficiency is high. Consequently, the dosage of hydrophobic drugs may be dramatically reduced using self-assembling peptide vehicles. The encapsulated pyrene from the peptide coatings can be released into liposomes used to mimic the cell membrane.[147] The release rate has been found to be a few hours and proportional to the peptide-to-pyrene ratio during the encapsulation: the higher the ration, the slower the release rate. This is due to the difference in the density of peptide nanostructures coated on the pyrene crystals, as revealed by scanning electron microscopy. This example demonstrates that controllable release of drugs may be achieved by using ionic-complementary peptide vehicles.

Recent work in our group has shown the ability of such peptides interacting with an anticancer agent and oligonucleotides. The solubility of the hydrophobic anticancer agent ellipticine was significantly improved upon interaction with EAK16-II.[32] In addition, EAK16-II can also interact with oligodeoxynucleotides (ODNs) in a controlled manner at different solution pHs and peptide concentrations.[148] In addition, the encapsulation of ODNs with ionic-complementary peptide can protect the ODNs from degradation as indicated by fluorescence quenching studies. These results show the potential of ionic-complementary peptides in gene delivery as well.

Apart from delivery of hydrophobic compounds and hydrophilic genes, ionic-complementary peptides have shown success in the local delivery and release of peptide/protein drugs in a controlled manner. Biotinylated RADA16-II has been used to deliver insulin-like growth factor 1(IGF-1) to the myocardium.[149] The biotinylation does not change the self-assembly property of RADA16-II. IGF-1 is then incorporated into the biotinylated RADA16-II by using tetravalent streptavidin. This “biotin sandwich” approach allows specific and highly controlled delivery of IGF-1 to local myocardial microenvironments. After injection into the rat myocardium, the biotinylated nanofibers provide sustained IGF-1 delivery for 28 days and increase activation of Akt in the myocardium, indicating an improved cell therapy.

In summary, ionic-complementary peptides have shown the potential in constructing versatile delivery vehicles that can encapsulate both hydrophobic and hydrophilic molecules. The targeting/penetrating abilities can be possibly introduced by peptide design at a molecular level. The ability to manipulate the size of the self-assembled nano/micro-structures and complexes with various drugs would be essential to enhance the drug loading and release capacity and enable this type of peptides to be effective biocompatible carriers in cancer chemotherapy and gene therapy.

2.4 Molecular Assembly on Surfaces

The nanoscale assembly of molecules on surfaces play an important role in nanotechnology and many biological systems.[150-152] Many nanoscale devices require formation of regular/patterned arrays of thermodynamically stable nanostructures.[6] This can be achieved by surface-directed/assisted molecular assembly. However, it is still a challenge to precisely control the arrangement of molecular modules to form regular arrays at a surface or interface. Therefore, study and manipulation of molecular assembly at surfaces or interfaces has drawn increasing attention in recent years.[153]

2.4.1 Directed/Assisted Molecular Assembly into Patterned Nanostructures

The assembly of most molecules on surfaces has been found to be surface-directed/assisted. For instance, a hydrophobic graphite surface helps to organize molecules such as metal-organic complexes,[154] long alkyl chains and fullerenes,[155] peptides[41-43] and polymers[156] into patterned nanostructures. These patterned nanostructures often resemble the crystallography of the graphite. This occurs due to the combination of molecule-surface and molecule-molecule interactions that constrains the assembling molecules. Particularly, a flat surface constrains the motion of molecules to be two-dimensional when attached to a surface and thereby facilitates the special-organization of the molecules. The most important interactions for molecular assembly into well-defined architectures on surfaces include Van der Waals forces, hydrogen bonds, electrostatic interactions and metal

coordination. More often, competitive interactions occur simultaneously and the successful outcome of the assembly process requires not only balanced intermolecular interactions but also favorable molecule-surface interactions.[154]

The formation of well-ordered supramolecular nanostructures from functional organic molecules on surfaces has attracted much interest in view of their potentials for use in electronic, magnetic and optic devices. Recently, one-dimensional nanostructures of a perylene-based n-type semiconductor molecule (PTCDI) on both glass and mica surfaces have been fabricated with the solvent-vapour annealing method.[157] In this study, concentrated chloroform solutions of PTCDI were drop-casted or spin-coated onto a mica or glass surfaces to form a thin films. The thin films were then annealed in chloroform vapour to allow packing of PTCDI molecules on the surface. After 24 hour annealing, long nanobelt-like one-dimensional nanostructures were observed. The lengths of the nanobelt assemblies can be feasibly controlled by the nature of the surface and the concentration of PTCDI during casting. It has been found that the nanobelts formed on glass are longer and thinner than those on mica under the same condition. In addition, higher concentrations of PTCDI favour the formation of extended nanobelts. These one-dimensional assemblies with tuneable length have potential applications in nanowire-based organic optoelectronics and quantum devices.[153]

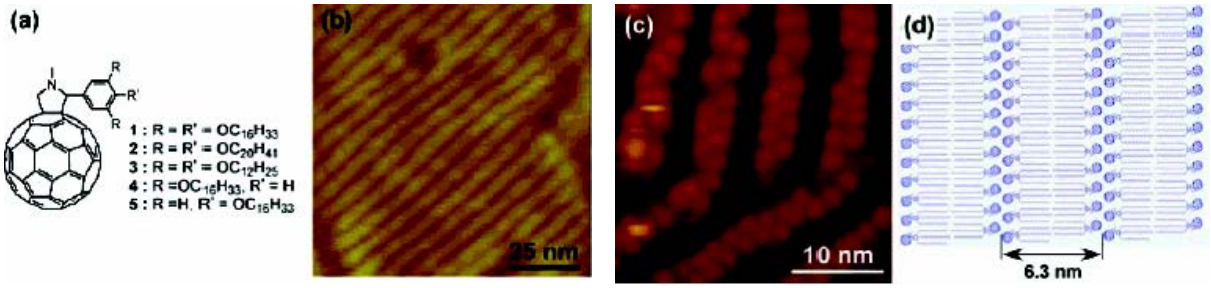

Figure 2.8 Assemblies of a fullerene derivative on HOPG. (a) Structure of fullerene derivatives. (b) AFM image of the fullerene derivative 1 with three hexadecyl chains on HOPG spin-coated from $CHCl_3$ solution. (c) High-resolution STM image of the fullerene derivative 1 on HOPG. (d) Schematic illustration showing the molecular organization of derivative 1 in the lamellae.[155]

Interestingly, a highly ordered pyrolytic graphite (HOPG) surface has been shown to direct the assembly of fullerenes (C_{60}) into one-dimensional architectures.[155] To form these well-ordered nanostructures, long alkyl chains were attached to the fullerenes, as shown in Figure 2.8a, to induce epitaxial assembly on HOPG and to act as insulating barriers to separate the fullerene nanowires. These fullerene derivatives in chloroform solution were then spin-coated onto freshly cleaved HOPG under suitable conditions to achieve submonolayer coverage so as to reveal structural details of the interfacial layer. The AFM images show that fullerene derivatives formed one dimensional lamellar stripes on HOPG (Figure 2.8b). The observed stripes in different domains were arranged at 60º or 120º with respect to each other, reflecting the symmetry of the underlying graphite lattice. A high-resolution STM image revealed the zigzag-type arrangement of C_{60} in the lamellar structure, as shown in Figure 2.8c. The conformation of alkyl chains and arrangement of the fullerene derivatives were revealed by the periodicity of the nanostripes, which were twice the length of the fullerene derivatives in an *all-trans* conformation. Accordingly, it was proposed that the lamellae are composed of fully extended alkyl chains and the molecules are arranged in a head-to-head bilayer architecture (Figure

2.8d). This hypothesis was supported by the examination of the effect of alkyl chain length on the spacing of the fullerene nanostripes. It is hoped that the distance between adjacent fullerene nanowires may be ultimately tailored at the nanoscale level through the attached the alkyl chain length.

Peptides/proteins can also form ordered structures on surfaces. It was reported that the peptide GAV-9 with a sequence NH_2-VGGAVVAGV-$CONH_2$ can grow epitaxially into ordered nanofilaments on both hydrophilic mica and hydrophobic HOPG surfaces (Figure 2.9).[158] The formation of these nanofilaments monitored by *in-situ* AFM was found to follow three preferred orientations at 120° to each other and in a threefold symmetry pattern. Interestingly, the nanofilament height on these two surfaces was found to be different, indicating that the peptide molecules were orientated differently. The height of the nanofilament on mica is similar to the peptide length, whereas that on the HOPG surface is similar to is height. This observation suggests the following interfacial orientations on the two surfaces: peptide adopts an "upright" orientation on mica due to the electrostatic interaction between the positively charged N-termini and the negatively charged mica; a horizontal orientation on HOPG is preferred due to the hydrophobic interaction between the peptide and the surface. Examination of the peptide secondary structures shows that it adopts random coil structure in solution but anti-parallel β-sheets on mica surface, indicating that these ordered nanostructures are surface-directed. Surface-directed/assisted peptide assembly by emploiting surface hydrophobicity/hydrophilicity may be a useful approach to fabricate tailored nanostructures.

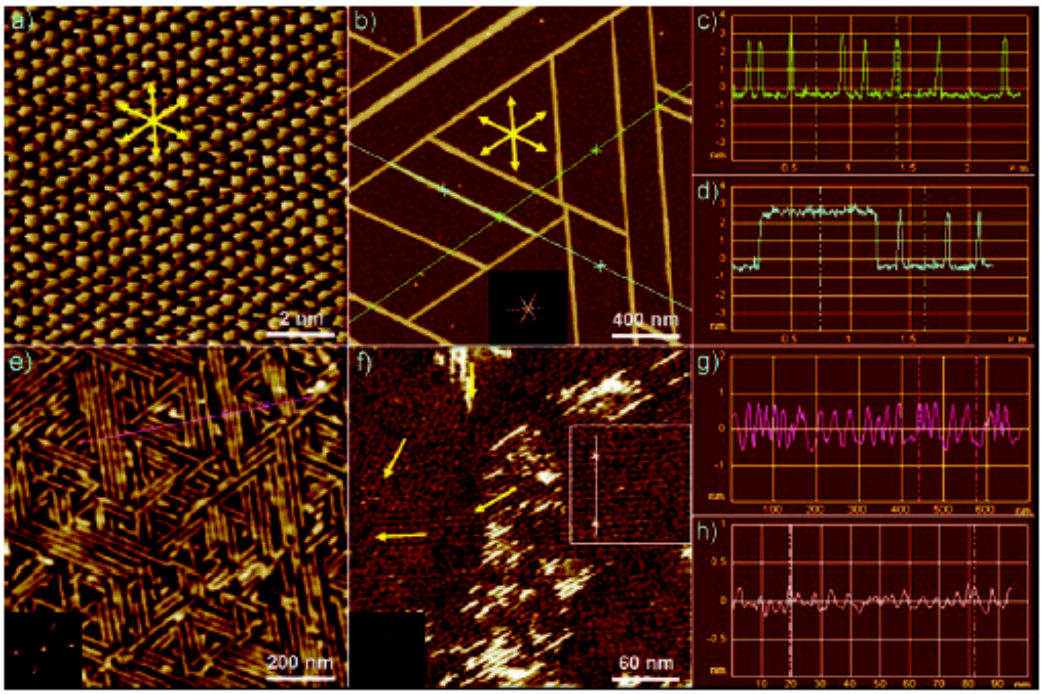

Figure 2.9 AFM images and analysis of GAV-9 nanofilaments. (a) Atomic lattice of the mica surface; (b) GAV-9 fibrils on mica; inset is the Fourier transform image; (c) cross-section of the green line marked in (b); (d) cross-section along a fibril marked by the blue line in (b); (e) GAV-9 on HOPG; inset is the Fourier transform image; (f) layers of GAV-9 on HOPG with yellow arrow indicating their orientations; inset is Fourier transform of the marked region; (g) cross-section of the pink line marked in (e); (h) cross-section of the white line marked in (f).[158]

2.4.2 Induced Biomolecular Aggregation

In addition to directing and regulating molecular assembly, a surface can induce or catalyze protein/peptide aggregation. Recently, studies have shown the importance of surfaces in amyloid fibril formation.[40,43,159,160] The size and shape of amyloid-β (Aβ) peptide aggregates, as well as the kinetics of their formation, exhibited a pronounced dependence on the physicochemical properties of the surface.[41-43] On hydrophilic mica, the Aβ peptide formed linear assemblies with an average height

of 5-6 nm, whereas uniform, elongated sheets with height of 1 nm were found on hydrophobic graphite.[43] Amyloid formation of Aβ peptide was found to follow a nucleation and growth mechanism by direct observation of its assembly on mica using *in situ* AFM.[43,130] The formation of amyloid fibrils on mica occurs when protofibrils appear on the surface as seeds and are elongated by the addition of Aβ molecules and protofibrils to the active sites of the seeds. Such seed-dependent amyloid fibril growth of Aβ was also observed in real-time using total internal reflection fluorescence microscopy (TIRFM) on the glass surface by Ban *et al*.[159] Interestingly, they noticed some differences between fibril growth on the glass surface and in solution, particularly fibril length, indicating the effect of surfaces on the Aβ aggregation.

Similarly, fibrillization of α-synuclein, a protein associated with Parkinson's disease, has been found to be surface dependent.[40,161] Hoyer *et al.*[40] reported that α-synuclein formed elongated β-sheets on a negatively charged mica surface, but not on HOPG, suggesting that negatively charged surfaces promote α-synuclein assembly. Such an argument was supported by the study of *Necula et al.* on fibrillization of recombinant α-synuclein in the presence of anionic lipids or surfactants.[161] They found that the fibrillization can be greatly accelerated at low micromolar concentrations with the presence of micelles in the solutions. Other anionic surfaces provided by anionic phospholipid vesicles also induced α-synuclein assembly, with resulting filaments originating from their surface. These findings provide new insights into the role of anionic surfaces in α-synuclein fibrillization, underlying that anionic membranes may participate in amyloid fibrillization *in vivo*.

Other evidence of surface-induced/catalyzed amyloid fibril formation has been reported by Zhu *et al*.[160] In their investigation, a recombinant amyloidogenic light chain variable domain SMA formed fibrils on negatively charged mica but not on hydrophobic or positively charged surfaces. Fibril growth could occur from the deposited oligomeric units as well as the preformed amorphous cores on

the surfaces. In addition, fibril formation was accelerated significantly on surfaces compared to that observed in bulk solution. Also, the mechanism of SMA fibril formation on the surface was significantly different from that in solution. However, the surface-induced assembly may be more physiologically relevant since the *in vivo* protein deposits are associated with surfaces.

In summary, the observed assembly of various molecules ranging from organics, fullerenes to peptides, on surfaces lead to the following conclusion: the surface effect on molecular assembly/aggregation could be a general phenomenon. Although the underlying mechanisms are still unclear, the substrate or surface is crucial to many of these molecular or biological assemblies. Study of the substrate/surface effect on supramolecular assembly using a typical model system may therefore shed new light on many complicated biological events and better control molecular architectures on surfaces. Our aim is to study the substrate/surface effect on the assembly of an ionic-complementary peptide not only to understand the mechanisms of molecular assembly but also to control such processes in order to build supramolecules with desired structures and functions.

Chapter 3*
Surface-Assisted Peptide Assembly: Controllable Nanofiber Growth

3.1 Introduction

Molecular assembly at a surface plays an important role in many nanotechnology and biological applications.[150-152] Surface/substrate-directed assembly has been explored to construct a variety of nanosystems. For example, a hydrophobic graphite surface was reported to direct molecules, such as long alkyl chains, fullerene derivatives,[155] peptides[41-43] and polymers,[156] to organize into various patterns. The resulting nanostructures can be used to construct nanoscopic devices, such as (bio)sensors, information storage units, optical computers and solar cells.[44-47] Another example is the spontaneous organization of the negatively charged virus M13 into ordered monolayer structures on the surface of a positively charged, multilayered LPEI/PAA polymer film.[162] These ordered, self-assembled viral structures can be used to fabricate more powerful batteries and grow functional nanoparticles and nanowires.[162,163]

In biomedical studies, some surfaces have been found to induce protein/peptide aggregation. Recent reports have shown the importance of substrates in amyloid fibril formation.[40,43,159,160] The size and shape of amyloid-β (Aβ) peptide aggregates, as well as the kinetics of aggregation, exhibited pronounced dependence on the physicochemical properties of the substrate.[43,130,159] The fibrillization of α-synuclein, a protein associated with Parkinson's disease, has been found to depend on the nature of the micelle surface in incubation solution.[40] It was reported that the *in vitro* fibril formation of some proteins, such as SMA, a recombinant amyloidogenic light chain variable domain, is sensitive to the contact surface of test tube materials and a stir bar.[160] All these observations point to a notion

*This chapter is based on a paper "H. Yang, S.Y. Fung, M. Pritzker, P. Chen, Surface-Assisted Assembly of an Ionic-Complementary Peptide: Controllable Growth of Nanofibers, *J. Am. Chem. Soc.* 2007" (in press).

that the substrate effect on protein/peptide assembly and aggregation is important and critical to many nanoscale biomedical processes.

Our understanding of the substrate-assisted assembly and aggregation of biomolecules however remains incomplete. This is partially due to the complexity of biomolecules and the experimental difficulties in nanoscale *in-situ* examination of the assemblies. A relatively simple, self-assembling peptide with residues that possess a variety of molecular interactions occurring in proteins could be a good model molecule to investigate such complicated processes. The purpose of this work is thus to study the substrate/surface effects on the nano-assembly of a model peptide, to better understand the assembly kinetics and further to control the peptide aggregation at a surface.

The model peptide used is an ionic-complementary, self-assembling peptide, EAK16-II (Figure 3.1). [21,26,86] This peptide is capable of hydrogen bonding, electrostatic and hydrophobic interactions. The amino acid sequence of this peptide bears a repetitive, alternating charge distribution (type II: $--++--++$) leading to ionic complementarity.[50,86] In addition, alternation of the hydrophobic (A) and hydrophilic (E and K) residues results in an amphiphilic feature. Such an amino acid sequence allows the peptide to self-assemble into β-sheet rich nanofibers in solution.[21,26,50,86] Our previous studies have shown that many factors, such as peptide sequence[26,27] and concentration,[21,51] salt type and concentration,[22,51,52] and solution pH,[26] affect the self-assembled micro-/nanostructures of the peptide and its derivatives. The simple, regular structure and our previous knowledge of EAK16-II provide a good basis to study the substrate/surface effect on the peptide aggregation and to possibly control this process.

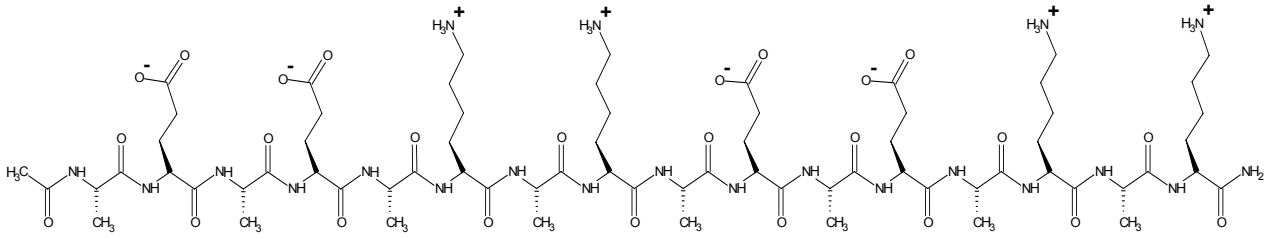

AcN-AEAEAKAKAEAEAKAK-CNH_2

Figure 3.1 Molecular structure of EAK16-II

The main tool used was *in-situ* Atomic Force Microscopy (AFM). This technique is especially suitable for real-time monitoring the assembly of biomolecules in solution. First, this method enables the repetitive imaging of mechanically delicate biomaterials with minimum lateral forces between the probe and sample. Second, it is possible to directly study the dynamics and kinetics of the assembly of proteins/peptides under the solution conditions appropriate for biological events.[164] Third, the kinetics of each individual assembly can be quantified. The surface used in this study was mica, which is negatively charged even at a low pH value of 3,[165] and provides an atomically flat surface that enables high resolution AFM imaging. To complement the AFM surface observations, Dynamic Light Scattering (DLS) and zeta potential measurements were employed to monitor the assembly process and the charge of the peptide in bulk solution, respectively. It is known that the surface charge of a particle plays an important role in aggregation of colloidal dispersions, polyelectrolytes and proteins.[166,167] These solution properties of EAK16-II should provide essential information and evidence in relation to surface-assisted assembly.

We in particular investigated the surface-assisted EAK16-II assembly at different solution pHs. It is expected that a change of the solution pH would alter the charge status of the peptide and its electrostatic interaction, which in turn should affect the peptide-peptide and peptide-surface interactions. As a result, the assembly behavior of EAK16-II on the substrate may be modified. This

will provide a way to control the surface-assisted assembly, leading to construction of functional nanostructures. These findings are also related to amyloid fibrillogenesis, providing a simple model to understand peptide/protein aggregation.

3.2 Materials and Methods

3.2.1 Materials

The peptide EAK16-II ($C_{70}H_{121}N_{21}O_{25}$, molecular weight 1657 g/mol) has a sequence of AEAEAKAKAEAEAKAK (Figure 3.1), where A corresponds to alanine, E to glutamic acid and K to lysine. At neutral pH, A is neutral, hydrophobic residue, while E and K are negatively and positively charged, respectively. This peptide was purchased from CanPeptide Inc. (Québec, Canada) with a purity of >95% (purified by reverse-phase High-Performance Liquid Chromatography). The N-terminus and C-terminus of the peptide were protected by acetyl and amino groups, respectively, to minimize end-to-end electrostatic interaction between peptides.[27]

The EAK16-II stock solutions were prepared in pure water (18.2 MΩ; Millipore Milli-Q system) at concentrations of 12 μM and 120 μM, and stored at 4°C before use. Unless otherwise noted, the 12 μM peptide stock solution was used for all AFM studies while the 120 μM peptide stock solution was for TEM imaging. Reagent grade sodium hydroxide with purity of 99+% and hydrochloric acid (36-38% by weight) were obtained from BDH Chemicals Ltd. (Toronto, Canada) and Fisher Scientific, Inc. (Nepean, Canada), respectively.

Grade V-4 muscovite mica ($KAl_2(AlSi_3)O_{10}(OH)_2$, SPI Supplies, West Chester, USA) was used as the supporting surface. A mica slide was fixed on an AFM sample plate using a double sided tape. An adhesive tape was used to remove the outer layer of mica to generate a fresh surface prior to each experiment.

3.2.2 *In-situ* AFM Imaging

To monitor how a single EAK16-II nanofiber assembles on a mica surface under desired experimental conditions and avoid any drying effects, *in-situ* AFM imaging was performed on a PicoScan^{TM} AFM (Molecular Imaging, Phoenix, AZ) in a liquid cell (custom-made). The cell was mounted on a freshly cleaved mica surface and injected with 500 μl of pure water, 1 mM HCl, 10 mM HCl, 1 mM NaOH or 10 mM NaOH solution. 100 μl of the 12 μM EAK16-II stock solution was then injected into the liquid cell with a microsyringe to obtain a final peptide concentration of 2 μM. This slightly diluted the concentrations of HCl and NaOH solutions (0.83 mM and 8.33 mM); however, the same initial concentrations (1 and 10 mM of HCl or NaOH solutions) before the injection of the peptide solution were used throughout this study. The pH values of the final solutions in the liquid cell are indicated in Table 3.1.

Atomic force microscopy images were obtained using a scanner with a maximum scan area of 6×6 μm^2. All AFM experiments were conducted in an environmentally controlled chamber at room temperature to avoid evaporation of the working solution. Silicon nitride cantilevers with a nominal spring constant of 0.58 N/m (DNP-S, Veeco Probes, Santa Barbara, USA) and a typical tip radius of 10 nm were used in AFM tapping mode. To obtain the best imaging quality, the typical tapping frequency was set between 16 kHz and 18 kHz and the scan rates were controlled between 0.8 and 1 Hz (~5 min to take each AFM image). All AFM images were collected at a resolution of 256×256 pixels. In general, the elapsed time associated with each image refers to the point when EAK16-II stock solution was injected into the liquid cell containing a desired working solution. An initial image of a newly cleaved mica surface immersed in the working solution was taken to confirm the absence of contaminating dust particles.

The lengths of EAK16-II fibers on the mica surface at different times were measured with the Image J software (http://rsb.info.nih.gov/ij/). The width and height of EAK16-II nanofibers were

determined by the cross-section analysis tool of the PicoScan™ software (Molecular Imaging, Phoenix, AZ). The peptide fiber widths reported were obtained using the deconvolution method reported by Fung *et al*.[21] In each solution condition, at least 50 nanofibers were collected and analyzed from the AFM images of at least three independent experiments.

3.2.3 TEM Imaging

Transmission Electron Microscopy (TEM) was performed with a Philips CM20 electron microscope (Philips Electronics Ltd. Guildford, UK) at an accelerating voltage of 200 kV. Images were digitalized using a Gatan 679 slow-scan CCD camera and analyzed using DIGITALMICROGRAPH (version 2.1, Gatan Inc. Pleasanton, CA). A 120 μM EAK16-II stock solution was diluted with pure water 5 times first, and then 10 μl of the diluted solution was incubated on a 400-mesh carbon-coated formvar copper grid (Marivac Ltd., St. Laurent, QC) for 10 min. Excess solution was drawn off the edge of the grid with tissue paper. After air drying for 20 min, the grid was negatively stained with 2% (wt/vol) uranyl acetate for 5 s. Excess stain was drawn off with tissue paper and the grid air-dried before TEM imaging.

3.2.4 Dynamic Light Scattering

Dynamic Light Scattering experiments were performed using a Zetasizer Nano ZS (Malvern Instruments, Worcestershire, UK) with the appropriate viscosity and refractive index settings and the temperature maintained at 25°C during the measurement. A small-volume (45 μl) black quartz cuvette with a 3 mm light path was used. A 0.3 mM EAK16-II solution was prepared in pure water, 1 mM HCl, 10 mM HCl or 10 mM NaOH, and sonicated for 10 min and then filtered (0.22 μm) before the measurement was taken. The scattered light intensities of samples at the angle of 173° were collected at various times. The pH of 0.3 mM EAK16-II dissolved in pure water, 1 mM HCl, 10 mM HCl and 10 mM NaOH was measured to be 3.9, 3.1, 2.0, and 11.9, respectively. The viscosity and

refractive index of pure water, 1 mM HCl, 10 mM HCl and 10 mM NaOH at 25 °C were also measured by a Cannon Ubbelohde Semi-Micro viscometer (size 75, Cannon Instrument Company, State College, PA) and refractometer (Bausch & Lomb, Inc., Rochester, New York, USA)), respectively, and found to be very close to those of pure water at 25 °C.

Under each condition, two samples were used and triplicate measurements were made for each sample. The sample was monitored frequently within the first day, twice a day for the following 4 days and once every 2 or 3 days for the following 3 weeks. The intensity-based size distribution of peptide assemblies in solution was obtained with the multimodal algorithm CONTIN,[168] provided in the software package Dispersion Technology Software 5.0 (Malvern Instruments, Worcestershire, UK).

To study the kinetics of peptide assembly in solution, the total light intensity of the peptide solution was monitored over time. The light intensities reported as a function of time were the average values obtained from three measurements of each sample. The light intensity of the peptide dissolved in pure water was plotted versus time and fitted to a single exponential function:

$$I(t) = I_{eq} + A\exp(-k_{app}t) \qquad (3.1)$$

where *I(t)* is the light intensity at time *t*, I_{eq} is the maximum light intensity at the end of the observed exponential phase, *A* is the pre-exponential coefficient and k_{app} is the apparent rate constant.

3.2.5 Zeta Potential Measurements

The surface charge of EAK16-II assemblies in solution was determined by zeta potential measurements on a Zetasizer Nano ZS (Malvern Instruments, Worcestershire, UK) at 25°C. A freshly prepared 0.18 mM EAK16-II solution was used for each measurement. The pH of the peptide solution was adjusted to the desired value using small amounts of 2 M NaOH or 2 M HCl. A correction of the

peptide concentration for the volume change was not made for this measurement because the change in peptide concentration (<1%) due to the addition of NaOH or HCl was negligible. Samples were injected into a disposable cell (folded capillary DTS-1060 from Malvern, Worcestershire, UK) with a volume of ~1 ml and analyzed at constant voltage. The zeta potential distribution (in mV) was automatically calculated from the electrophoretic mobility distribution based on the Smoluchowski formula.[169,170] For each solution condition, the zeta potentials were repeated with two independent samples; at least three measurements were carried out for each sample. The zeta potentials reported herein correspond to the average of the peak values of the zeta potential distributions from the repeated measurements.

3.3 Results

3.3.1 Real-Time Observation of EAK16-II Nanofiber Growth on Mica

Figure 3.1 (panels a-d) shows a sequence of the in-situ AFM images of EAK16-II nanofibers taken on the same location of a mica substrate immersed in an aqueous solution containing 2 μM EAK16-II. It can be seen that the length of nanofibers increases with time. A couple of short nanofibers (~200 nm in length) initially appearing after ~21 min incubation (Figure 3.2a) are observed to continually grow on mica (Figure 3.2b-d). After ~81 min, the nanofiber length increases to ~2.3 μm. The green arrows indicate the two ends of a fiber, while the red arrow points to a reference spot to show that the nanofiber can grow at both ends (bidirectional growth). The elongation from the two ends of a fiber may result from the addition of peptide monomers or oligomers at the two active ends. At this stage, we cannot distinguish whether a monomeric or oligomeric addition is occurring.

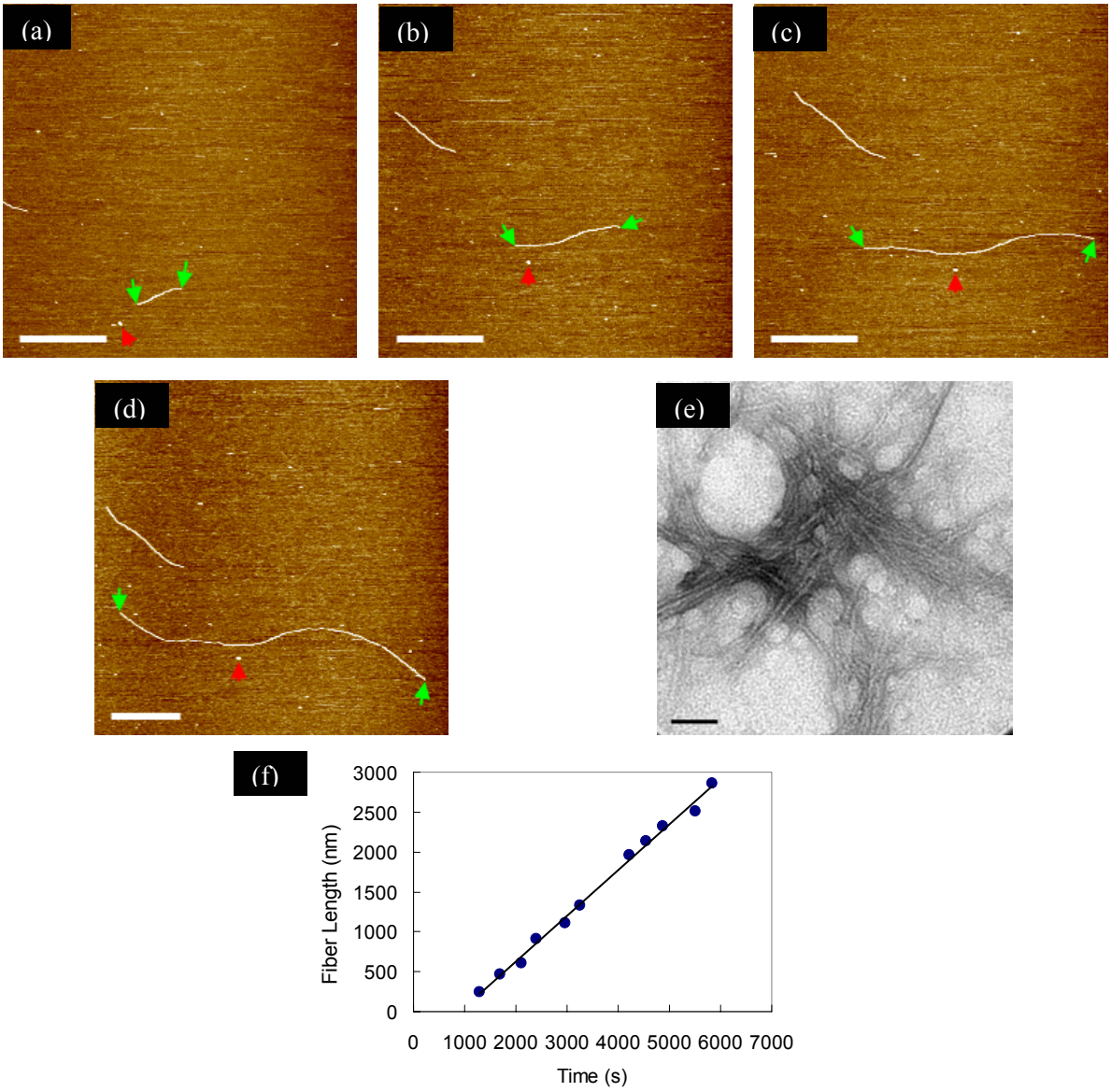

Figure 3.2 Time evolution of EAK16-II nanofiber growth on mica in pure water at (a) 1285 s, (b) 2107 s, (c) 3251 s, and (d) 4874 s. Time zero is when peptide solution is added into the AFM liquid cell. The scale bar represents 500 nm. The green arrows point at two ends of a fiber and the red arrow points at a small globule serving as a reference location on mica. (e) TEM image of EAK16-II self-assembled nanofibers. The scale bar represents 50 nm. (f) Variation of EAK16-II nanofiber length on mica with time

From the AFM images, the width and height of newly grown part of fibers on the surface are similar to those of the nanofiber "seeds", which are presumably formed in solution. This suggests that nanofibers formed in bulk solution and on the surface are similar. The width and height of these nanofibers are ~7 nm (after tip deconvolution) and ~1.5 nm, respectively. Since the fiber width measured by AFM is usually affected by the AFM tip,[21] the fiber width was also examined by TEM for comparison (Figure 3.2e). The TEM image shows that a single EAK16-II nanofiber has a width of ~5 nm, which compares well with the AFM results. The uniform fiber width and height may indicate a special arrangement of peptide molecules in the nanofiber and a possible fiber growth mechanism, as will be discussed later.

The uniform width of nanofibers enables precise analysis of the growth rate of an individual fiber length. Figure 3.1f shows a plot of the variation of the peptide fiber length (measured between two green arrows) with time. The length of the fiber monitored in Figures 3.1a-d increases linearly with the incubation time at a rate of 0.57 nm/s over the experiment. The lengths of other fibers also show a predominant linear growth although the growth rates vary from one nanofiber to another. This may be due to the (minute) differences in the fiber characteristics and/or the change of the local environments. It is also worth noting that the growth rate in our study may represent the initial growth state since the time period of *in-situ* AFM imaging is usually less than 2 h. In some cases, the active ends of a growing fiber can be terminated when they encounter other fibers or other small surface features (dots or globules in the AFM image). This will lead to the fiber network formation on the mica surface. These small surface features may be peptide globular aggregates or some other components in solution (e.g., impurities). The presence of some globules/small dots through out all AFM images is reasonable since EAK16-II has been shown to form both globules and fibers especially when the peptide concentration is very low.[27] However, unlike the nanofibers, these

globules and small dots do not grow on the surface. If one active end is blocked, the nanofiber can grow from the other end; such a growth pattern can be termed unidirectional fiber growth.

From the analysis of at least 50 independent, growing nanofibers with two active ends on mica, an average growth rate of 0.74 ± 0.40 nm/s is obtained. The observed linear growth of nanofibers might indicate that the fiber elongation occurs by the addition of peptide monomers to the active ends. To relate this growth rate to the number of monomers added, the width of the β-strand EAK16-II molecule was estimated using ChemSketch software (Toronto, Canada). This software determined the width to be 0.3-0.5 nm from the distance between the top-most and bottom-most atoms in the van der Waal-based structure (i.e., direction in and out of the plane of the structure shown in Figure 3.1). Thus the observed growth rate corresponds to the attachment of one or two monomers to the active ends of a nanofiber "seed" every second by presuming that the arrangement of peptides in the nanofiber follows a cross-β fashion (see Section 3.4.2).

The increase in the fiber length as a function of time can be described by the following linear relation, within our AFM observation period:

$$\begin{cases} t < \tau_0, l = l_0 \\ t \geq \tau_0, l = l_0 + (t - \tau_0)v \end{cases} \tag{3.2}$$

where l is the fiber length at time t; l_0 is the length of a nanofiber "seed"; τ_0 is the time when a nanofiber "seed" deposits on mica; v is the fiber growth rate on mica. Although each nanofiber has a different growth rate, one can use an average growth rate at the same solution condition to estimate the length of the nanofiber on the surface at a given time with these equations. One can also estimate the deposition time τ_0 of a "seed" by monitoring its growth rate. For instance, if the length of a nanofiber "seed" is known (e.g., l_0 ~54.6 nm in 12 μM peptide stock solution, obtained from the statistical analysis of nanofiber length in 10 mM HCl, see Section 3.3.2), τ_0 for "seed" deposition

(Figure 3.2) is estimated to be ~ 918 s for a fiber that has a growth rate of 0.57 nm/s (l = 2855.9 nm at t = 5833 s).

The assemblies in self-assembly systems are typically polydispersed with various sizes.[171-173] As will be shown in Section 3.3.3, we also observed this behavior for EAK16-II dissolved in solution. A manifestation of this polydispersity is the formation of large peptide aggregates as fiber clusters on the mica surface, as shown in Figure 3.3. Over time, many nanofibers begin to grow from these fiber clusters (Figure 3.3a-d). This suggests that the large aggregates consist of nanofiber bundles/entanglements; and the active ends of these fibers on the outer edges of the fiber clusters can continue to grow radially outward.

In order to investigate the rate at which these nanofibers grow from the clusters, the area covered by the fiber clusters on the mica substrate has been analyzed and plotted as a function of time in Figure 3.3e. It can be seen that the area covered by the fiber clusters also increases linearly with time. Since the nanofiber width remains uniform, the area increases linearly due to a linear increase of the nanofiber length. This suggests that the nanofiber growth from the fiber clusters is similar to that from the single nanofiber "seeds" except that each nanofiber in the former case grows at one end while it can grow at both ends in the latter. The equivalent growth rate of nanofiber from the fiber clusters can be obtained to be 3.21 nm/s through dividing the area of peptide aggregates by the width of nanofibers (15.6 nm prior to deconvolution). This value is almost 4 times higher than that of the average bidirectional growth rate of nanofibers (0.74 ± 0.40 nm/s). The much faster growth rate of nanofibers from the fiber clusters may be due to the peptide concentration being locally higher around the fiber clusters.

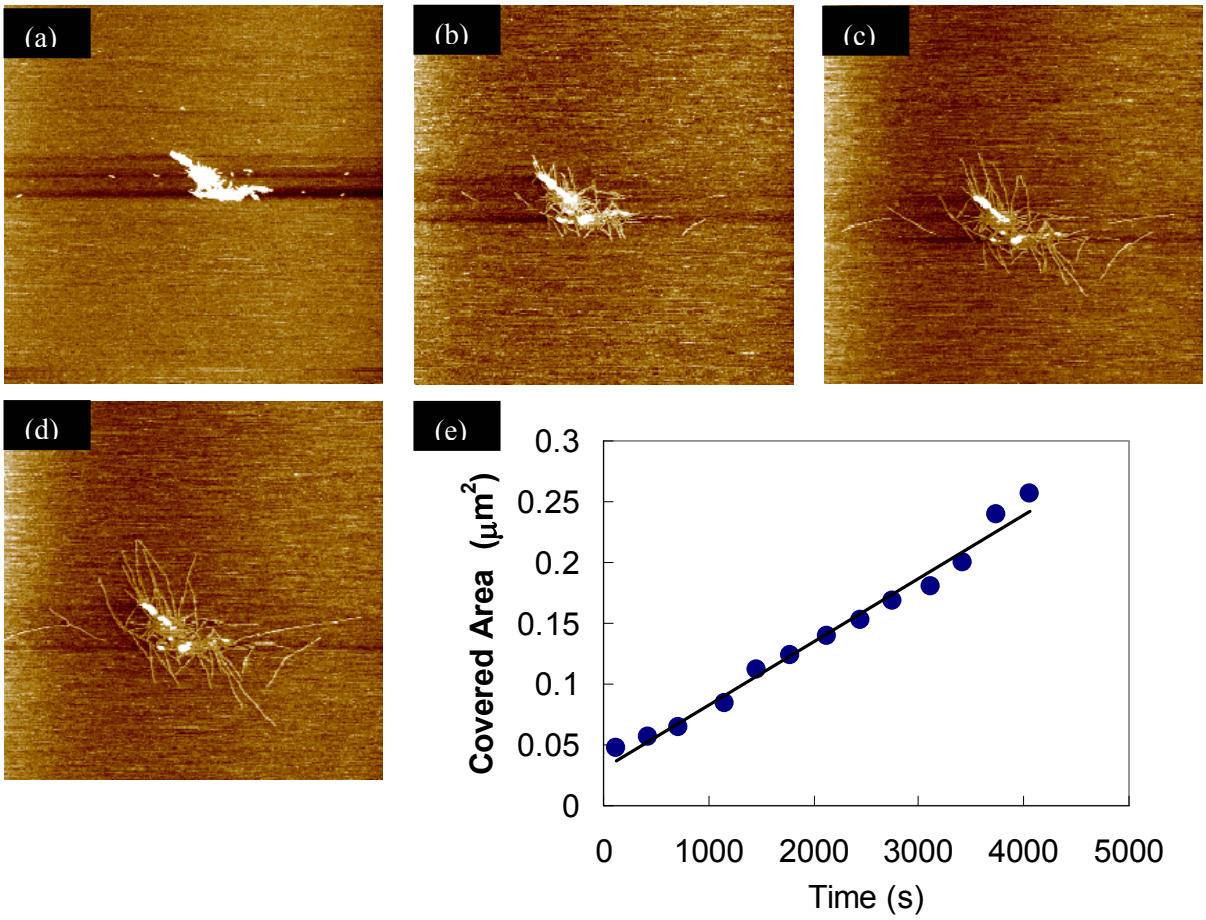

Figure 3.3 Time evolution of EAK16-II nanofiber growth from fiber clusters in pure water at (a) 120 s, (b) 1320 s, (c) 2520 s, and (d) 3120 s. The area covered by the clusters as a function of time is plotted in (e). Each *in-situ* AFM image corresponds to a scan area of 2000 nm × 2000 nm.

3.3.2 Effect of Solution pH on EAK16-II Nanofiber Growth on Mica

EAK16-II is ionic-complementary and contains four positively charged residues (K, pKa of 10.54) and four negatively charged residues (E, pKa of 4.05) at neutral pH (Figure 3.1).[174] Thus, it is expected that the charge status of this peptide can be tuned by adjusting the solution pH. In an acidic environment, the peptide becomes positively charged; whereas, it becomes negatively charged under basic conditions. A change in the peptide charge can affect its affinity to the negatively charged mica surface and the self-assembly behavior. Figures 3.4 (panels a-d) shows AFM images of the assembled

nanostructure formed after injecting a 100 μL EAK16-II stock solution into 500 μL of 1 mM HCl, to yield a final peptide concentration of 2 μM and a solution pH value of 3.4. Only 2 min after the injection, many short nanofibers ranging in length from ~30 to 100 nm are observed on the mica substrate (Figure3.4a). A slight increase in the nanofiber length is observed over time. After 17 min, the lengths range from ~110 to 490 nm (Figure 3.4d). A representative analysis of the variation of nanofiber length with time is plotted in Figure 3.4e. The nanofiber length increases linearly with time at a rate of 0.078 nm/s, which is ~7 times slower than that observed in pure water (Figure 3.2f). The pH (3.4) of this solution is lower than the pKa of the glutamic acid and results in the partial neutralization of the glutamic acid residues and leads to a net positive charge of the peptide molecule. Repulsive forces between positively charged molecules may explain the observed decrease in the fiber growth rate. On the other hand, the more positively charged peptide nanofibers and molecules should more easily adhere to the negatively charged mica substrate, resulting in a significant increase in the amount of adsorbed EAK16-II nanofibers on mica at the start of the incubation time (compare Figure 3.2a with Figure 3.4a).

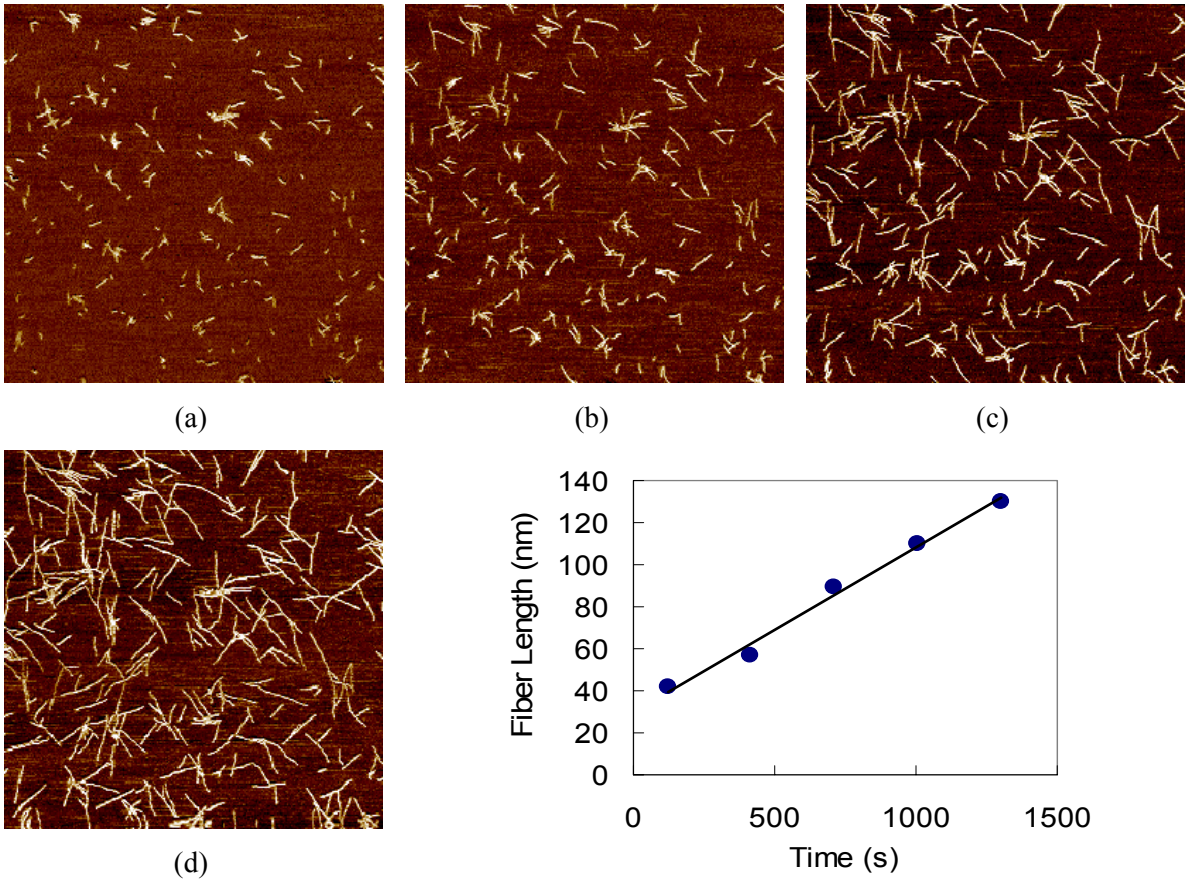

Figure 3.4 EAK16-II nanofiber growth on mica substrate in 1 mM HCl solution at (a) 120 s, (b) 420 s, (c) 720 s, and (d) 1020 s. The EAK16-II nanofiber length on mica in 1 mM HCl solution is plotted as a function of time in panel (e). Each *in-situ* AFM image corresponds to a scan area of 2000 nm × 2000 nm.

The assembly of EAK16-II in 10 mM HCl on mica was also investigated. Figure 3.5 (panels a and b) shows the *in-situ* AFM images of EAK16-II nanofibers on the mica surface in this solution having a measured pH of 2.2. Within about 2 min after the addition of the peptide solution to the HCl solution, short nanofibers are observed to densely cover the surface (Figure 3.5a). After ~19 min, no significant change in fiber length is observed (Figure 3.5b), indicating that very little growth of these

fibers occurs in such a solution. The very acidic environment could make the EAK16-II molecules positively charged enough to inhibit peptide-peptide and peptide-nanofiber assembly. On the other hand, this would tend to strengthen the affinity of the nanofibers to the negative mica surface relative to that observed in pure water and 1 mM HCl solution, and lead to a significant increase in the amount of EAK16-II adsorbed as nanofiber "seeds" on the surface (compare Figure 3.4a and Figure 3.5a).

The fact that very little growth of the nanofibers occurs after adsorption under highly acidic conditions may provide a method to characterize the dimensions of the nanofibers formed in the bulk solution. The nanofibers are stable upon injection into 10 mM HCl solution (see Section 3.3.3). Therefore, the size of nanofibers in Figure 3.5 (panels a and b) should reflect that of the nanofibers dissolved in the peptide stock solution. Figure 3.5c shows the length distribution of nanofibers shown in Figure 3.5a. The nanofibers in the peptide stock solution (12 μM) predominantly have lengths ranging from ~30 to 60 nm (average length of 54.6 ± 19.5 nm).

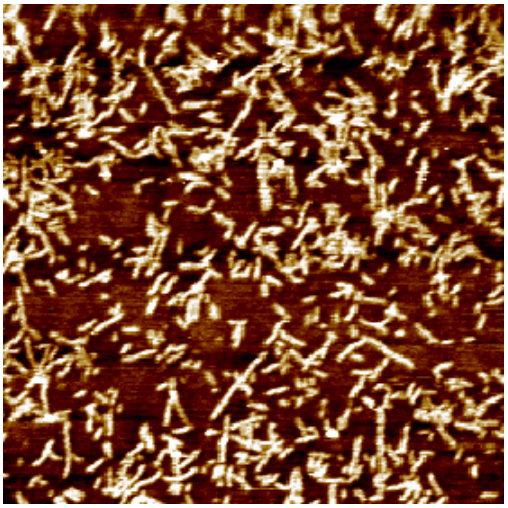

(a)

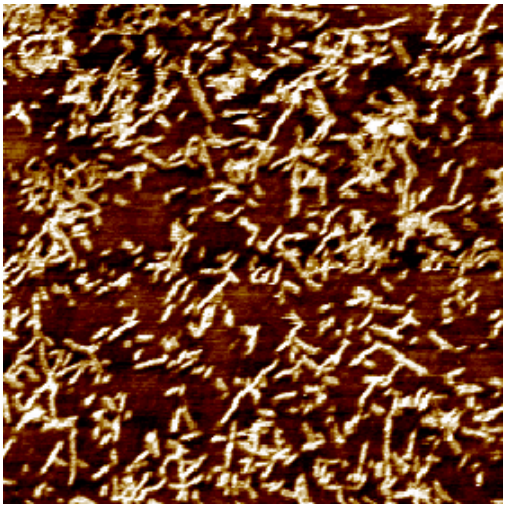

(b)

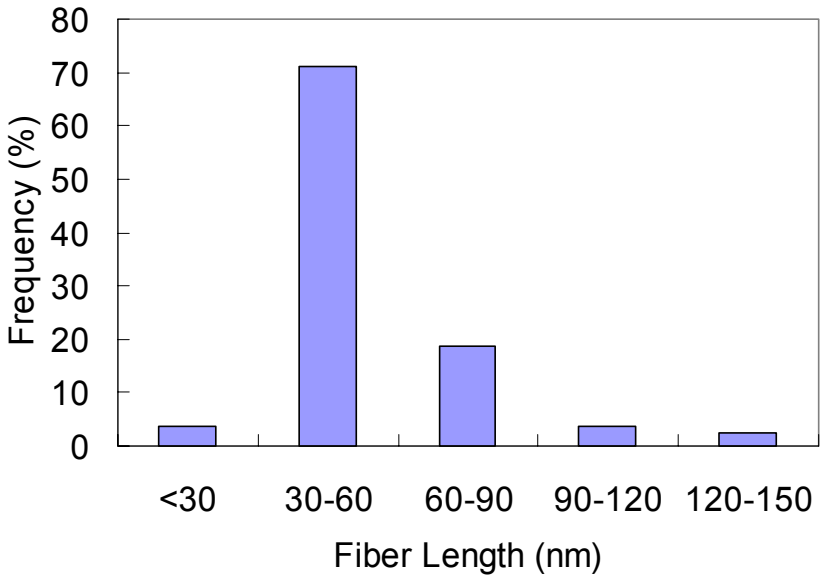

(c)

Figure 3.5 EAK16-II nanofiber growth on mica in 10 mM HCl solution at (a) 120 s and (b) 1140 s. The fiber length distribution of EAK16-II in 10 mM HCl is plotted in panel (c). Each *in-situ* AFM image corresponds to a scan area of 1000 nm × 1000 nm.

EAK16-II molecules can become negatively charged when the solution pH is greater than the pKa (10.54) of the lysine residues. Figures 3.6 (panels a-c) shows the *in-situ* AFM images of EAK16-II nanofibers growing on the mica substrate in 1 mM NaOH (final pH 9.9). Several short nanofibers with lengths ranging from ~20 to 55 nm are dispersed on the mica surface after 197 min incubation. The length of these fibers increases slightly with time (Figure 3.6b and c). A representative plot of the fiber length as a function of time is shown in Figure 5d. The fiber length again increases linearly with time, similar to that observed in the other solutions. However, the growth rate is only 0.014 nm/s, much smaller than that in pure water and 1 mM HCl. When the NaOH concentration is further increased to 10 mM (pH 11.5 after the injection of peptide stock solution), no nanofibers are observed

on the mica substrate in the first hour of incubation; after 1.5 hr incubation, only a few fibers are observed (Figure 3.7). These nanofiber "seeds" do not grow during the experimental period.

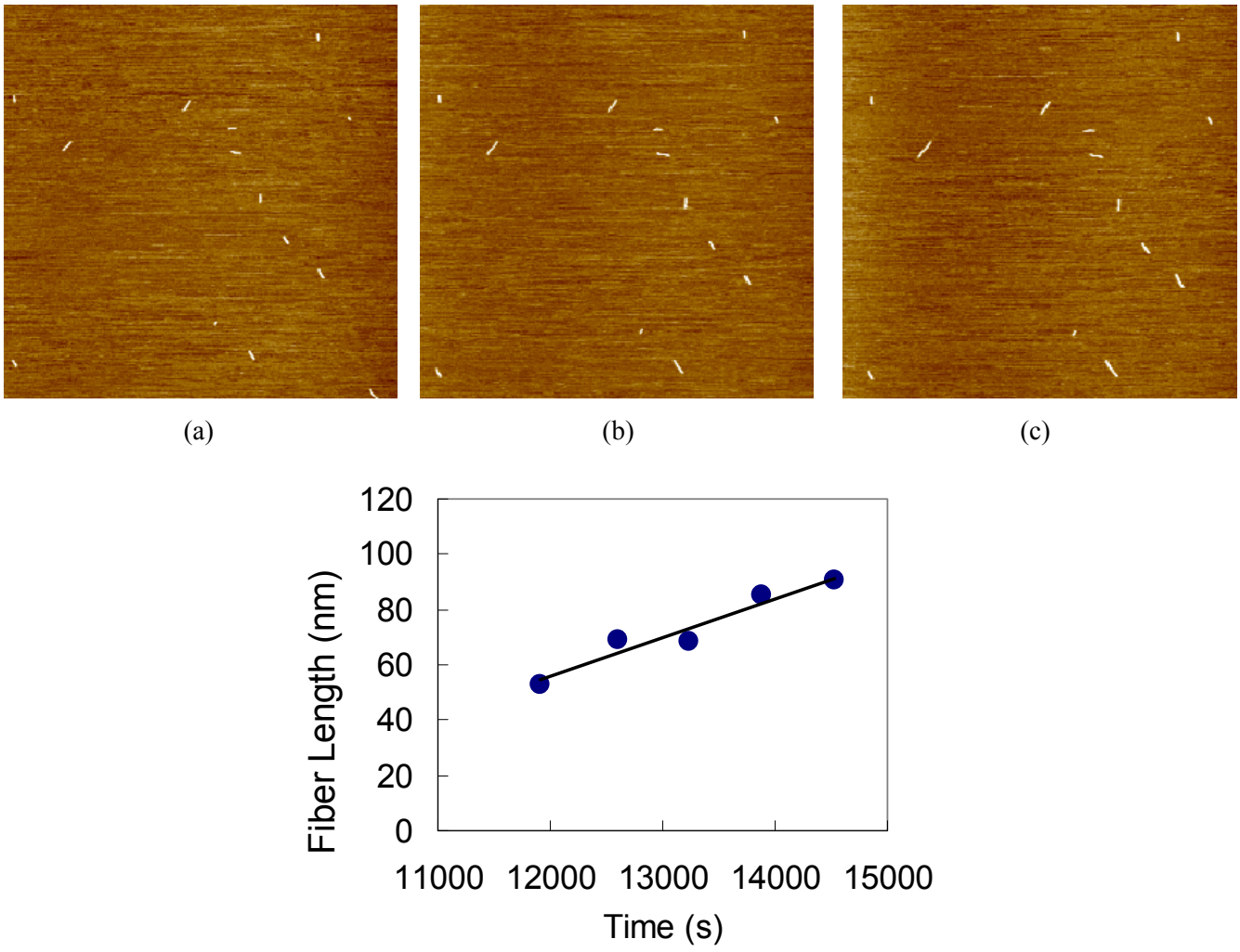

Figure 3.6 EAK16-II nanofiber growth on mica in 1 mM NaOH solution at (a) 11820 s, (b) 12420 s, and (c) 13020 s. The EAK16-II fiber length on mica in 1 mM NaOH solution is plotted as a function of time in panel (d). Each *in-situ* AFM image corresponds to a scan area of 2000 nm × 2000 nm.

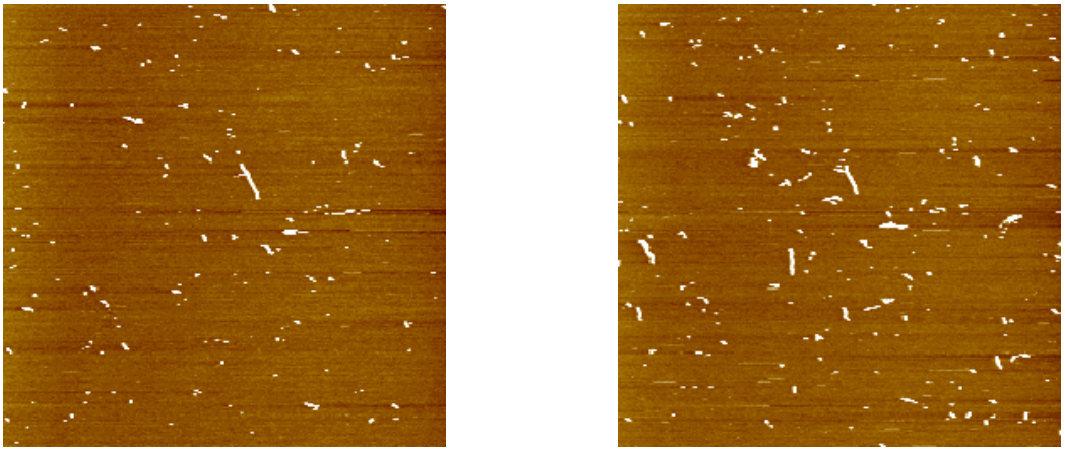

(a) (b)

Figure 3.7 EAK16-II nanofiber growth on mica in 10 mM NaOH solution at (a) 5400 s and (b) 6660 s. Each *in-situ* AFM image corresponds to a scan area of 2000 nm × 2000 nm.

A statistical analysis was conducted to obtain the distribution of EAK16-II nanofiber growth rates under the different solution conditions. The frequencies of the fiber growth rates within the following ranges are assigned to generate the histogram shown in Figure 3.8: very slow (<0.01 nm/s), slow (0.01-0.2 nm/s), intermediate (0.2-0.5 nm/s) and fast growth (>0.5 nm/s). In pure water solution, most nanofibers grow at a fast growth rate above 0.5 nm/s, while the peptide nanofibers grow predominantly at a slow speed of 0.01-0.2 nm/s in 1 mM HCl and even more slowly (<0.01 nm/s) in 1 mM NaOH solution. The average growth rates of the peptide nanofibers in the different environments are summarized in Table 3.1.

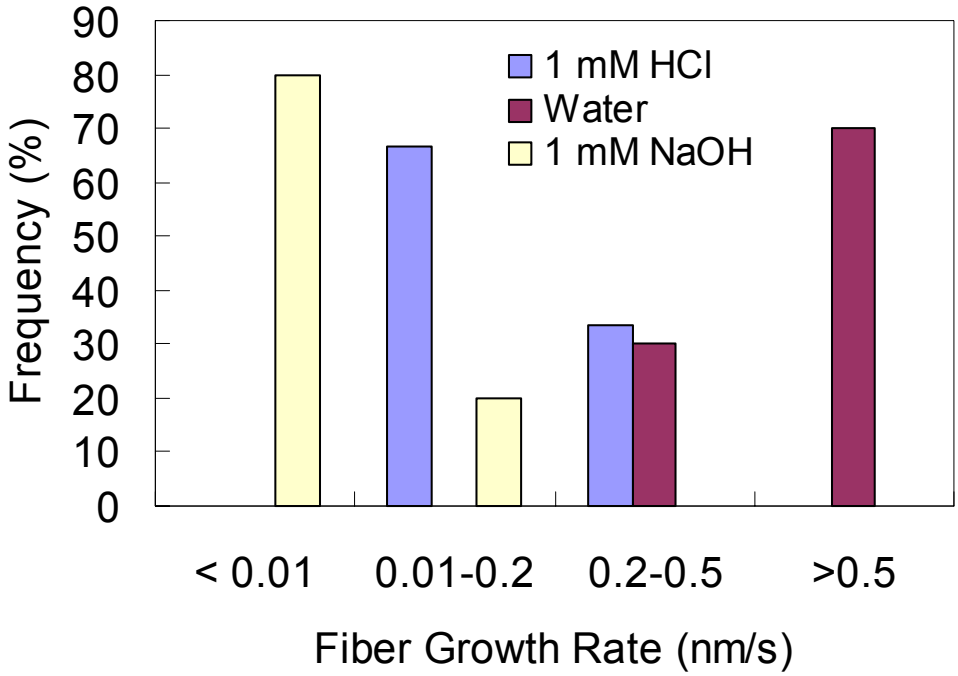

Figure 3.8 Histogram of EAK16-II nanofiber growth rates in pure water, 1mM HCl and 1 mM NaOH solutions.

Table 3.1 Effect of pH of 100 μl 12 μM EAK16-II obtained by preparation in pure water and then addition to various solutions on fibril growth on mica

Solution conditions	Final pH	Fibril deposited on mica	Fibril growth on mica	Average growth rate (nm/s)
EAK16-II in 10 mM HCl	2.2	Yes	No	0
EAK16-II in 1 mM HCl	3.4	Yes	Yes	0.17 ± 0.10
EAK16-II in pure water	5.0	Yes	Yes	0.74 ± 0.40
EAK16-II in 1 mM NaOH	9.9	Yes	Yes	0.008 ± 0.003
EAK16-II in 10 mM NaOH	11.5	Yes	No	0

3.3.3 Self-Assembly of EAK16-II in Bulk Solution

Dynamic Light Scattering (DLS) of EAK16-II in solution

To better analyze and understand the assembly behavior of EAK16-II on mica, the self-assembly process of EAK16-II in the bulk solutions was monitored using DLS. Figure 3.9a shows the time evolution of the scattered light intensity of 0.3 mM EAK16-II in pure water, 1 mM HCl, 10 mM HCl and 10 mM NaOH solutions. For the peptide dissolved in pure water, the scattered light intensity rapidly increases with time at the outset before leveling off and slowly approaching a plateau after ~300 h (12.5 days), indicating that the self-assembly of the peptide has reached steady-state. However, such an equilibrium state in peptide assembly will be changed when the peptide is in contact with the mica surface. Upon the adsorption on the surface, the active ends of the nanofiber "seeds" and fiber clusters can continue to grow. The dramatic change of EAK16-II assembly due to the presence of a surface indicates that the nanofiber growth on mica is indeed a surface-assisted phenomenon.

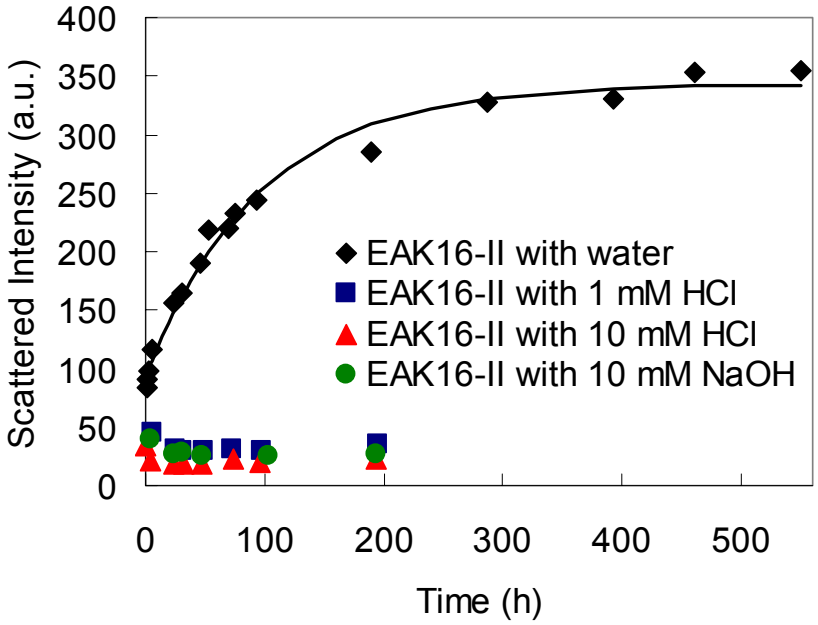
Scattered Intensity (a.u.)
400
350
300
250
200
150
100
50
0
0
100
200
300
400
500
Time (h)
EAK16-II with water
EAK16-II with 1 mM HCl
EAK16-II with 10 mM HCl
EAK16-II with 10 mM NaOH

(a)

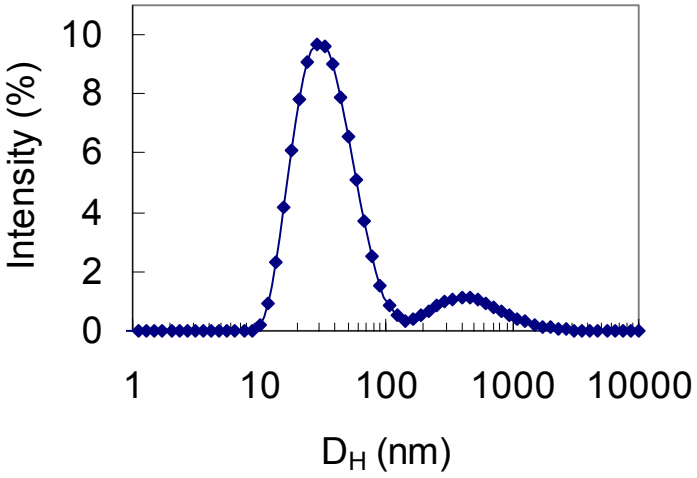
Intensity (%)
10
8
6
4
2
0
1
10
100
1000
10000
D_H (nm)

(b)

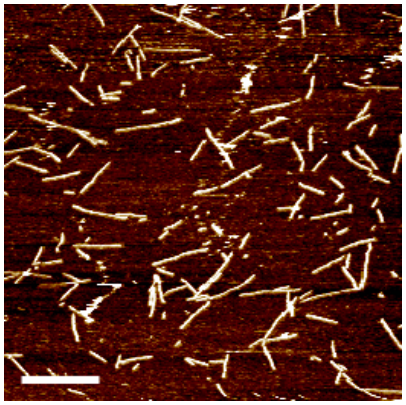

(c)

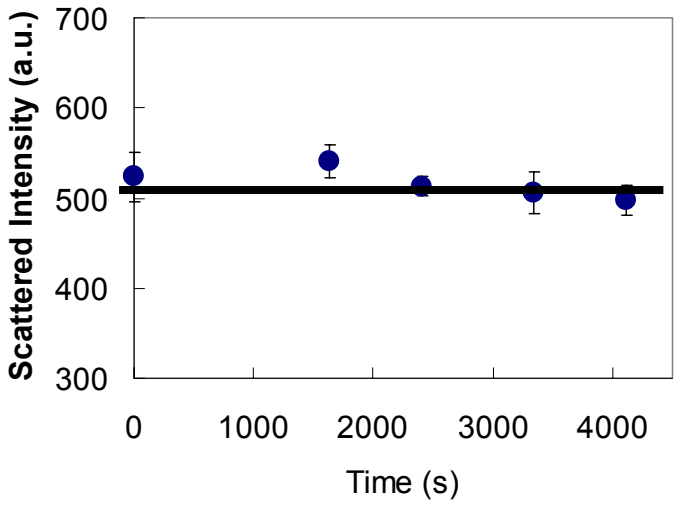

(d)

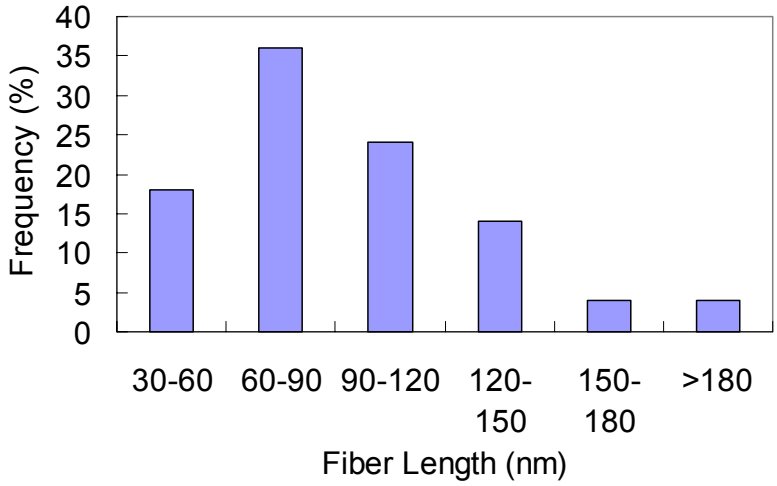

(e)

Figure 3.9 (a) Variation of scattering intensity of 0.3 mM EAK16-II in various aqueous solutions with time. The solid line represents a fitting curve to the equation (1). (b) Representative size distribution (based on the scattered intensity) of EAK16-II obtained in pure water after 55 h. (c) AFM image of 0.3 mM EAK16-II (prepared in pure water) after 550 h, obtained in 10 mM HCl solution. (d) Light intensity of EAK16-II aggregates in 10 mM HCl as a function of time. (e) The fiber length distribution obtained from AFM image in (c). Scale bar represents 200 nm.

On the other hand, the scattered light intensity shows no significant change with time in the case of the peptide dissolved in 1 mM HCl, 10 mM HCl and 10 mM NaOH solutions. This suggests that the peptide does not tend to self-assemble in these acidic and basic solutions. It has been reported that very acidic conditions can significantly slow the kinetics of the assembly of an amyloid peptide.[105] This may be due to the charge repulsion among peptide molecules under these solution conditions.

Figure 3.9b shows a representative hydrodynamic diameter distribution based on the light intensity of the peptide in pure water after 55 h incubation. This shows two distinct size populations, one centered at ~33 nm and the other at 320 nm. The first population may correspond to the peptide nanofibers, while the second one may be associated with the fiber clusters. The presence of these two size populations in solution is consistent with the *in-situ* AFM observation (Figures 3.2 and 3.3) of the co-existence of nanofibers and large fiber aggregates.

To compare the dimensions of the nanofibers observed by AFM with those obtained by DLS, AFM images of the aged peptide (0.3 mM EAK16-II in pure water after 550 h, having reached equilibrium state) were taken in 10 mM HCl (Figure 3.9c). The nanofibers observed on mica are taken to be those that originally formed in pure water for the following reasons. As shown above, EAK16-II nanofibers do not further grow on the mica substrate under very acidic solution conditions (e.g., Figure 3.5). Also, nanofibers formed in pure water have been found to remain stable for at least 1 hr after their addition to a 10 mM HCl solution, as indicated in Figure 3.9d which shows very little change in the scattered light intensity of this solution over this period. This assures a new method using AFM to characterize the peptide assemblies in bulk solution, in addition to the well-known Cryo-TEM technique, i.e., AFM imaging of peptide assemblies in an acidic solution.[25,109,175]

Images of 50 individual nanofibers obtained by AFM were analyzed to generate a distribution of their lengths (Figure 3.9e). This analysis shows that all nanofibers have lengths greater than 30 nm and the highest frequency is observed for lengths between 60 and 90 nm. The average nanofiber length is calculated to be 93.4 ± 37.8 nm. Based on the assumption that the nanofibers have a cylindrical shape, their length can be converted to a hydrodynamic diameter using the following equation:[105]

$$D_h = L \times (\sqrt{1-x^2} / \ln \frac{1+\sqrt{1-x^2}}{x}) \qquad (3.3)$$

where $x = \frac{d}{L}[1 + \frac{0.37 \times (L-d)}{L}]$, L is the fiber length and d is the fiber width. The use of this equation yields a hydrodynamic diameter of 31 ± 8 nm (n=50), which is very close to that obtained from the DLS experiment in water (~33 nm, Figure 3.9b). It should be noted that this estimation is approximate since the assumption that the nanofiber has a cylindrical shape may not be entirely correct. In fact, the EAK16-II nanofibers are ribbon-like, with their heights (~1-2 nm) being much smaller than their widths (~7 nm). In addition, these ribbon-like nanofibers may not be as rigid as a cylinder. However, no simple equation is available to correlate the hydrodynamic diameter with such a structure. Usually, a more complicated approach or analysis is required for fiber-like structures.[176,177] Regardless, this rough estimation shows a reasonable correlation between the AFM observation and the DLS measurement.

Zeta potential of EAK16-II

Zeta potential measurements were made to determine the surface charge of EAK16-II assemblies in solution. The net surface charge of particles is an important parameter to predict their tendency to aggregate and adsorb onto surfaces. Theoretically, the larger the zeta potential, either positive or

negative, of a particle, the more stable the resulting suspension will tend to be (i.e., no aggregation). Figure 3.10a shows zeta potentials of 0.18 mM EAK16-II solution as a function of solution pH. From this analysis, an isoelectric point (pI) for the EAK16-II system is found to be 6.3, which is comparable to the calculated pI value of 6.7 for EAK16-II molecule.[50] Note that the pI being measured in these experiments is not for EAK16-II monomers alone, but rather for a mixture of monomers and aggregates that exist in these EAK16-II solutions. Figure 3.10 (panels b-d) shows the AFM images of 2 μM EAK16-II obtained in 1 mM HCl (final pH 3.4), pure water (final pH 5.0) and 1 mM NaOH (final pH 9.9) after 30 min incubation. Densely dispersed and shorter nanofibers are observed at lower pH (1 mM HCl), while sparsely dispersed and longer nanofibers are observed at pH 5.0 close to the pI of the EAK16-II system. At pH 9.9, which is above the pI, no fibers are observed over the first 30 min.

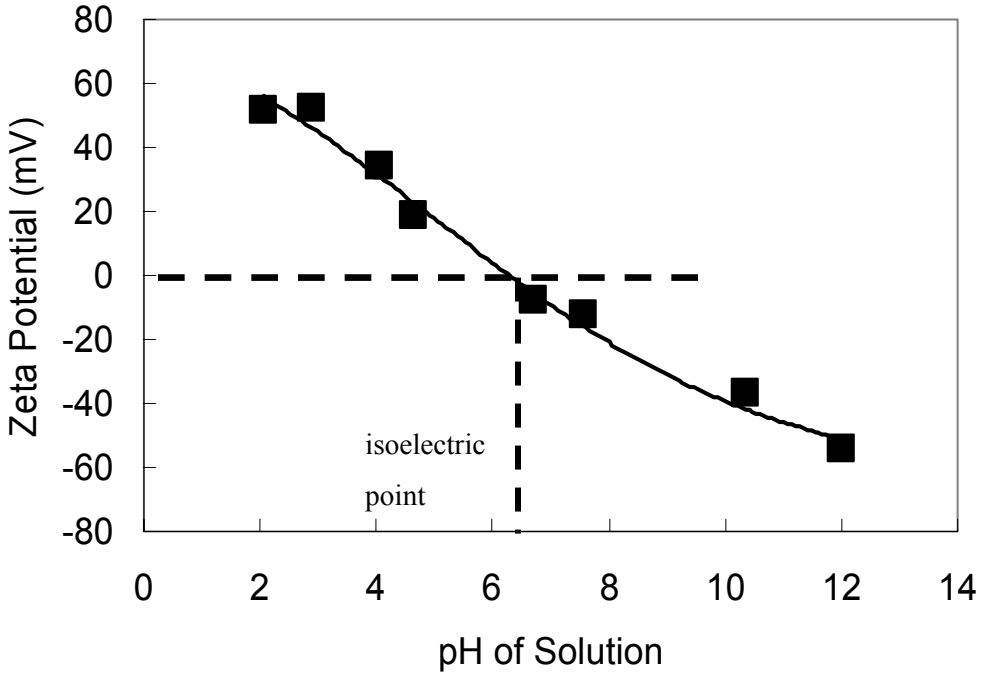

(a)

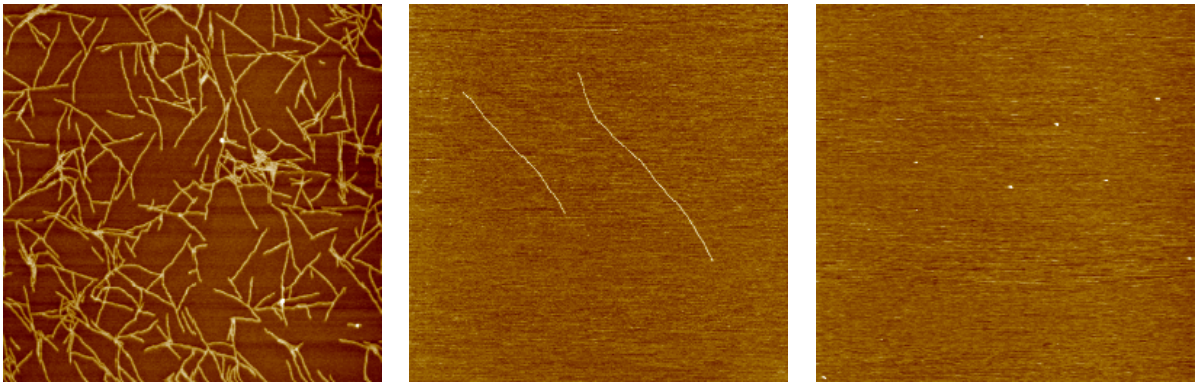

(b) 1 mM HCl
pH 3.4

(c) Pure water
pH 5.0

(d) 1 mM NaOH
pH 9.9

Figure 3.10 (a) Zeta potential of EAK16-II as a function of pH. The standard deviation of zeta potentials are less than 4 mV. (b)-(d) AFM images of EAK16-II on mica in various solutions after 30 min. Scan area is 2000 nm x 2000 nm.

Comparing the zeta potential results with the AFM observations, it can be clearly seen that the charge status of the EAK16-II system is crucial to the assembly of EAK16-II on mica. At low pH, the peptides/nanofibers are positively charged (very positive zeta potential) and so have a strong affinity for the negatively charged mica surface, leading to a dense dispersion on the surface (Figure 3.10b). However, the electrostatic repulsion between peptides tends to retard fiber growth (Figures 3.4 and 3.5, Table 3.1) and yield shorter lengths. In pure water, on the other hand, the attraction between the peptide and the mica surface is moderate, but less repulsion between peptide molecules/fibers results due to a close to zero zeta potential. Thus, on the same time scale, fewer but longer peptide nanofibers than in 1 mM HCl are observed on mica (Figure 3.10c). The absence of nanofibers in 1 mM NaOH (Figure 3.10d) is likely due to the large electrostatic repulsion between the negatively charged peptide and the mica surface. Under this condition, nanofibers appear only after a long incubation time (197 min) and the fiber growth rate is very low (Figure 3.6 and Table 3.1)

3.4 Discussions

3.4.1 Control of Nanofiber Growth on Mica by Adjusting Solution pH

Surface-assisted assembly of EAK16-II on mica appears to be governed by two principal interactions: 1) peptide-surface interaction that enables nanofiber "seeds" and fiber clusters to adsorb onto mica and serve as "nuclei"; 2) peptide-peptide interaction that enables elongation of the nanofiber "nuclei". A simple way to control this process is to modulate the two interactions by adjusting the solution pH.

Peptide-surface interaction

At different pHs, the amount of nanofibers deposited on the mica surface at the same time scale can be significantly altered and follows the order: 10 mM HCl > 1 mM HCl > pure water > 1 mM NaOH > 10 mM NaOH. This is because the charge status of the peptide monomers and aggregates can be changed according to different solution pHs. By adjusting the solution pH, one could control the

adsorption of the nanofiber "seeds" to mica, which will determine the density of growing nanofibers on the surface.

The adsorption of the nanofiber "seeds" on a surface is a prerequisite for surface-assisted nanofiber growth. The deposited nanofiber "seeds" serve as the nuclei for subsequent fiber growth. A high affinity for a surface will concentrate peptides at the surface and facilitate peptide-peptide association. This also explains why nanofiber growth of EAK16-II on mica is possible at a peptide concentration of 2 μM, much lower than its critical aggregation concentration (CAC) of ~60 μM.[21] The importance of the surface charge on the adsorption of peptides and proteins onto surfaces of mica and micelles has been demonstrated by M. Zhu *et al.*[160] and M. Necula *et al.*[161] It is also worth noting that the surface restricts the mobility of the adsorbed nanofibers and may influence their growth mode.

Peptide-peptide interaction

While the peptide-surface interaction initiates surface-assisted assembly, the growth of deposited nanofiber "seeds" is mainly controlled by peptide-peptide interaction. The growth rate of EAK16-II nanofibers on mica in various solutions follows the order: pure water > 1 mM HCl > 1 mM NaOH > 10 mM HCl ≈ 10 mM NaOH ≈ 0 (Table 3.1 and Figure 3.8). This is because the peptide-peptide association can be significantly affected by the electrostatic repulsion. The fastest nanofiber growth occurs in pure water, where the electrostatic repulsion is minimum. The electrostatic repulsion increases in acidic or basic solutions, which resists the peptide-peptide association, leading to slower or no fiber growth. By adjusting the solution pH, one could control the growth of the nanofiber "seeds", which further determines the length of the growing nanofibers at a given time period.

Overall, the surface-assisted nanofiber growth of EAK16-II can be controlled by adjusting the solution pH to have the desired amount and dimension (long or short) of the nanofibers. The amount

of nanofibers deposited on the surface can be regulated at the step of "nucleation" (i.e., the adsorption of the nanofiber "seeds" to mica); the strength of the electrostatic repulsion between peptide molecules will determine the growth rate of the nanofibers and further control the length of nanofibers at a specific time. The controllable nanofiber growth on a surface may be beneficial to fabricate many peptide-based functional nanostructures.

3.4.2 Proposed Model of EAK16-II Nanofiber Growth on Mica

All AFM images have shown that the nanofibers formed on mica have a uniform width of ~7 nm and a height ranging from ~1 to 2 nm. Our previous results have shown that EAK16-II predominantly adopts a β-sheet secondary structure in aqueous solution.[26] The height of a single β-sheet of EAK16-II can be estimated to be ~1 nm. Comparison of this value with the observed nanofiber height of EAK16-II (~1-2 nm) suggests that the EAK16-II nanofibers observed on mica are probably made of one or two β-sheet layers. The width of nanofibers of ~7 nm from the AFM results is very close to the length of an EAK16-II molecule in β-strand conformation (~5.9 nm). Thus, we may propose that EAK16-II adopts a cross-β sheet arrangement when forming nanofibers (i.e., the peptide β-strands are arranged perpendicularly to the direction of fiber elongation).

Accordingly, a simple model of EAK16-II nanofiber growth on the mica surface may be proposed in Figure 3.11. EAK16-II nanofiber "seeds" first adsorb on mica. These nanofibers are probably made of single or double layers of β-sheets. The two active ends of the nanofiber can further associate with peptide monomers or oligomers, and continue to grow. Peptide-peptide interactions may involve hydrogen bonding between backbones, electrostatic attraction between charged residues and hydrophobic interaction between alanine (A) residues. When a peptide monomer interacts with a β-strand at one active end, the electrostatic interaction, due to the ionic complementarity, may allow it to shift in the direction perpendicular to the fiber length, as shown in Figure 3.11. This may explain

why nanofibers are sometimes observed to have a wavy shape along its length. This model may also explain why the nanofibers have a consistent width. However, whether these β-sheets preferentially adopt an anti-parallel or parallel fashion is still unclear since both arrangements can occur in an ionic-complementary peptide. Further experiments, such as solid state NMR and X-ray fiber diffraction, are required to distinguish these two arrangements.

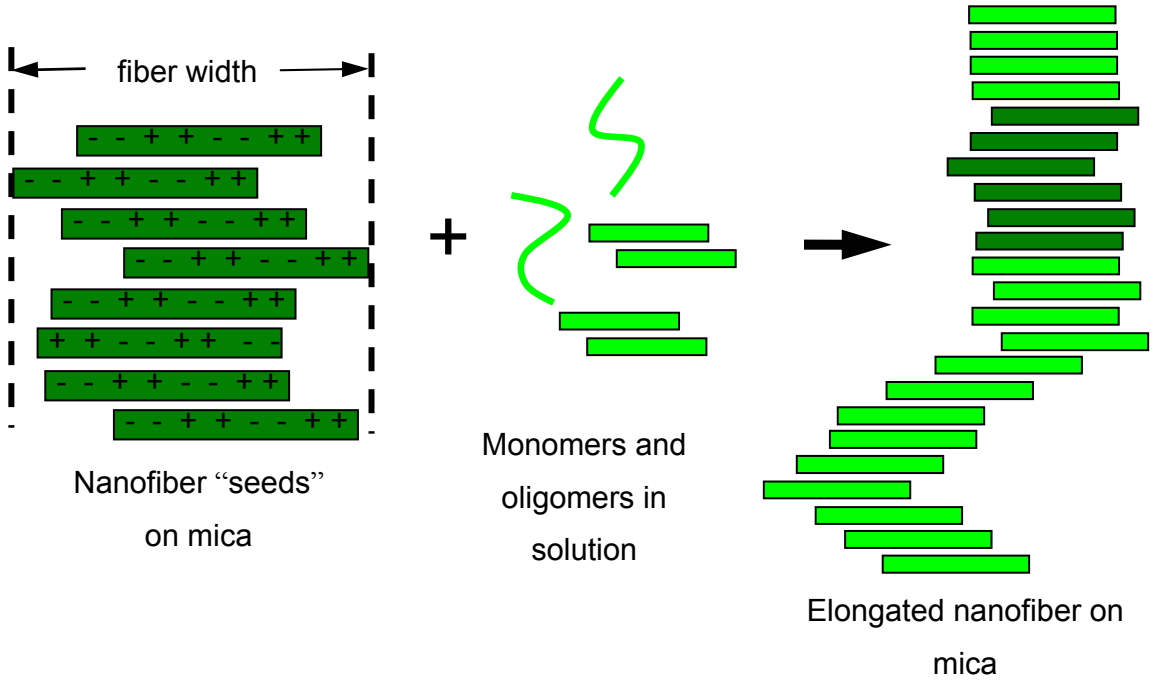

Figure 3.11 Proposed model of EAK16-II nanofiber growth on mica.

3.4.3 Comparison of EAK16-II Assembly with Amyloid Fibrillization

The surface-assisted assembly of EAK16-II has many similarities to amyloid fibrillization, which is a main characteristic of many conformational diseases.[9,10] Surface-assisted EAK16-II nanofiber growth seems to follow a nucleation and growth mechanism. The deposited nanofiber seeds or fiber clusters can serve as nuclei on the hydrophilic, negatively charged mica surface for surface-assisted nanofiber growth. This mechanism is similar to that of protein/peptide fibrillogenesis in bulk solution.[105,178-185]

The growth of the deposited nanofiber "seeds" is bidirectional (i.e., from two active ends); such a growth pattern has been found in the fibrillization of synthetic human amylin,[186] β-amyloid[130] and prion protein either in solution or on a surface.[12,187] The nanofiber growth from the fiber clusters is radial and unidirectional, which is also similar to amyloid fibrillization on mica and glass substrates.[130,159,160] The kinetics of EAK16-II assembly is significantly increased upon adsorption on a negatively charged mica surface at a very low peptide concentration (2 μM). This is much the same as the finding that anionic micelles can greatly accelerate fibrillization of recombinant α-synuclein at low micromolar concentrations.[161] These similar characteristics between EAK16-II and other disease-related peptides/proteins suggest that a simple model peptide can be used to study the surface effect of the more complicated amyloid fibrillization.

This study has demonstrated that the assembly of EAK16-II on the negatively charged mica surface can be controlled by modulating the peptide surface charges. The repulsion between negatively charge peptides and mica inhibits their adsorption and their growth. This may provide means to control amyloid fibrillization on negatively charged cell membranes. It has been found that the binding of amyloid-β peptides to cell membranes facilitates amyloid fibrillization, which in turn disturbs the structure and function of the membranes (e.g., membrane fluidity and ion channels).[38,39] If the amyloid peptides/proteins becomes very negatively charged, their ability to bind to the cell membrane and surface-induced fibrillization may be significantly reduced. This could be achieved by introducing negatively charged molecules (e.g., polyglutamates) grafted with a binding motif to these amyloid peptides/proteins.

3.5 Conclusions

The growth of EAK16-II nanofibers on a mica surface has been observed via *in-situ* AFM. The growth kinetics of single nanofibers can be directly quantified. In pure water, the average nanofiber

growth rate is 0.74 ± 0.40 nm/s. The nanofiber growth appears to follow a nucleation and growth mechanism that involves the adsorption of nanofiber "seeds" or fiber clusters formed in stock solution, to serve as nuclei, and fiber elongation at the active ends of these nuclei. Dynamic light scattering experiments indicate that the nanofiber growth is a surface-assisted phenomenon; nanofibers that no longer grow in solution can start to grow once they adsorb onto the surface. Such surface-assisted nanofiber growth can be controlled by adjusting the solution pH to regulate both nucleation and growth steps. The amount of nanofiber "seeds" that adsorb on mica decreases as the solution pH increases. The growth rate of EAK16-II nanofibers in different solutions follows the order: pure water > 1 mM HCl > 1mM NaOH > 10 mM HCl ≈10 mM NaOH ≈ 0. This controllable nanofiber growth may be beneficial to the construction of functional, supramolecular structures. We have demonstrated that, at very acidic condition (10 mM HCl), *in situ* AFM is capable of directly "seeing" the assemblies formed in the bulk solution. The surface-assisted EAK16-II assembly has many similar characteristics to amyloid fibrillization on surfaces. This study provides a model to help understand and control surface-assisted fibrillization of disease-related peptides/proteins.

Chapter 4*
Modification of Hydrophilic and Hydrophobic Surfaces Using an Ionic-Complementary Peptide

4.1 Introduction

Surface modification plays an important role in materials science and interfacial engineering and has been widely used to improve the compatibility of given materials with other materials or environments. For example, biocompatibility is an important issue for materials used for transplantation and bioanalytic applications.[188,189] For such a purpose, the material surface usually has to be physically/chemically modified to improve the compatibility with the human body.[190,191] Surface modification can also impart additional functionalities to the materials; in particular, smart drug delivery vehicles have benefited from surface modification for cellular targeting and membrane penetration.[192-194]

Recent advances in surface modification have had a significant impact on the development of microfluidic bioanalysis,[195] immobilization of enzymes and DNA for the purpose of developing biocompatible biosensors[196] and the control of cell adhesion in tissue engineering and biomedical applications.[197,198] One achievement is the conjugation of both polyethylene glycol (PEG) and tri-peptide Arg-Gly-Asp (RGD) on polymethyl methacrylate (PMMA) to control cell adhesion and growth for keratoprosthesis applications.[199] Another is the surface modification of a conductive gold surface with a protein fragment containing a cell adhesion domain in order to grow and pattern neurons for potential use in multi-electrode array recording technology.[200] Furthermore, the use of a dipeptide Phe-Phe (FF) to modify graphite and gold electrodes has improved the electrochemical reactivity of these surfaces to detect hydrogen peroxide and NADH.[48,49]

*This chapter is based on a paper "H. Yang, S.Y. Fung, M. Pritzker and P. Chen, Modification of Hydrophilic and Hydrophobic Surfaces Using Ionic-Complementary Peptide, PLoS ONE 2007" (submitted)

Among the many emerging materials, self-assembling peptides show promise for use in surface modification. In this category is a special class of ionic-complementary peptides, whose sequences were derived from a fragment of a Z-DNA binding protein in yeast.[86] They have unique sequences with alternating hydrophobic and hydrophilic residues, imparting them with amphiphilic characteristics. They can self-assemble into β-sheet-rich nanofibrils and macroscopic membranes. These β-sheets were found to be very stable over a wide range of pHs (1.5-11), at high temperature (up to 90°C) and in the presence of denaturation agents (e.g., 0.1% SDS and 8 M urea) and some proteases.[50,86] These peptides have been studied for a wide number of applications, ranging from tissue scaffolding, biological surface patterning to drug delivery.[32,36,55,86,96,136,147,201,202] A special design of these peptides can form a self-assembled monolayer (SAM) on gold surfaces and facilitate cell patterning for purposes of investigating cell communications and signal transduction.[203]

The ionic-complementary peptides have several features that are advantageous for modifying surfaces. First, their amphiphilic nature allows them to interact with both hydrophobic and hydrophilic surfaces. Second, the charge state of the peptide residues can be adjusted by the solution pH, which can affect the interaction of the peptide with the surface and the peptide assembly on the surface. Third, the peptide sequence can be designed and synthesized to incorporate certain amino acids with desired functions, such as RGD for cell attachment[199] and residues containing COOH[204] and NH_2[205] groups for protein immobilization. Fourth, the self-assembled peptide nanostructures exhibit excellent chemical stability[50] with good *in vitro* and *in vivo* biocompatibility.[86,97,136,202] With these promising features, self-assembling peptide modified surfaces have great potential for use in (bio)molecular sensing and tissue engineering.

In this study, we demonstrate how a model ionic-complementary peptide EAK16-II assembles on a hydrophilic (mica) and a hydrophobic (HOPG) surface. This peptide has been extensively studied in our group.[21,26,27] We take this research one step further by examining how the assembly of

EAK16-II modifies mica and HOPG surfaces. The operation of AFM in liquid is the primary method used to observe the peptide assembly on the model surfaces. The hydrophobicity of the peptide-modified surfaces is characterized by water contact angle measurements. The stability of the modified surfaces in acidic and alkaline solutions is evaluated in terms of the surface coverage changes determined from AFM image analysis. The information obtained in this study is to provide a more complete picture of the peptide assembly on both hydrophilic and hydrophobic surfaces and help the fabrication of peptide-modified electrodes for (bio)molecular sensing and biocompatible templates for tissue engineering.

4.2 Materials and Methods

4.2.1 Materials

The ionic-complementary peptide EAK16-II ($C_{70}H_{121}N_{21}O_{25}$, molecular weight 1657 g/mol) has the sequence AEAEAKAKAEAEAKAK (Figure 4.1) where A corresponds to alanine, E to glutamic acid and K to lysine. At neutral pH, A is neutral, while E and K are negatively and positively charged, respectively. This peptide was purchased from CanPeptide Inc. (Quebec, Canada) with a purity >95% (purified by reverse-phase high-performance liquid chromatography). The N-terminus and C-terminus of the peptide were protected by acetyl and amino groups, respectively.

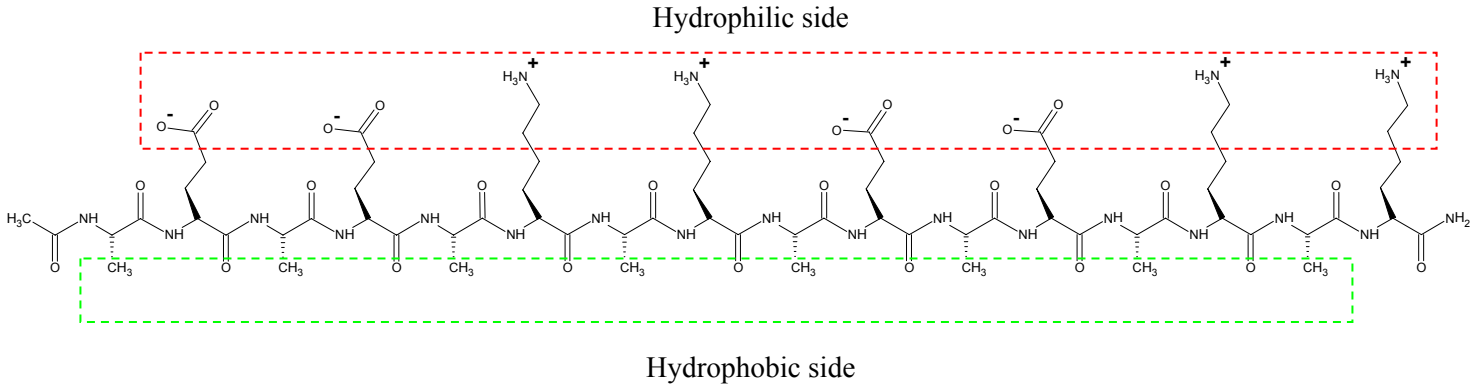

Figure 4.1 Schematic diagram of EAK16-II structure. The red portion shows the hydrophilic side of the peptide and the green portion shows the hydrophobic side of the peptide.

EAK16-II peptide stock solutions were prepared in pure water (18 MΩ; Millipore Milli-Q system) at concentrations of 12 μM and 29 μM. All peptide stock solutions were stored at 4 °C before use. Reagent grade sodium hydroxide with purity of >99% and hydrochloric acid (36.5-38%) were obtained from BDH Chemicals Ltd. (Toronto, Canada) and Fisher Scientific (Nepean, Canada), respectively.

Grade V-4 muscovite mica ($KAl_2(AlSi_3)O_{10}(OH)_2$) and highly ordered pyrolytic graphite (HOPG, ZYB grade) were obtained from SPI Supplies (West Chester, PA, USA). Mica is negatively charged even at pH 3[165] and serves as a model hydrophilic surface, whereas HOPG serves as a model hydrophobic surface. Mica and HOPG were first fixed on glass slides using double-sided tape. An adhesive tape was then used to remove the outer layer of mica and HOPG surfaces prior to contact with the EAK16-II solutions.

4.2.2 Preparation of EAK16-II Modified Surfaces

Appropriate amounts of the 12 μM or 29 μM EAK16-II stock solution were diluted to the desired concentrations (2 – 12 μM) for the experiments to measure the peptide surface coverage on mica and HOPG surfaces. The diluted EAK16-II solutions were added to a liquid cell with a freshly cleaved mica or HOPG surface at the bottom and immobilized for a time period varying from 1 min to 160 min to allow the peptide to adhere and assemble on the surface. The EAK16-II-treated surface was then thoroughly rinsed with pure water three times. To avoid any drying effects on the adherence and assembly of the peptide on the surface, AFM imaging was carried out in pure water.

For contact angle measurements, 30 μl and 300 μl of the 29 μM EAK16-II stock solution were placed on a freshly cleaved mica or HOPG surface and allowed to contact each surface for 2 hours under a Petri-dish cover to reduce contamination. Each modified surface was then thoroughly rinsed with pure water three times to remove unattached peptides and air-dried prior to measuring the contact angle of a water drop on the surface.

To study the stability of EAK16-II-modified surfaces under different environments, the following procedure was adopted. First, a freshly cleaved mica or HOPG substrate was placed on an AFM sample plate on which an AFM liquid cell was mounted. Then, 500 μl of 4 μM EAK16-II solution was poured into the liquid cell when a mica substrate was used, while 500 μl of a 6 μM EAK16-II solution was contacted with HOPG substrates. These samples were then incubated for ~10 hours to ensure a high degree of EAK16-II surface coverage. During this incubation period, all samples were sealed in an environmental chamber saturated with pure water to avoid evaporation of peptide solution. These EAK16-II treated surfaces were then rinsed with pure water three times to remove unattached peptides. The stability of these EAK16-II-modified surfaces was assessed through

AFM images to analyze the changes in peptide surface coverage after exposure to different environments: water, 10 mM HCl and 10 mM NaOH.

4.2.3 AFM Imaging in Liquid

The AFM imaging in liquid was performed on a PicoScan™ AFM (Molecular Imaging, Phoenix, AZ) in 500 μl of pure water, a 10 mM HCl or 10 mM NaOH solution (last two solutions were used to assess the stability of EAK16-II-modified surfaces). A scanner with a maximum scan area of 6 × 6 μm^2 was used. Silicon nitride cantilevers with a nominal spring constant of 0.58 N/m (DNP-S, Digital Instruments, Santa Barbara, CA) and a typical tip radius of 10 nm were used for tapping mode operation. For the best imaging quality, the tapping frequency was typically set between 16 kHz and 18 kHz and the scan rates controlled between 0.8 and 1 Hz. To minimize interference of the AFM tip on peptide nanofibers, the amplitude of the tip displacement between each tap was controlled so that the tapping would not break any nanofibers. All images were obtained in an environmentally-controlled chamber at room temperature to avoid evaporation of the solution. All AFM images were obtained at a resolution of 256 × 256 pixels.

4.2.4 Quantitative Analysis of AFM Images

The width and height of EAK16-II nanofibers on mica and HOPG surfaces were determined using the cross-sectional analysis tool of the PicoScan software. The peptide fiber widths reported herein were obtained using the deconvolution method reported by Fung *et al.*[21] The surface coverage of EAK16-II on mica and HOPG was analyzed with Image J software (http://rsb.info.nih.gov/ij/). For each sample, at least five images (6 μm × 6 μm) at different locations were analyzed to obtain the average surface coverage of the peptide assemblies. The AFM tip size effect was not taken into account in estimating the surface coverage of the EAK16-II nanofibers on the mica and HOPG substrates. Therefore, the surface coverage values reported in this study are apparent values and higher than the true values.

This should be sufficient since our objective is to show the trends on the effect of incubation time and peptide concentration on the coverage of EAK16-II nanofibers on mica and HOPG surfaces. Another purpose of the surface coverage measurements is to compare the stability of EAK16-II-modified surfaces in various environments.

4.2.5 Contact Angle Measurement

Contact angle measurements were made to determine changes in the hydrophobicity of the surfaces upon their modification by EAK16-II. A sessile drop of water (30 μl) was manually deposited on the unmodified and EAK16-II-modified surfaces placed inside a sealed, water-saturated chamber (to prevent evaporation). A sequence of images of the water drop was then recorded over a period of 5 minutes in 5-second intervals. The recorded images were analyzed by the Axisymmetric Drop Shape Analysis-Profile (ADSA-P) program[206] to yield a water contact angle. All the experiments were controlled by a refrigerated bath/circulator digital controller (NESLAB Instrument, Inc., Georgetown, Ontario) to ensure that the temperature remained at 20 ± 0.1 °C during the measurements. The water contact angle for each surface reported herein represents the static one and the average value was obtained from three different drops.

4.3 Results and Discussion

4.3.1 EAK16-II Assembly on Hydrophilic Mica Surface

The AFM images (Figure 4.2a-i) show that EAK16-II can adhere to a mica surface and assemble into nanofibers after a certain time in pure water. In the presence of 4 μM EAK16-II, a few single and unbranched short fibers are observed after 1 minute of incubation (Figure 4.2a). With time, longer and more fibers appear on the mica surface (Figures 4.2b and c). After 10 minutes, fiber networks are observed (Figures 4.2d-i). The evolution of the surface coverage of EAK16-II nanofibers with the

incubation time is plotted in Figure 4.2j. The surface coverage of EAK16-II nanofibers increases rapidly with time over the first 30 or 40 minutes before leveling off to a plateau of about 27% after ~1 hour, indicating that saturation has been reached.

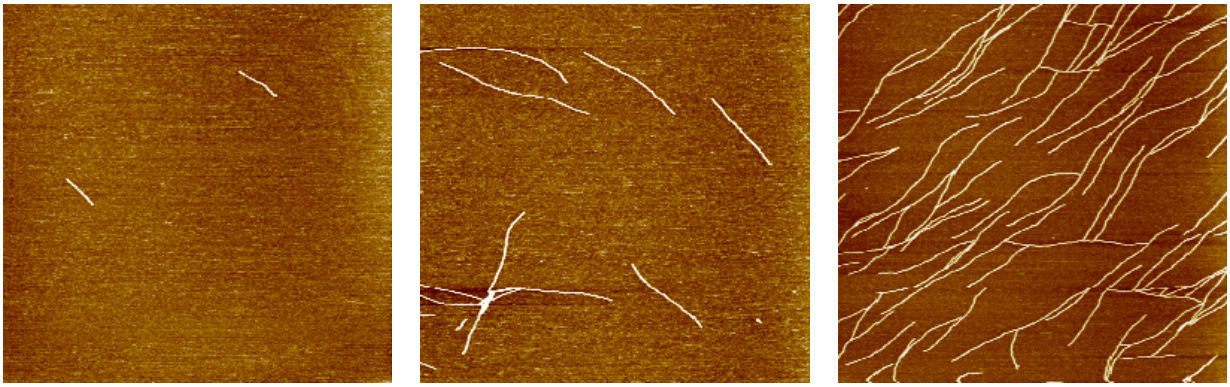

(a) 1 min (b) 2 min (c) 5 min

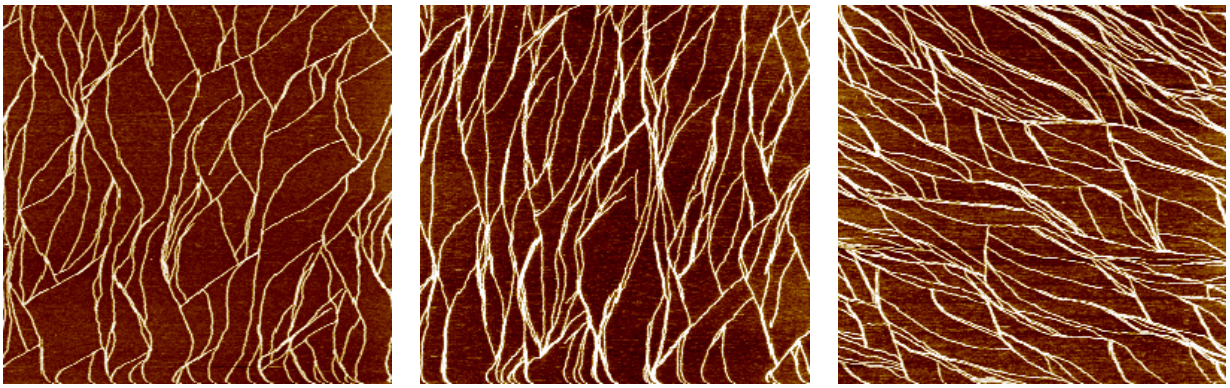

(d) 10 min (e) 23 min (f) 40 min

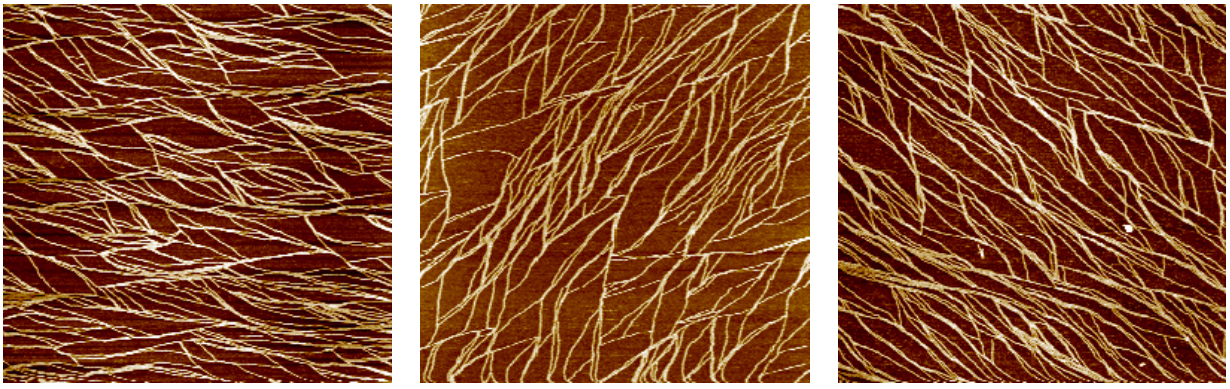

(g) 80 min (h) 120 min (i) 160 min

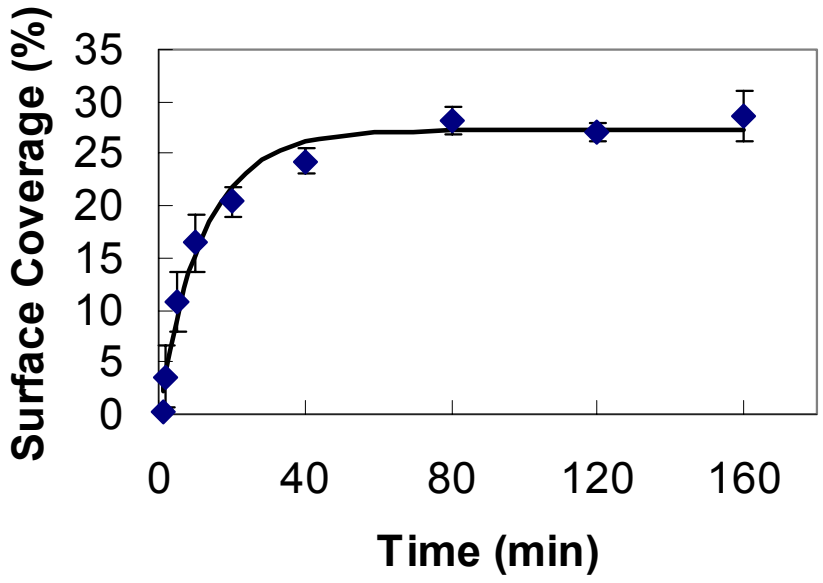

(j)

Figure 4.2 Time evolution of 4 μM EAK16-II assembly on the mica surface. AFM images collected at various incubation times: (a) 1 min; (b) 2 min; (c) 5 min; (d) 10 min; (e) 20 min; (f) 40 min; (g) 80 min; (h) 120 min; (i) 160 min. Surface coverage of EAK16-II on mica as a function of incubation time is plotted in panel (j). Each image corresponds to a scan area of 2000 nm × 2000 nm.

As expected, the surface coverage of EAK16-II nanofibers on mica is affected by the peptide concentration. Figure 4.3 shows images obtained at different peptide concentrations after an incubation time of 10 min. Only a few short fibers are observed on mica at a low EAK16-II concentration of 1 μM (Figure 4.3a). When the EAK16-II concentration is raised to 2 μM, the number and length of the nanofibers increase (Figure 4.3b). A further rise in the concentration to above 4 μM leads to the formation of fiber networks, which become denser as the peptide concentration continues to increase (Figure 4.3c-e). Quantitative analysis of the images yields the variation in surface

coverage of EAK16-II nanofibers with peptide concentration shown in Figure 4.3f. This indicates that the peptide concentration may serve as an operating variable to control the surface coverage on the mica surface.

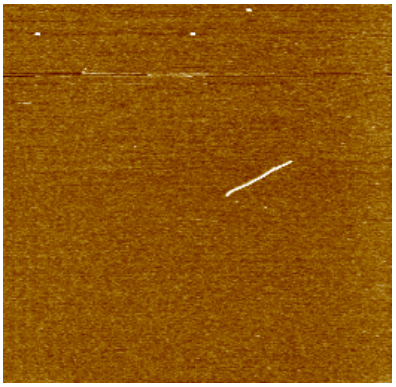

(a) 1 μM

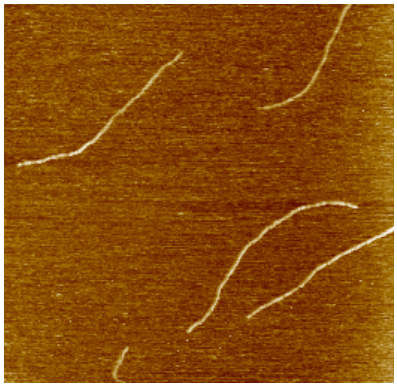

(b) 2 μM

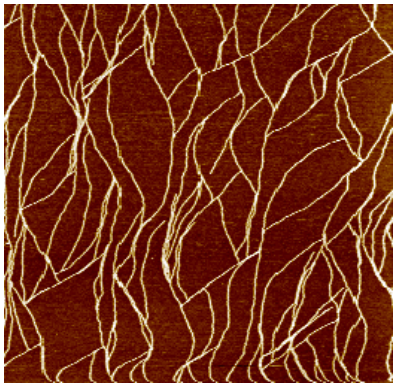

(c) 4 μM

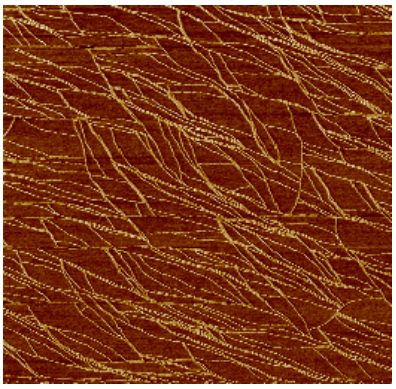

(d) 8 μM

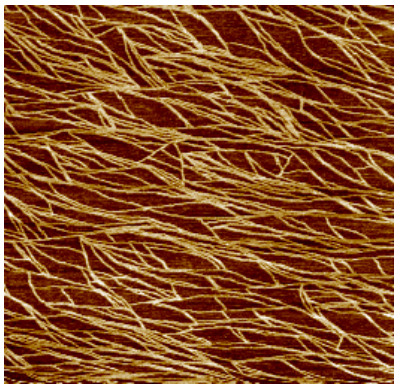

(e) 12μM

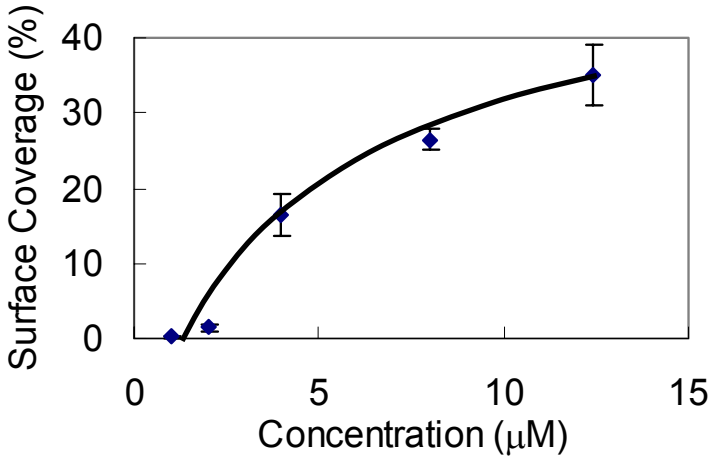

(f)

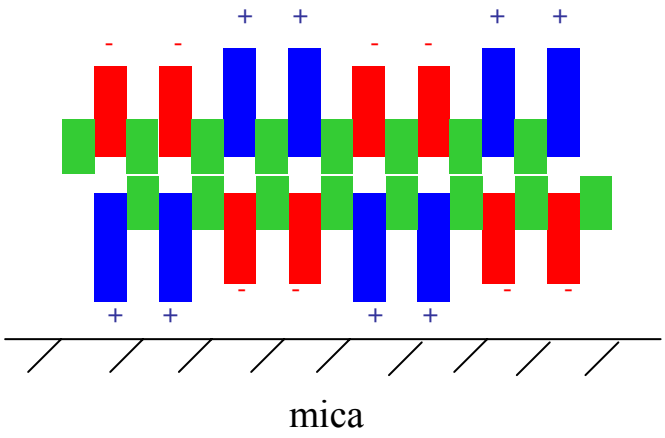

(g)

Figure 4.3 Effect of EAK16-II concentrations on the surface coverage of peptide assemblies on mica. AFM images of EAK16-II-modified mica surfaces at 10 min incubation with various peptide concentrations: (a) 1 μM; (b) 2 μM; (c) 4 μM; (d) 8 μM; (e) 12 μM. Surface coverage of EAK16-II assemblies on mica as a function of peptide concentrations is plotted in panel (f). Proposed molecular arrangement of EAK16-II assembly on mica is plotted in panel (g). Each image corresponds to a scan area of 2000 nm × 2000 nm.

The width and height of the nanofibers are observed to be independent of peptide concentration and incubation time, and estimated to be ~7.0 ± 2.6 nm and ~1.8 ± 0.2 nm, respectively, after AFM tip deconvolution.[21] These dimensions may provide information on the molecular arrangement of EAK16-II in the nanofibers and form the basis for the proposed structure shown in Figure 4.3g. It has been reported that EAK16-II forms β-sheets in pure water and salt solutions.[27,50,86] In a β-sheet structure, successive side chains of a polypeptide extend to opposite sides of the pleated sheet, resulting in a distance of ~0.7 nm between two adjacent residues on one side of the sheet.[207] A 16-residue β-strand would therefore have a length of 5.6 nm. Considering the N and C-terminal protection groups contribute an additional length of about 0.4 nm (estimated from Chemsketch software, Toronto, Canada), the total length of an EAK16-II β-strand would be approximately 6 nm. This length is close to the fiber width (7.0 ± 2.6 nm) observed on the mica surface. The height of a single EAK16-II molecule in a β-strand conformation is ~0.9 nm (estimated from Chemsketch software). By comparing the height of a single EAK16-II molecule with that of the EAK16-II nanofibers, we may infer that the nanofibers on the mica surface are made of two β-sheet layers stacked on top of one another. With such a structure, charged residues of the bottom layer peptide are oriented toward the hydrophilic mica surface and those of the top layer peptide toward the aqueous solution. The two β-sheet layers are held together by hydrophobic interactions between the hydrophobic residues of the two EAK16-II molecules. This arrangement minimizes the contact of the hydrophobic residues with either mica or the solution.

In the proposed model (Figure 4.3g), the modification of the mica surface by the peptide nanofibers is due to the electrostatic attraction between the peptide and the surface. The negatively charged mica surface can attract positively charged lysine residues at neutral pH. This electrostatic attraction is expected to be the major driving force for the adsorption and adhesion of the peptide on

mica (see Section 4.3.4). Since a chemical bond between the peptide and mica surface is unlikely to form, the adhesion of the peptide to the mica surface may be classified as physical adsorption. The growth of short peptide nanofibers into long fibers and fiber networks is thought to occur by the attachment of monomers and small protofibers onto the fiber ends at the mica surface, which has been characterized as surface-assisted nanofiber growth (see Chapter 3).

4.3.2 EAK16-II Assembly on Hydrophobic HOPG Surface

The AFM images of EAK16-II nanofibers formed on HOPG are shown in Figure 4.4. At a low EAK16-II concentration (2 μM), a few long peptide nanofibers are observed after 25 min incubation time (Figure 4.4a); a longer incubation time of 2 hours results in more nanofibers on the surface, which are either parallel or aligned 60° or 120° to each other (Figure 4.4b). Such an orientation of the fibers presumably arises due to the hexagonal crystal structure of the HOPG (0001) surface and reflects the importance of the substrate to the peptide nanofiber orientation. When the EAK16-II concentration increases to 6.2 μM, nanofibers arranged at 60° or 120° to each other are observed within 10 minutes of incubation (Figure 4.4c). As the incubation time increases to 2 hours, more nanofibers appear (Figure 4.4d). These results show that EAK16-II can assemble into patterned nanofibers on a HOPG surface.

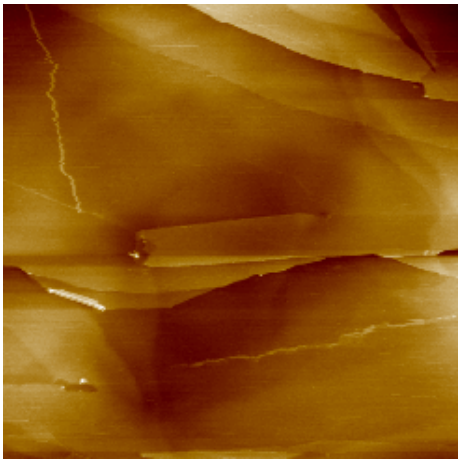

(a) 2 μM, 25 min

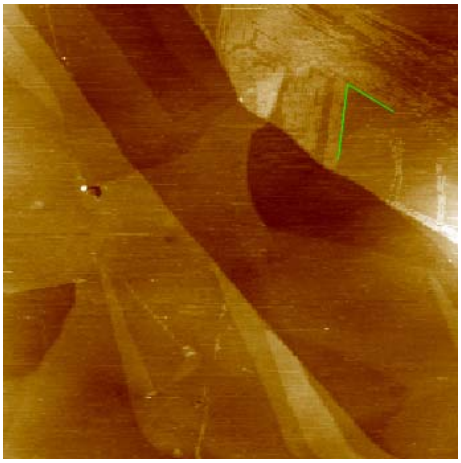

(b) 2 μM, 120 min

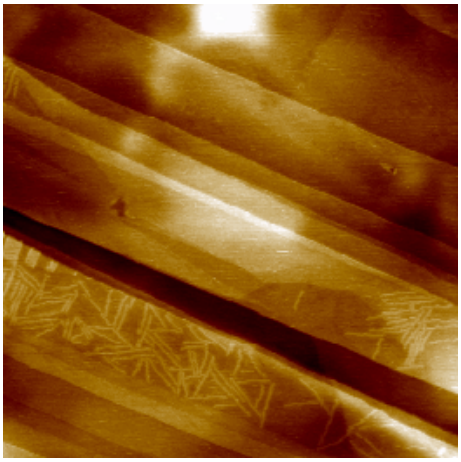

(c) 6 μM, 10 min

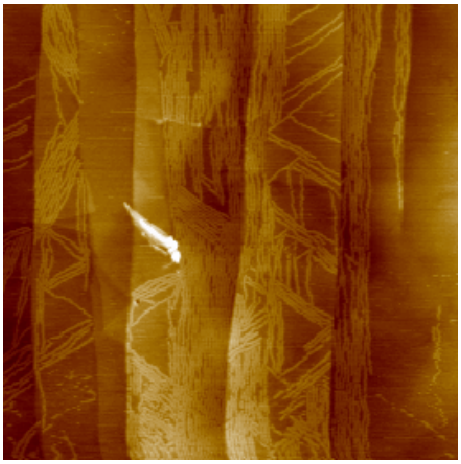

(d) 6 μM, 120 min

Figure 4.4 AFM images of EAK 16-II modified HOPG surfaces at different concentrations and time periods. (a) 2 μM 25 min, (b) 2 μM 120 min, (c) 6 μM 10 min and (d) 6 μM 120 min. Each image corresponds to a scan area of 1000 nm × 1000 nm

Unlike the case with mica, the affinity of EAK16-II to HOPG is likely due to hydrophobic interactions. As mentioned, the peptide has an amphiphilic structure in which the alanine residues lie on one side of the backbone, while the lysine and glutamic acid residues lie on the other side (Figure 4.1). When the peptide assembles in a β-strand arrangement,[27] it can attach to the surface by a

hydrophobic interaction in which the alanine side is oriented toward HOPG and the lysine and glutamic acid groups face the solution, resulting in side-on adsorption (i.e., peptide molecules lie down with their long axes parallel to the substrate surface).[208] Thus, each fiber would be made up of only a single layer of peptides on the surface, different from the situation with mica where two layers may be stacked on top of one another. This reasoning is supported by the observation that the fibers in Figure 4.4 at both peptide concentrations have a uniform width and height of 6.2 ± 2.0 nm and 0.9 ± 0.2 nm, respectively. The height of these nanofibers is close to that of a single peptide molecule in an extended β-strand.

Another question to address is whether the self-assembled nanofibers preferably form on the HOPG surface along the edges between adjacent terraces or on the terraces. It is known that the electrodeposition of metal ions occurs preferably along step edges of a surface.[209,210] In addition, Gettens *et al.* reported that the protein fibrinogen tends to adsorb on the step edges of HOPG rather than on the terraces.[208] However, our observation from the AFM image (Figure 4.5a) indicates that the EAK16-II nanofibers are primarily on the terraces and not at the step edges of HOPG. Figure 4.5b shows cross-sectional profiles of the HOPG surface along the two line segments indicated in Figure 4.5a. One line segment (green) crosses two closely-spaced fibers lying on the same terrace of HOPG, as indicated by the corresponding cross section showing that the height of the surface is the same on either side of the two bumps corresponding to the fibers (bottom plot in Figure 4.5b). On the other hand, very few of the nanofibers are oriented along the step edges. As an example, the red line segment crosses an edge without intersecting any fibers (Figure 4.5a and top plot in 4.5b). A possible explanation for this phenomenon is as follows. When adopting a β-sheet secondary structure, EAK16-II has a unique structure with charged residues on one side and hydrophobic residues on the other side. The strongest interaction of the peptide with a hydrophobic surface would involve contact of the

hydrophobic side of the peptide with the terrace of the substrate. Therefore, it is not necessary for the peptide to selectively align itself along an edge.

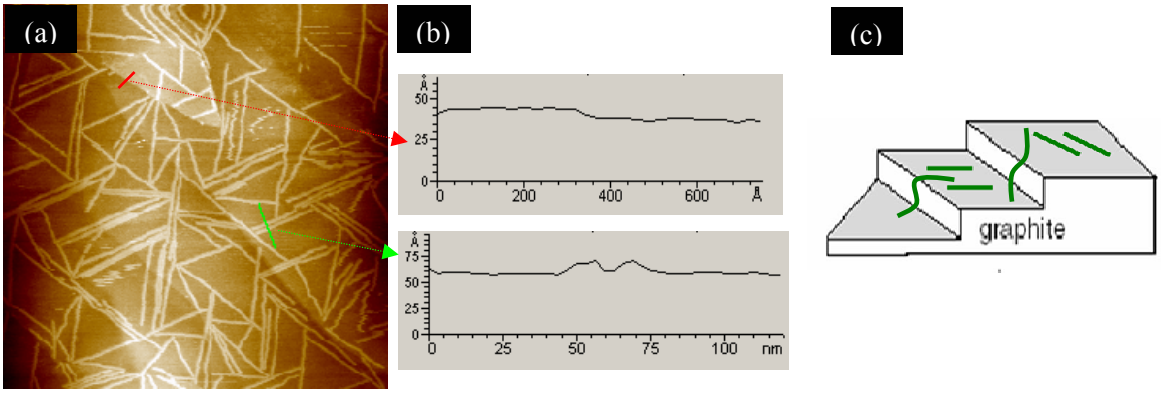

Figure 4.5 The preferred location of EAK16-II self-assembled nanofibers on the HOPG surface. (a) A representative AFM image of EAK16-II on HOPG surface over a scan area of 800 nm × 800 nm; (b) cross sectional analysis of EAK16-II nanofibers on one terrace (green line) and a step edge of HOPG (red line); (c) schematic diagram of EAK16-II nanofibers on HOPG surface.

Another interesting feature of the patterns formed on HOPG is that long EAK16-II nanofibers can actually drape over step edges from one terrace to the next. One advantage of such behavior is that surface defects such as edges and kinks may not significantly inhibit the formation of the EAK16-II nanofiber structure. Thus, the EAK16-II nanofibers can be evenly distributed, allowing control of their density over the entire surface.

Previous research has shown that HOPG surface can direct peptides and proteins to form patterned nanostructures. Examples are elastin-like peptides[42], de novo proteins[41] and amyloid proteins.[43] These patterned nanofibers also tend to align themselves at angles of 60° and 120° to one

another. However, the detailed mechanism of how proteins or peptides assemble at liquid/inorganic substrate interfaces still remains unclear.

Based on the analysis of the EAK16-II and HOPG structures, we herein propose a model of EAK16-II assembly into nanofibers on HOPG. The length of an EAK16-II molecule in β-strand is ~6 nm, which is comparable to the fiber width observed on the HOPG surface (~6 nm after deconvolution for the AFM tip size effect). In addition, the HOPG surface is made of hexagonal lattices, as shown in Figure 4.6a. In order to attain the largest hydrophobic contact between EAK16-II and the HOPG surface, it is expected that a peptide molecule would arrange itself to cover as many carbon atoms as possible. From the length of each C-C bond (0.246 nm) in the graphite lattice and the dimension of an EAK16-II β-strand, one extended strand would cover 29 carbon atoms in a row (Figure 4.6a). The peptide can assume the three possible orientations on the HOPG shown as green stripes in order to meet this requirement. The peptide strands can then line up parallel to one another to form nanofibers in the directions indicated by the three purple arrows at an angle of 60° or 120° to one another. Such a pattern is very similar to the fiber orientation shown in the AFM image in Figure 4.6b. The special orientation of peptide fibers is also indicated by the characteristic 6-fold symmetry of the 2-dimensional Fourier transform of the image (Figure 4.6b inset)

A comparison of the height of the patterned nanofibers (0.9 ± 0.2 nm) with that of a single peptide strand (~0.9 nm) suggests that these fibers consist of single layer β-sheets. These single layer sheets likely adsorb through the hydrophobic interaction between the alanine residues of the peptide and HOPG surface, leaving the hydrophilic lysine and glutamic acid residues facing the aqueous solution (Figure 4.6c). If such a structure forms, the EAK16-II-modified HOPG surface should be more hydrophilic than an unmodified surface, as examined further in the following section.

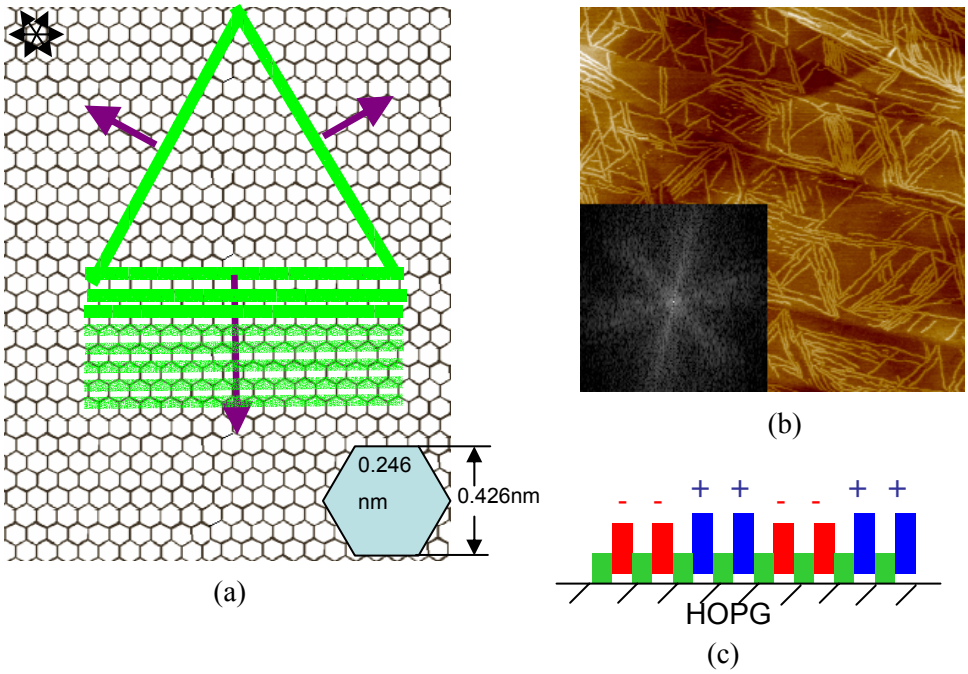

Figure 4.6 Proposed model of EAK16-II assembly on HOPG surface. (a) Schematic representation of EAK16-II strands assembled on HOPG; (b) AFM image of EAK16-II on HOPG surface over a scan area of 1000 nm × 1000 nm; the inset is the two-dimensional Fourier transform of the AFM image, showing a characteristic 6-fold symmetry; (c) schematic diagram of EAK16-II in a β-strand conformation on HOPG.

4.3.3 Water Contact Angles of EAK16-II Modified Surfaces

Contact angle measurements were conducted to determine whether the hydrophobicities of mica and HOPG surfaces change upon modification by EAK16-II. Figure 4.7 and Table 4.1 summarize the water contact angle measurements on mica and HOPG surfaces before and after the modification with EAK16-II. The water contact angle on a freshly cleaved mica surface is less than 10° (Figure 4.7a), indicating that the surface is very hydrophilic and almost completely wettable.[211] Once mica is

modified with EAK16-II nanofibers, the water contact angle of the surface increases to about 20° (Figure 4.7b and Table 4.1). This increase could result from the amphiphilic nature of the peptide molecule enhancing the hydrophobicity of the surface after the modification. However, a water contact angle of 20° indicates that the EAK16-II-modified mica surface still remains hydrophilic. On the other hand, the water contact angle of an EAK16-II-modified HOPG surface decreases to about 39° (Figure 4.7d). This value is much lower than that obtained on a freshly cleaved HOPG surface, which ranges between 82° and 60° likely due to variations in surface morphology (Figure 4.7c and Table 4.1). This result indicates that HOPG becomes more hydrophilic after treated with EAK16-II and is consistent with what would be expected from the proposed single layered β-sheet structure with lysine and glutamic acid oriented toward the aqueous solution (Figure 4.6c).

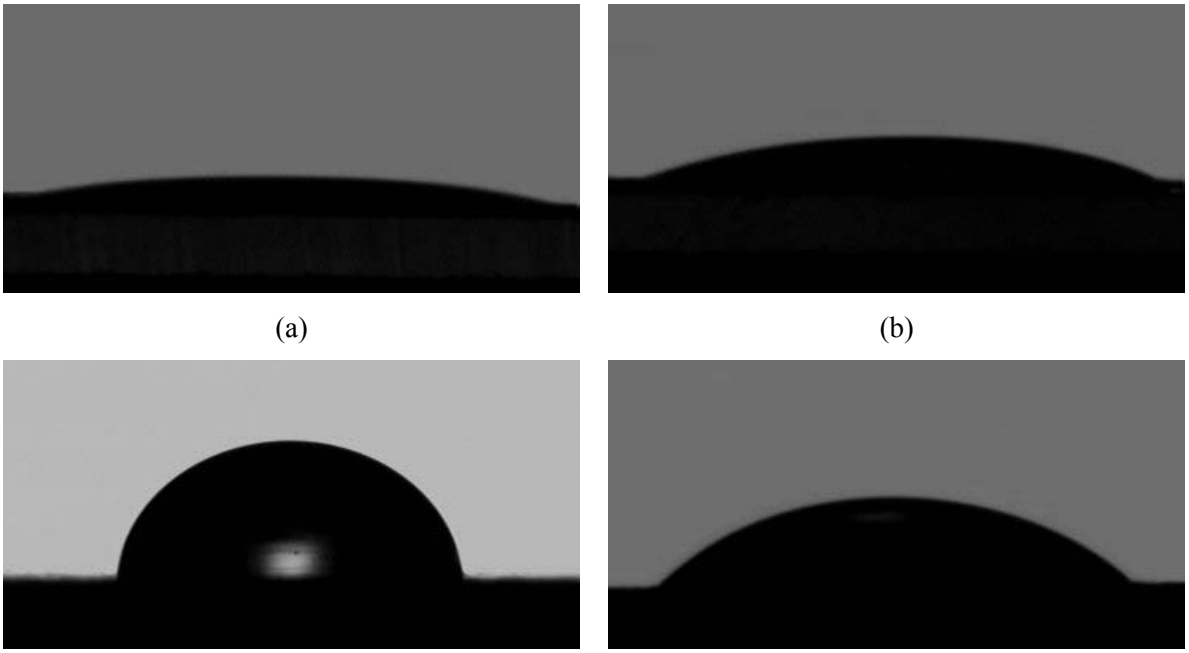

Figure 4.7 Photographs of water contact angles of mica and HOPG surfaces and their EAK16-II modified surfaces: (a) mica; (b) EAK16-II-modified mica; (c) HOPG; (d) EAK16-II-modified HOPG.

Table 4.1 Contact angles measured on mica, HOPG and their EAK16-II-modified surfaces

surfaces	mica	EAK16-II/mica	HOPG	EAK16-II/HOPG
contact angle	< 10°	20.3° ± 2.9°	71.2° ± 11.1°	39.4° ± 4.3°

4.3.4 Stability of EAK16-II Modified Surfaces in Acidic and Alkaline Solutions

To gain more insight concerning the structures of EAK16-II on mica and HOPG surfaces proposed in sections 4.3.1 and 4.3.2, we investigated the stability of the assembled nanostructures on these two surfaces in acidic and alkaline solutions. Also, in view of the possible practical applications of such modified surfaces, information regarding their stability in different environments would be useful. The stability is interpreted from the change in the surface coverage by the EAK16-II. As shown in Figure 4.8a-c and Table 4.2, EAK16-II remains on a mica surface as randomly oriented nanofibers in pure water, 10 mM HCl and 10 mM NaOH solutions, although differences in the surface coverage of EAK16-II are observed. After contact of the EAK16-II modified mica surface with the 10 mM HCl solution for 10 hours, the surface coverage of nanofibers does not change much (21.4 ± 3.5%) from that obtained prior to contact with the acid (23.7 ± 7.3%). However, the surface coverage decreases significantly to 7.7 ± 3.7% after the modified mica surface has been immersed in a 10 mM NaOH solution for 10 hours. These results indicate that an EAK16-II-modified mica surface is stable in an acidic solution but not in an alkaline solution. It has been reported that EAK16-II nanofibers remain stable in the bulk of acidic and alkaline solutions.[26] Thus, the decrease of the amount of nanofibers on mica surface under alkaline conditions may be due to a weakening of the peptide-surface interaction due to a change of the charge of the EAK16-II residues. Under acidic or neutral conditions, EAK16-II can adsorb on mica through the electrostatic interaction between positively charged lysine and the negatively charged surface. At pH 12 (10 mM NaOH), the lysine residues of EAK16-II become

neutral, making the peptide nanofibers negatively charged overall due to the glutamic acid residues. The repulsion between the negatively charged fibers and the negatively charged mica surface would cause the detachment of peptide nanofibers from the mica surface. If this interpretation is correct, it further demonstrates that the electrostatic interaction is a major driving force in the adsorption of EAK16-II onto mica surfaces.

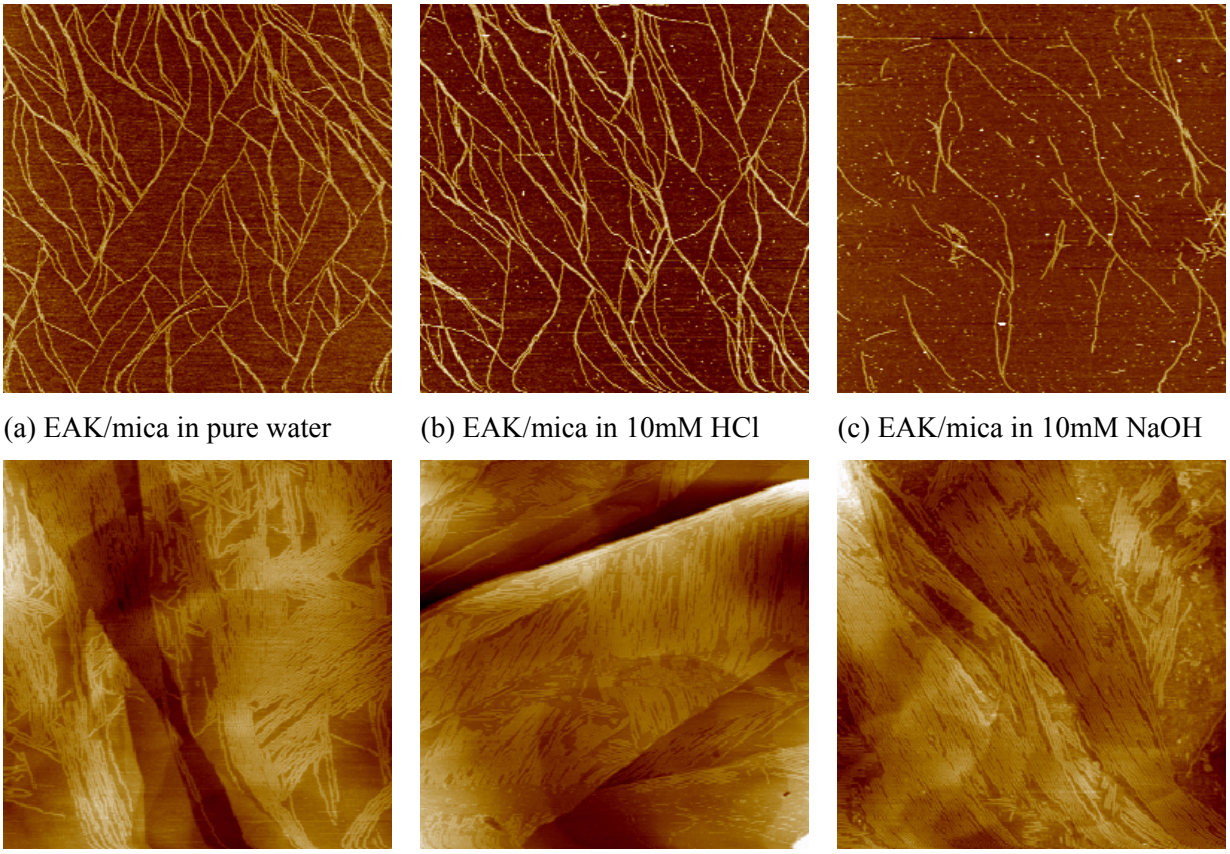

(a) EAK/mica in pure water (b) EAK/mica in 10mM HCl (c) EAK/mica in 10mM NaOH

(d) EAK/HOPG in pure water (e) EAK/HOPG in 10mM HCl (f) EAK/HOPG in 10mM NaOH

Figure 4.8 AFM images of EAK16-II modified mica and HOPG surfaces after immersion in pure water, 10 mM HCl and 10 mM NaOH solutions for 10 hours. Scan areas are 2000 nm × 2000 nm for mica surface and 1000 nm × 1000 nm for HOPG surface. (a) Mica, water; (b) mica, 10 mM HCl; (c) mica, 10 mM NaOH; (d) HOPG, water; (e) HOPG, 10 mM HCl; (f) HOPG, 10 mM NaOH.

Table 4.2 Surface coverage on EAK16-II-modified mica and HOPG surfaces after 10 hours under different environments

surface coverage %	water	10mM HCl	10mM NaOH
mica	23.7±7.3	21.4±3.5	7.7±3.7
HOPG	65.6±7.4	63.9±7.3	65.1±3.8

In the case of the EAK16-II-treated HOPG surface, the surface coverage of peptide nanofibers does not change in either the acidic or alkaline environment from that observed previously in pure water. As shown in Figure 4.8d-f and Table 4.2, the surface coverages of peptide nanofibers are 65.6 ± 7.4%, 63.9 ± 7.3% and 65.1 ± 3.8% after immersion in water, 10 mM HCl and 10 mM NaOH solutions, respectively, for 10 hours. These results indicate that the EAK16-II-modified HOPG surface is stable under neutral, acidic and alkaline conditions. This also supports our proposal that the association of the peptide with HOPG surface is mainly through hydrophobic interaction, which should not be strongly affected by the charge state of the peptide. Also, the fact that fibers remain stable on a modified HOPG surface in an alkaline solution, but not on a modified mica surface, provides further support that the loss of stability in the latter case is due to a change in the mica-EAK16-II interaction but not to chemical attack on the nanofibers.

The use of amphiphilic self-assembling peptides for surface modification offers a number of advantages. First, the modification process occurs spontaneously by adsorption of peptide fibers onto the surface followed by molecular self-assembly to elongate pre-deposited fibers on the surface. This process can be achieved by simply immersing the substrate into an aqueous peptide solution under suitable conditions. Second, the peptide secondary structure and self-assembled nanostructures have been shown to exhibit excellent chemical stability by resisting degradation in acidic or alkaline

environments and even in the presence of denaturation reagents,[21,26,97] while exhibiting good *in vitro* and *in vivo* biocompatibility.[86,97,136,202] Third, various substrates, including gold,[212,213] can be modified by these peptides through various molecular interactions, which may not depend on specific thiol-gold chemistry. Fourth, since the solution pH affects the charge state of the peptide, it provides another means by which the surface charge of the modified substrate can be adjusted for specific applications. Furthermore, the peptide sequence can be specially designed and synthesized to incorporate certain amino acids with desired functions. With these promising features, surfaces modified by self-assembling peptides may be useful in biosensor technology and tissue engineering.

The advantages of using EAK16-II-modified HOPG surfaces specifically for a number of applications are as follows. First, the hydrophobicity of the modified surface can be significantly reduced to improve its water wettability. The improvement of the water wettability of a given hydrophobic surface by EAK16-II could be utilized to help stabilize hydrophobic compounds in aqueous systems. If successful, this could have significant implications for hydrophobic drug delivery.[32,147] Second, the biocompatibility of the HOPG surface may be improved by EAK16-II, which has been found to support mammalian cell attachment.[97] Third, outward orientation of charged residues (K and E) toward the solution may provide electrostatic interaction and covalent linkage with other analytes and biomolecules so that chemical or enzymatic reactions on the surface can be accelerated. This could be important in electrochemical sensor and biosensor applications as well as the catalysis of biochemical reactions. For example, the carboxylate group of the glutamic acid residues on EAK16-II can be covalently linked to the amine group of an enzyme (e.g. glucose oxidase, GOx) Thus, the enzyme molecules can be immobilized on a graphite surface with the assistance of EAK16-II assembled nanostructures. Since HOPG is electronically conductive, this modification could make it a promising enzymatic biosensor (see Appendix A). It is also worth noting that the charge state of a peptide or protein can be changed by adjustment of the solution pH. For

example, the surface charge of EAK16-II-modified HOPG can be altered to be positive (K) or negative (E) in acidic or basic solutions, respectively, to selectively bind with target molecules.

4.4 Conclusions

The ionic-complementary peptide EAK16-II has been shown to assemble on both mica and HOPG surfaces to form nanofibers. The interaction between the peptide and mica is mainly through electrostatic attraction, whereas the adsorption of peptides and nanofibers on HOPG occurs through hydrophobic interaction. EAK16-II forms randomly orientated nanofibers with uniform width on the hydrophilic mica surface. In contrast, EAK16-II nanofibers with preferential orientations at angles of 60° or 120° to each other are observed on the hydrophobic HOPG surface. This orientation resembles the crystallographic structure of the graphite surface. After modification with EAK16-II, the contact angle of mica surface increases from <10° to 20.3 ± 2.9°, but the surface remains hydrophilic. However, the hydrophobicity of the HOPG surface is significantly reduced as seen from a contact angle change from 71.2 ± 11.1° to 39.4 ± 4.3°. An EAK16-II-modified mica surface is stable in acidic solution, but not in alkaline solution, while the modified HOPG surface is stable in both acidic and alkaline solutions for at least 10 hours. This work has shown the potential of using ionic-complementary peptides to modify both hydrophobic and hydrophilic surfaces and may open up the possibility of other surface modifications beyond traditional thiol-gold technology. In addition, the controllable peptide assembly on HOPG surface has an exciting potential application in constructing biocompatible electrodes for biosensors.

Chapter 5*
Mechanical Force-Induced Peptide Assembly at Liquid/Solid Interfaces

5.1 Introduction

Self-assembling peptides have emerged as new nanobiomaterials and received considerable attention in the areas of nanoscience and biomedical engineering.[1,8,55] They are either fragments of naturally existing proteins or derived by *de novo* biomolecular design. Among the many self-assembling peptides is a class of ionic-complementary peptides, which contain a repetitive charge distribution and alternating hydrophobic and hydrophilic residues in the amino acid sequence, resulting in the unusual properties of amphiphilicity and ionic complementarity. Such peptides can self-assemble into various stable nanostructures via electrostatic interactions, hydrogen bonds and hydrophobic interactions.[8,50,86] Their self-assembled nanostructures have a wide range of potential applications such as templates for nano-fabrication,[24,35,70,111] scaffoldings for tissue repair and tissue engineering,[36,37] nanocarriers for anti-cancer drug and gene/siRNA delivery[32,147] and surface modifiers for enzyme immobilization in biosensors.

Many applications of self-assembling peptides involve interface and surface patterning with peptide micro-/nanostructures. Therefore, understanding and controlling the peptide assembly on a surface becomes critical in developing these applications. Our previous studies have shown that the surface can facilitate and/or direct the assembly of a model ionic-complementary peptide, EAK16-II; (See Chapter 3) the surface-assisted peptide assembly follows a nucleation and growth mechanism, and the assembly kinetics can be influenced by the surrounding environment such as solution pH.(See Chapter 3) Although the solution conditions can be used to help control the density of peptide nanostructure formed globally over an entire surface, it would be useful, for example, in the

*This chapter is based on a paper " H. Yang, S.Y. Fung, M. Pritzker and P. Chen, Mechanical Force-Induced Peptide Assembly at Liquid/Solid Interfaces, *Angew. Chem, Int. Ed.*" (submitted)

fabrication of nanoscale devices to develop techniques that can produce patterns over local regions of a surface. Scanning probe lithography has been successfully used to pattern self-assembled monolayers (SAMs) on surfaces by mechanically scratching the SAM-covered surface using contact mode Atomic Force Microscopy (AFM).[44,214,215] Mechanical force/stress has recently been shown to induce chemical reactions[216] and to deliver single molecules to specific locations,[217] opening up the field of nano-mechanochemistry. It would therefore be important to determine whether a mechanochemical approach can be extended to molecular self-assembly, peptide self-assembly here in particular, through the application of a relatively gentle mechanical force by a tapping AFM tip. Note that molecular self-assembly is often governed by weak, non-covalent interactions. To the best of our knowledge, an investigation on this topic has not been reported in the literature.

More specifically, our aim is to determine whether the mechanical force applied by a tapping AFM tip can be used to better control the nanostructure of a model peptide that self-assembles over desired regions of a substrate and produce patterns that otherwise would not be possible. The primary effect of such a mechanical force is expected to break the peptide-assembled nanostructures; these broken fragments may serve as new nuclei for subsequent assembly or nanostructure growth. If so, the process of breaking peptide-assembled nanostructures by an AFM tip alone could form the basis for a nanolithography method to pattern the surface.

5.2 Materials and Methods

5.2.1 Materials

The ionic-complementary self-assembling peptides EAK16-II ($C_{70}H_{121}N_{21}O_{25}$, Mw = 1657 g/mol) and EFK16-II ($C_{118}H_{153}N_{21}O_{25}$, Mw = 2265.6 g/mol) have sequences of AEAEAKAKAEAEAKAK and FEFEFKFKFEFEFKFK, respectively; where A and F correspond to alanine and phenylalanine, E to glutamic acid and K to lysine. At neutral pH, A and F are neutral hydrophobic residues, while E and

K are negatively and positively charged, respectively. These peptides were purchased from CanPeptide Inc (Québec, Canada). The N-terminus and C-terminus of these peptides were protected by acetyl and amino groups, respectively, to minimize end-to-end electrostatic attraction between peptides.[27] The purity of EAK16-II is above 95% (purified by reverse-phase high-performance liquid chromatography), while that of EFK16-II is ~60% (crude).

EAK16-II and EFK16-II stock solutions were prepared in pure water (18.2 MΩ; Millipore Milli-Q system) at a concentration of 30 μM and 44 μM, respectively, and stored at 4 °C before use. Reagent grade sodium hydroxide with purity of 99+% and hydrochloric acid (36-38% by weight) were obtained from BDH Chemicals Ltd. (Toronto, Canada) and from Fisher Scientific (Nepean, Canada), respectively.

Grade V-4 muscovite mica ($KAl_2(AlSi_3)O_{10}(OH)_2$) and HOPG (ZYB grade), both obtained from SPI Supplies (West Chester, PA, USA), were used as the two model surfaces for AFM imaging. Mica and HOPG were fixed on the AFM liquid sample plate using double-sided tape. An adhesive tape was used to remove the outer layer of the mica and HOPG surfaces and expose fresh layers prior to the addition of peptide solution.

5.2.2 *In-Situ* AFM Imaging

To monitor in real-time the effect of the mechanical force applied by the AFM tip on EAK16-II nanofibers on substrates, *in-situ* AFM imaging was performed on a PicoScan™ AFM (Molecular Imaging, Phoenix, AZ) in a liquid cell (custom-made). The liquid cell was mounted on freshly cleaved mica or HOPG and filled with 500 μl pure water. Peptide stock solution was then injected into the liquid cell with a micro-syringe. The final peptide concentration in the liquid cell was 2, 4 or 6 μM, as indicated in the figure captions and the main text. After certain time periods, the peptide nanofibers formed on the surfaces were then scanned with the AFM tip to apply a mechanical force.

For the experiments on the effect of solution conditions, the liquid cell was filled with 1 mM HCl, 10 mM HCl or 10 mM NaOH solution instead of pure water prior to the injection of the peptide stock solution.

The amplitude of the AFM tip was calculated with the following equation from the AC mode user's manual (Molecular Imaging, Phoenix, AZ):

$$Amplitude \quad (nm) = \frac{Display \quad Voltage \quad (V)}{20 \times Input \quad Gain} \times 4.3 \times Sensitivity \quad (\frac{nm}{V}) \tag{5.1}$$

The sensitivity of the AFM tip operating in liquid was obtained from amplitude-distance spectroscopy and found to be 18.0 ± 0.8 and 14.7 ± 1.5 nm/V for HOPG and mica substrate, respectively. The display voltage was ~1 V during imaging. Thus, the amplitude of silicon nitride cantilever oscillation in liquid was calculated to be ~3-4 nm.

Atomic force microscopy images were taken using a scanner with a maximum scan area of 6 × 6 μm^2. All AFM experiments were conducted in an environmental-controlled chamber at room temperature to avoid evaporation of the working solution. Silicon nitride cantilevers with a nominal spring constant of 0.32-0.58 N/m (DNP-S, Digital Instruments) and a typical tip radius of 10 nm were used for tapping mode in liquid. To obtain the best imaging quality, the tapping frequency was usually set between 16 and 18 kHz and the scan rates were set to 0.814 Hz (~5 mins for each AFM image). All AFM images were obtained at a resolution of 256 × 256 pixels.

In general, the indicated times in the figures refer to the moment when the EAK16-II stock solution was injected into the liquid cell containing the desired solutions. The indicated concentrations for the acid and alkaline solutions refer to the original concentrations added to the liquid cell. An initial image of a newly cleaved mica/HOPG surface under the working solution was taken to confirm the absence of contaminating particles.

The surface coverage of EAK16-II nanofibers on the HOPG surface at different time periods was measured with the Image J software (http://rsb.info.nih.gov/ij/). The width and height of EAK16-II nanofibers were determined by the cross section analysis tool of the PicoScan software. The peptide nanofiber widths reported herein were obtained using the deconvolution method reported by Fung *et al.*[21]

5.2.3 Surface Tension Measurements

The experimental set-up for the Axisymmetric Drop Shape Analysis-Profile (ADSA-P) technique to study the dynamic surface tension of 30 μM EAK16-II in various solutions was described in more detail in an earlier publication.[101] Briefly, a pendant drop of the peptide solution was formed at the tip of a vertical Teflon needle (0.92 mm inner diameter) connected to a motor-driven micro-syringe (1 ml, release speed of 0.04 ml/s). The sample was placed in a temperature-controlled environmental chamber, saturated with the corresponding solvent vapor to maintain a constant humidity. The entire system was placed on a vibration-free table. The images of the pendant drop were magnified by an optical microscope and then captured by a CCD camera before being transferred to a computer. The surface tension of every sample was measured for 2 hours. During each run, images were acquired at 0.5 s intervals for the first 70 s and then at 20 s intervals for the remaining time. Software was used to digitize the images and generate a profile of the pendant drop. A theoretical curve governed by the Laplace equation of capillarity was then fitted to the profile, generating the surface tension value as a fitting parameter.[218] The standard deviation of the surface tension values obtained was less than 0.2 mJ/m^2.

5.3 Results and Discussions

The studied peptide EAK16-II has a molecular structure shown in Figure 5.1a. This peptide predominately adopts a β-sheet secondary structure, resulting in a unique amphiphilic structure with

hydrophilic residues on one side and hydrophobic residues on the other side. Such a molecular structure may allow it not only to self-assemble but also to interact with both hydrophilic and hydrophobic surfaces (Figure 5.1b and c). Negatively charged mica and hydrophobic HOPG were used to create liquid/hydrophilic and liquid/hydrophobic interfaces, respectively. It is expected that the positively charged lysine residues can interact with the mica surface, while the hydrophobic interactions occur between the alanine residues and the HOPG surface.

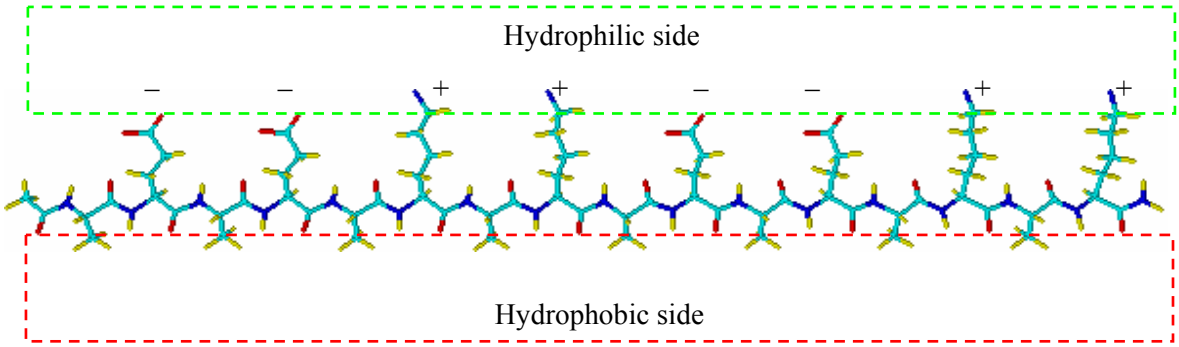

(a)

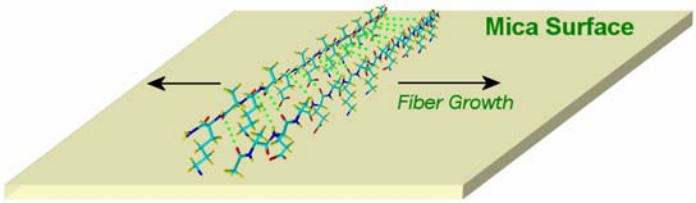

(b)

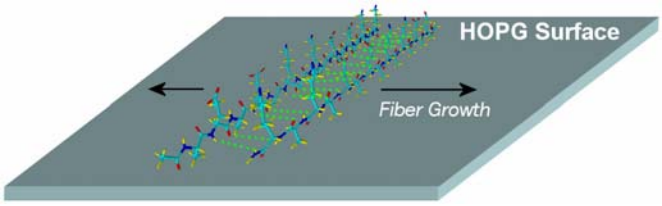

(c)

Figure 5.1 (a) Schematic diagram of EAK16-II molecular structure. Interfacial orientation of EAK16-II assemblies on (b) negatively charged hydrophilic mica surface and (c) hydrophobic HOPG surface. The green dotted lines represent hydrogen bonds between two peptide backbones.

The experiments were carried out by first depositing EAK16-II nanofibers on two model surfaces: negatively charged mica and hydrophobic highly ordered pyrolytic graphite (HOPG); *in-situ* AFM was then applied not only to generate the mechanical force on the peptide nanofibers formed on the surfaces during tip scanning, but also to monitor the force-induced/directed peptide assembly in real-time (in the presence and absence of peptide molecules in the solution). The total work applied from a tapping AFM tip to the biomolecules could be manipulated by adjusting the amplitude of the tip oscillation, the size of the scan area and scan speed.

5.3.1 Cutting EAK16-II Nanofibers by a Tapping AFM Tip

Figure 5.2a-c shows that EAK16-II nanofibers formed on a mica surface can be broken up by an AFM tip in tapping mode operation in pure water. Initially, continuous nanofibers are imaged when scanning over a large area of 2 μm × 2 μm (Figure 5.2a). However, when the scan is performed over the 500 nm × 500 nm dotted area, the nanofibers in this region appear to be discontinuous and broken (Figure 5.2b). The repetitive scanning at the same location leads to further truncation and displacement of the segments of the nanofibers (Figure 5.2c). This result shows that in the absence of dissolved peptide in solution, the applied mechanical force from the AFM tip can cut the nanofibers into shorter segments and relocate them(Figure 5.2c).

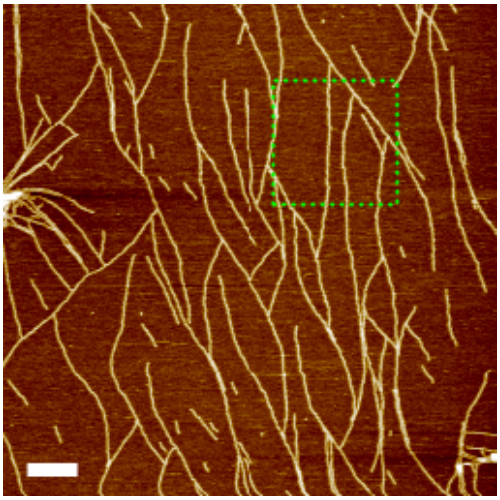

(a)

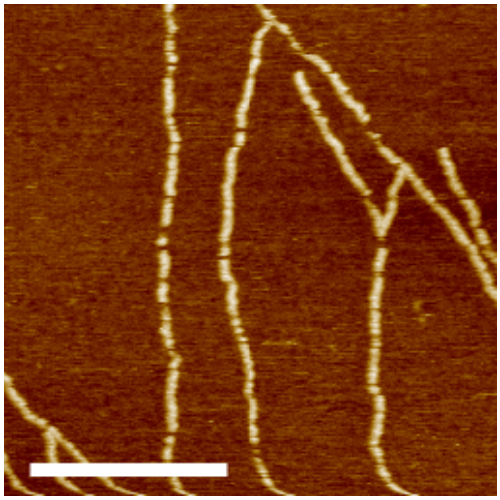

(b)

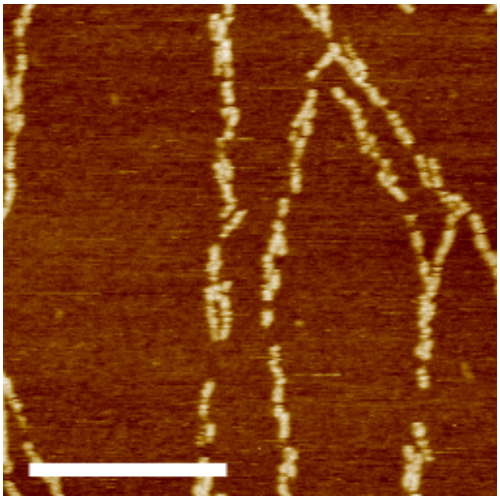

(c)

Figure 5.2 AFM images showing the effect of the mechanical force applied by the AFM tip on EAK16-II nanofibers adsorbed on mica in pure water. (a) 2 μm × 2 μm scan area; (b) zoom-in scan of the dotted area in (a); (c) 4th scan at the same location as (b). The scale bar corresponds to 200 nm.

The effect of the scan area on the breakage of the peptide nanofibers on the mica surface may be related to differences in the total work done by the AFM tip at different scan sizes. The total work that an AFM tip does on a nanofiber can be approximated using the following equation:

$$W_{total} = \sum_{n=1}^{m} F_{spring} \cdot S_n \qquad (5.2)$$

where F_{spring} represents the tension in the spring that the AFM tip applies to the nanofiber during each tap; S_n represents the total displacement of the AFM tip during interaction (attraction or repulsion) with the nanofiber during the n^{th} tap; m is the total number of taps by the AFM tip on a nanofiber during a scan. The damping force (due to friction) and the driving force (that drives the oscillation of the cantilever) are ignored as they are negligible when compared to F_{spring}. When the AFM tip scans the surface, it applies an intermittent force to the surface during each tap. This intermittent force is determined by the mechanical properties (e.g., spring constant k) and the amplitude x of the oscillating tip, which is governed by Hooke's law, i.e., $F_{spring} = kx$. The amplitude of the tip oscillation/displacement calculated from Equation 5.1 has a typical value of ~3-4 nm for tapping mode AFM imaging in liquid. For a given tip, the spring constant is fixed and the amplitude is experimentally adjusted to be constant during each scan, leading to a near constant F_{spring}. Therefore, the total work done on the nanofiber is predominantly determined by the number of taps m. In our experiments, m can be calculated using the following equation:

$$m = \frac{w \cdot f}{a \cdot v \cdot \sin\alpha} \qquad (5.3)$$

where w is the width of the nanofiber, which is typically 7 nm for EAK16-II; f is the oscillation frequency of the AFM tip, usually set to 80% of the tip resonant frequency; α is the angle formed between the nanofiber and the scan direction; a is the scan distance in the horizontal direction and v is the scan speed (line/s). According to Equations 5.2 and 5.3, for a given scan speed and oscillation frequency, more work is done on a given location of a nanofiber as the scan range becomes smaller due to the increase in the number of taps per unit distance. If the total work applied by the AFM tip overcomes the total cohesive energy of the nanofiber, the nanofiber will break. This may explain our

observation that the AFM tip can effectively cut the nanofiber when scanning over a small area (e.g., 500×500 nm^2).

5.3.2 Mechanical Force-Induced EAK16-II Nanofiber Growth

An application of this discovery is to locally induce/control the growth/morphology of peptide nanofibers on surfaces. Previous studies have demonstrated that surface-assisted nanofiber growth follows a nucleation and growth mechanism (see Chapter 3). In the presence of EAK16-II molecules in solution, a nanofiber "seed" can continue to grow by the addition of EAK16-II molecules at the active ends of the "seed". The mechanical force of the AFM tip truncates the peptide nanofibers, which in turn can serve as the "seeds" for the growth of new nanofibers (Figure 5.3). After three zoom-in scans (500 nm × 500 nm) of an original single nanofiber, many new nanofibers appear (Figure 5.3c). These newly growing nanofibers may either repair the breakage (i.e., self-healing) or form a new branch depending on the orientation of the truncated nanofibers and the growth direction. As shown in the larger scale scan in Figure 5.3d, the nanofiber density is higher in the scanned area than at any other location. This provides a method to promote nanofiber formation at a desired location on a surface.

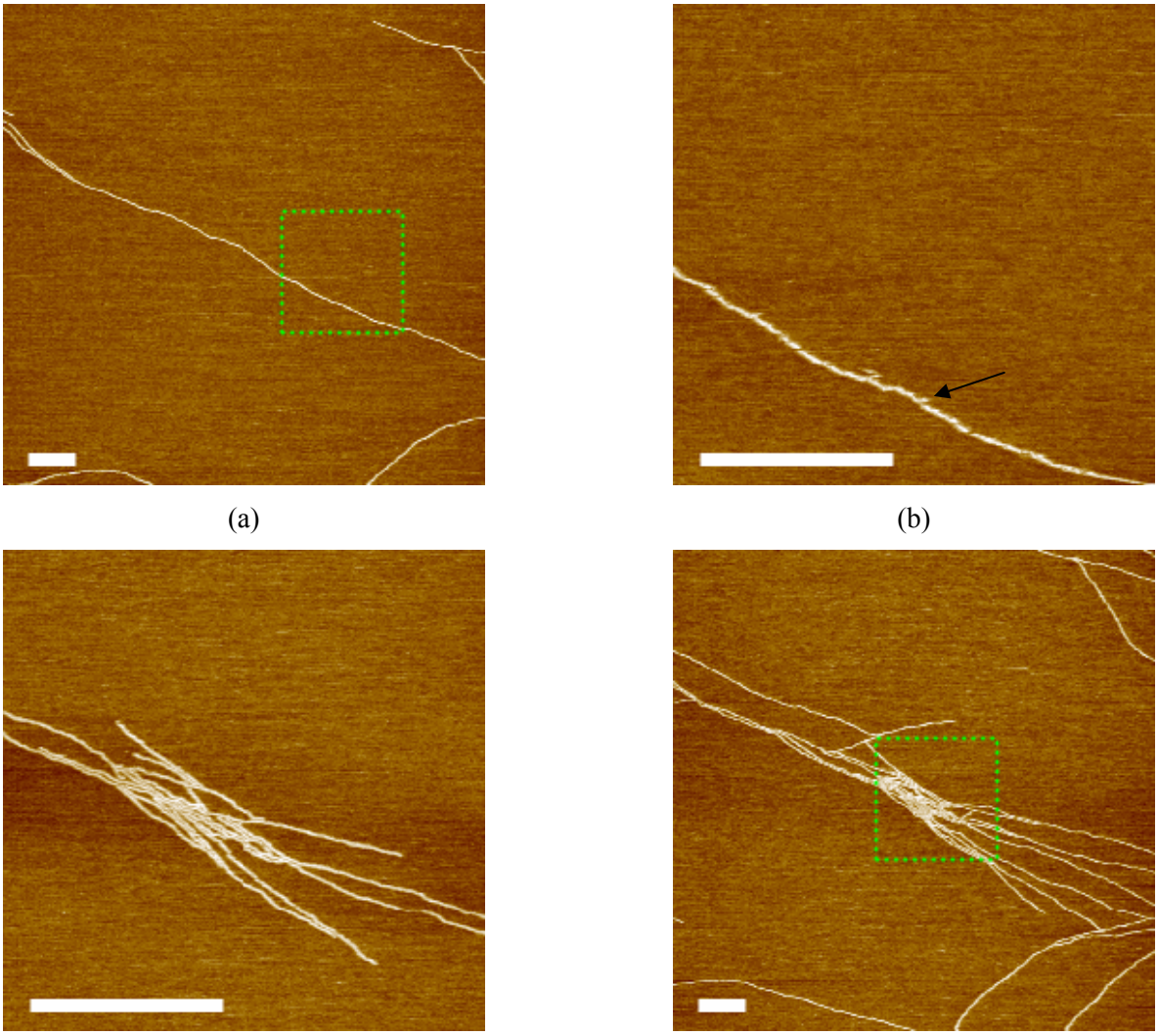

Figure 5.3 AFM images showing mechanical force-induced EAK16-II assembly on mica in 2 μM E AK16-II solution (a) 2 μm × 2 μm scan area; (b) zoom-in scan of dotted area; the arrow points to the broken nanofibers serving as new nuclei for subsequent nanofiber growth; (c) 3rd repetitive scan at the same location as (b) showing many new growing nanofibers; (d) large-scale scan after (c) showing that mechanical force can induce local nanofiber growth in the dotted area. The scale bar corresponds to 200 nm.

In addition to a mica surface, mechanical force-induced peptide assembly and nanofiber growth are also observed on a hydrophobic highly ordered pyrolytic graphite (HOPG) surface. In the absence of peptide molecules in solution, the continuous long nanofibers observed initially (Figure 5.4a) are truncated after the first zoom-in 500 nm × 500 nm scan (Figure 5.4b). Subsequent repetitive scans over the same region lead to shorter and fewer nanofibers remaining on the surface (Figure 5.4c). Evidently, some truncated nanofibers may detach from the HOPG surface. On the other hand, in the presence of peptide molecules in solution, repeated zoom-in scanning results in many short nanofibers on the HOPG surface (Figure 5.4d-g); the number of short nanofibers increases dramatically and covers the whole scan area (1 μm^2) after several cycles of scanning. On locations which do not receive continuous multiple scanning, the nanofibers are longer and more loosely covered in hexagonal patterns, resembling the crystallographic symmetry of the HOPG surface (Figure 5.4h).[43] Comparison of the surface coverage by the peptide nanofibers as a function of time with/without repetitive scanning (Figure 5.4i) clearly indicates that the mechanical force can induce nanofiber formation. This leads not only to a faster increase in the surface coverage but also to a coverage as high as ~80 % when equilibrium is reached, more than a two-fold increase over that achieved without the mechanical force.

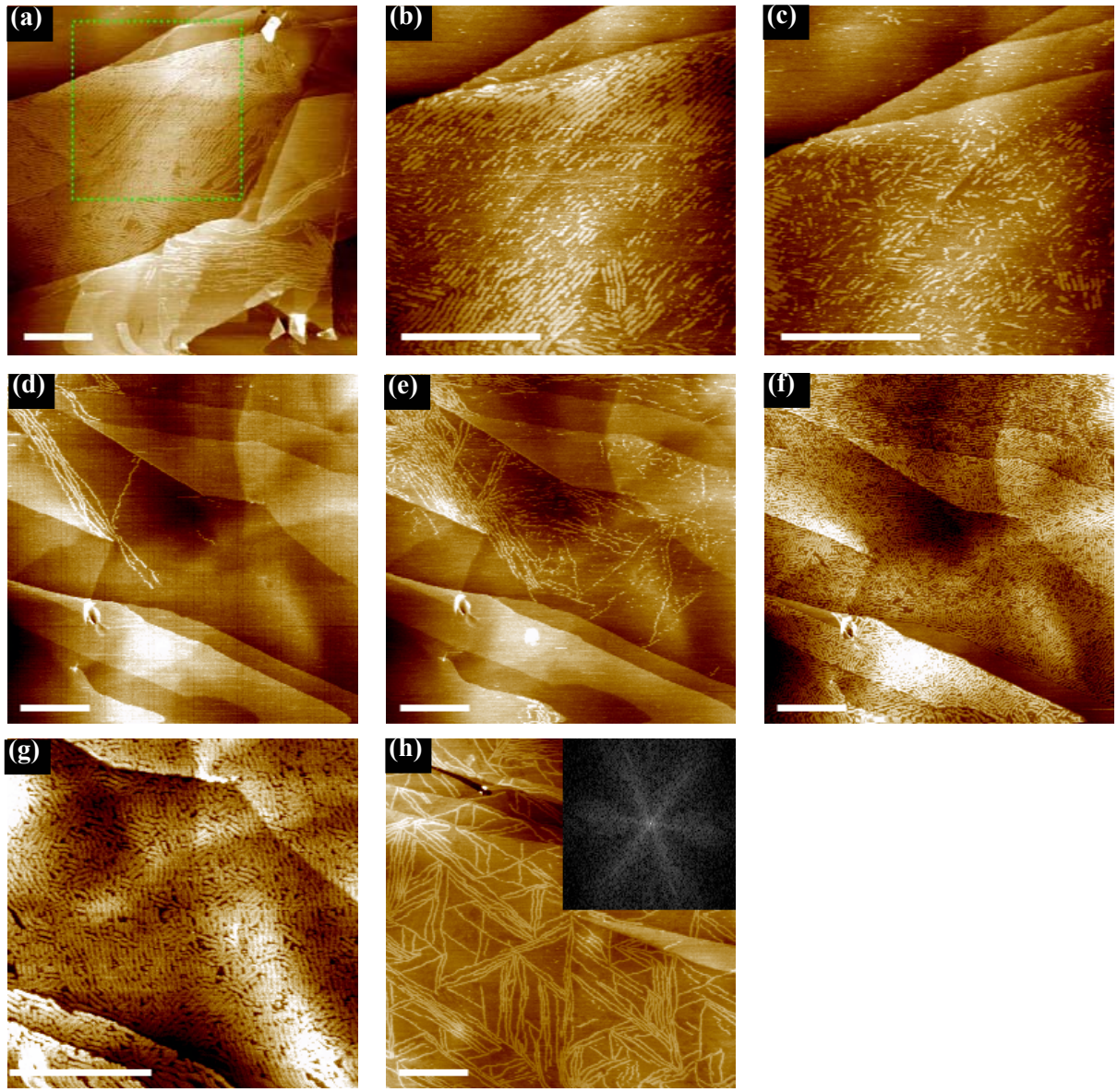
(a)
(b)
(c)
(d)
(e)
(f)
(g)
(h)

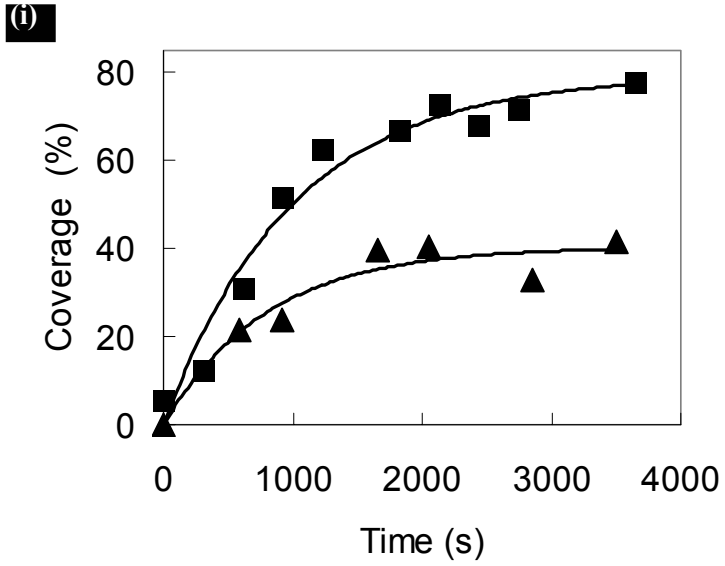

Figure 5.4AFM images of EAK16-II nanofibers adsorbed on HOPG in pure water (a-c) and 4 μM EAK16-II solution (d-g) under a mechanical force applied by a tapping AFM tip: (a) large-scale 1 μm × 1 μm scan; (b) 1st zoom-in scan of the dotted area in (a); long peptide nanofibers are broken into short nanofiber segments under the mechanical force; (c) 4th scan at the same location of (b) leads to further breakage of nanofibers into shorter ones; (d) 1st, (e) 2nd and (f) 10th 1 μm × 1 μm scan of the same location of (d); amount of peptide nanofibers on HOPG increased with the number of repetitive scans; (g) zoomed-in scan image after the 10th scan reveals many truncated nanofibers formed on HOPG; (h) a representative image of other locations that were not repetitively scanned; peptide nanofibers loosely covered the HOPG surface with a hexagonal pattern; inset FFT image shows the nanofiber are patterned in 6-fold symmetry; (i) surface coverage of peptide nanofibers as a function of time; squares represent the surface coverage of peptide at one location with repetitive scans and triangles correspond to that at different locations scanned only once. The scale bar corresponds to 200 nm.

From these observations, it can be concluded that the relatively gentle tapping force applied by the AFM tip during scanning is able to break the peptide nanofibers on both mica and HOPG. However, the effect on the two surfaces is different. The peptide nanofibers on the HOPG surface appear to be more easily broken than on mica. This may be due to the slight difference in the peptide nanostructures on the two surfaces. Our previous work has shown that the average nanofiber heights on mica and HOPG are 1.8 ± 0.2 nm and 0.9 ± 0.2 nm, respectively (See Chapter 4). On the basis of the height of a single β-sheet of EAK16-II (~0.9 nm, ChemSketch, Toronto, Canada), it appears that nanofibers on mica tend to consist of two β-sheet layers, while those on HOPG contain only a single layer. Presumably, the breakage of a double layer of β-sheets requires more energy than that of a single layer. Thus, a smaller scan area, such as 500 nm × 500 nm, is usually required to break the nanofibers on the mica surface, whereas a larger scan area of 1 μm× 1 μm is sufficient to cut the nanofibers on HOPG. Since these nanofiber segments function as new nuclei for growth, the local coverage of nanofibers on the surface increases.

The mechanical force-induced peptide assembly may provide insight into a number of biological events and help develop new biomedical applications. For example, it has been found that applying sonication to proteins can cause their aggregation into structures resembling amyloid fibrils.[219] Although sonication involves many aspects including mechanical/shear stress, local heating, the formation of liquid-gas interfaces and free radical reactions,[220] the result is the formation of active seeds that facilitate protein aggregation into amyloid fibrils. The result of our study suggests that sonication may be able to induce amyloid fibril formation through the creation of a mechanical force, which induces seed formation.

5.3.3 Fabrication of Patterned Nanostrucutures on HOPG

Thus far, we have demonstrated one approach of using an AFM tip to apply mechanical force and locally induce peptide assembly and nanofiber growth on both mica and HOPG surfaces. To fabricate patterns with specific shapes in desired locations, more precise control may be achieved by modifying the present nanolithography approach and exploiting the chemical properties of EAK16-II. An important aspect of this approach is the removal of the broken nanofibers from specific regions of the surface. This is possible due to the effect of pH on the adsorption of peptide molecules/nanofibers on HOPG. Experiments have shown that the peptide nanofibers adhere strongly to a HOPG surface in pure water, 1 and 10 mM NaOH solutions, but less so in 1 and 10 mM HCl solutions (Figure 5.5). This pH dependence may be due to the effect of pH on the peptide amphiphilicity, as supported by the surface tension data shown in Figure 5.6. In acidic solutions, the peptide solutions exhibit a much higher surface tension (~71 mJ/m^2), indicating that they are more hydrophilic and less able to adsorb to the hydrophobic HOPG surface. On the other hand, their lower surface tension in pure water and basic solutions indicates a higher hydrophobicity and tendency to adsorb on HOPG in these media. Once the peptide nanofibers adsorb onto this surface, they remain stable regardless of the pH (see Chapter 4). However, formed nanofibers can be removed by repetitive AFM tip scanning in an acidic solution.

It is worth noting that a related peptide EFK16-II is able to adsorb to the HOPG surface and form patterned nanofibers in 1 mM HCl solution as well as in neutral and basic conditions (Figure 5.5f). This is because the phenylalanine residues make EFK16-II more hydrophobic than EAK16-II. This observation also suggests that the hydrophobicity of the peptide molecules is important for their adsorption and assembly on HOPG.

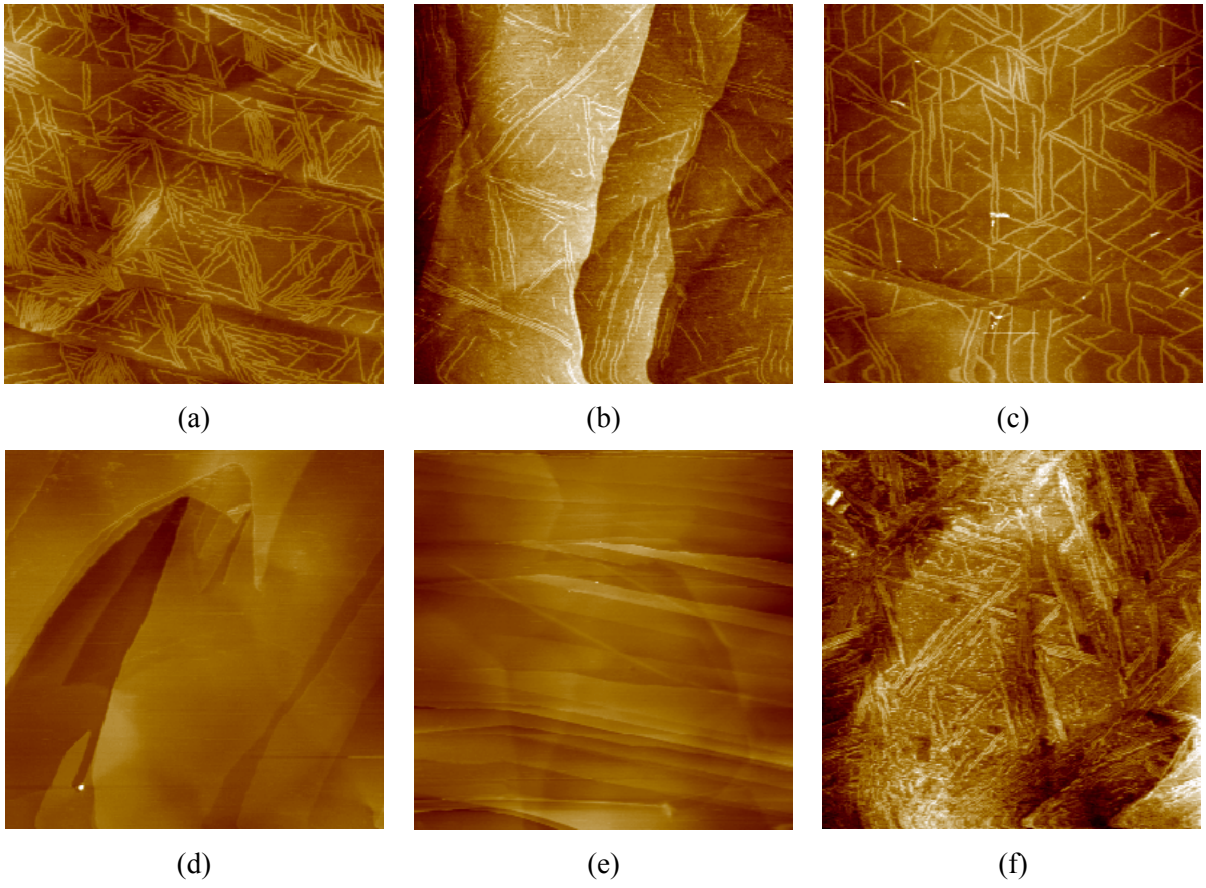

Figure 5.5AFM images of 6 μM EAK16-II assemblies on the HOPG surface under different environments: (a) pure water; (b) 1 mM NaOH; (c) 10 mM NaOH; (d) 1 mM HCl; (e) 10 mM HCl. (f) 6 μM EFK16-II on the HOPG surface in 1 mM HCl. All images were taken at 1000 nm × 1000 nm.

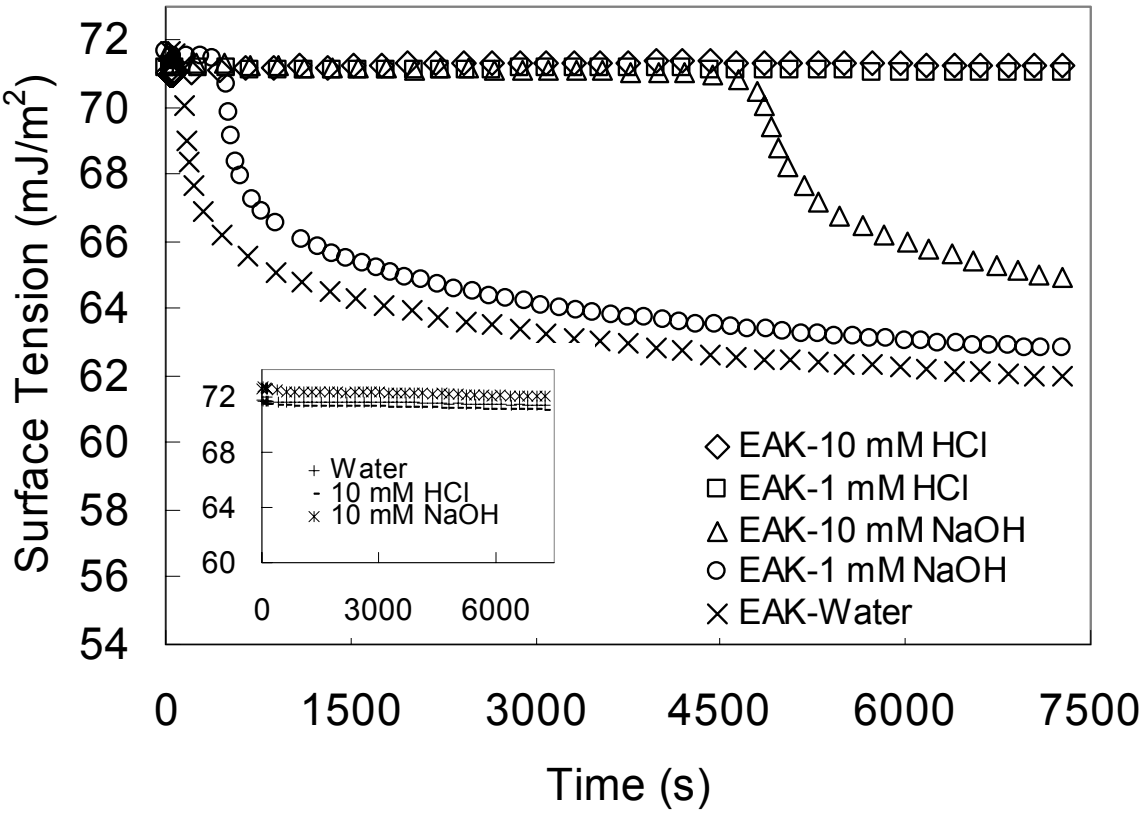

Figure 5.6 Dynamic surface tensions of 30 μM EAK16-II in various solutions: pure water (×);10 mM NaOH (Δ); 1 mM NaOH (○); 1 mM HCl (□); 10 mM HCl (◇). The inset shows the dynamic surface tensions of the solvents: water (+); 10 mM HCl (-); 10 mM NaOH (∗).

This property of weak adsorption of peptides to HOPG in acidic solutions forms the basis for an effective method to fabricate nanofiber patterns on HOPG that utilizes AFM tip nanolithography through a combination of bottom-up and top-down approaches. First, EAK16-II molecules (30 μM) are allowed to assemble into nanofibers on the HOPG surface in a neutral solution until the surface is almost fully covered by the peptide assemblies (Figure 5.7a). The EAK16-II–covered HOPG surface

is then submerged in a 10 mM HCl solution. Tapping mode AFM is applied to break the nanofibers in a particular region of the surface through repetitive scanning. In the acidic solution, nanofibers preferentially detach from the repetitively scanned portion of the substrate until the underlying HOPG surface appears (Figure 5.7b-d).

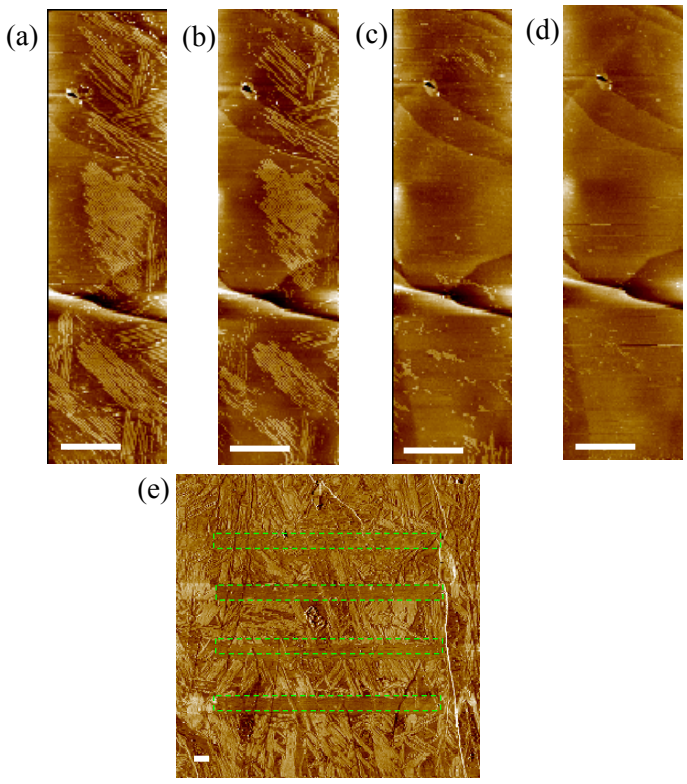

Figure 5.7 Results of AFM tip nanolithography performed in 10 mM HCl solution to fabricate EAK16-II nanofiber-patterned HOPG surface: (a-d) repetitive AFM scanning to break and remove peptide nanofibers to expose bare HOPG surface; (e) a representative AFM phase image of EAK16-II nanofiber patterned HOPG surface; peptide nanofibers were removed within the four strips (dotted area). Scale bar corresponds to 200 nm.

A representative peptide nanofiber pattern on HOPG is shown in the larger scale image in Figure 5.7e. Four parallel stripes were made by repetitive scanning in 10 mM HCl solution. Since the nanofiber-covered area is hydrophilic while the bare HOPG surface is hydrophobic (See Chapter 4), alternating hydrophilic and hydrophobic patterns can be created via this method. Such a structure could serve as a template to pattern proteins or enzymes by selective adsorption due to the variation in protein affinity based on differences in hydrophobicity of the surface. Many biomolecules and cells can also be immobilized on the patterned peptide nanofibers through functional amino acid residues to construct biosensors and protein/DNA chips and to study cell-to-cell communications.[97,203] Also, since HOPG is an electronic conductor and the regions covered by the peptide are likely to be passivated, it may be possible to use electrodeposition to produce nanoscale metal patterns and features.

This method, however, cannot be applied to the negatively charged mica since the solution pH significantly affects the electrostatic attraction between the peptides and the mica surface (see Chapter 4). The peptides dissociate from the surface at high pH even without a mechanical force from the AFM tip. On the other hand, peptides adsorb strongly at low pH and cannot be easily removed by AFM tapping. Thus, it will not be possible to selectively remove nanofibers from desired portions of the surface using this AFM nanolithography method.

5.4 Conclusion

Mechanical force applied by the tapping of an AFM tip can break EAK16-II nanofibers on both mica and HOPG surfaces. Such a process can be controlled by adjusting the scan area and the scan speed. The broken nanofibers can serve as seeds for new nanofiber growth. The mechanical force-induced peptide assembly allows one to locally grow nanofibers that densely cover specific regions of the surface. In addition, a new AFM lithography method based on applying a mechanical force with the

AFM tip to break the peptide nanofibers in an acidic solution is proposed to fabricate an alternating hydrophilic and hydrophobic patterned surface on HOPG. These patterned peptide nanofibers could serve as templates to immobilize protein/enzyme, DNA and cells for biomolecular sensing and other biomedical applications.

Chapter 6*
Design and Characterization of a Metal Ion Binding Self-Assembling Peptide for Metallic Nanowire Fabrication

6.1 Introduction

Molecular self-assembly is a widely recognized phenomenon in nature. Under certain conditions, amphiphilic molecules can spontaneously assemble into aggregates with certain size and structure. Self-assembling peptides are a novel class of amphiphilic molecules that are relatively easy to design and synthesize. In recent years, considerable advances have been made in the use of self-assembled nanostructures of these synthetic peptides as building blocks for functional biomaterials.[8,56] These biomaterials have many potential applications such as templates for nanowire fabrication,[29,35,70,71,73] platforms or scaffolds for tissue engineering,[86,96,97] delivery of proteins and peptide medicines[93,221] and biological surface engineering.[203]

Among the new class of self-assembling peptides are ionic-complementary peptides, whose sequence motif was serendipitously discovered from a Z-DNA binding protein in yeast.[97] These small peptides contain alternating hydrophobic and hydrophilic residues in sequence and possess a unique property of ionic complementarity. In solution, they can self-assemble into various nanostructures not only through hydrogen bonding, but also through electrostatic and hydrophobic interactions. Most of these peptides, such as EAK16-I and EAK16-II, readily self-assemble to form stable nanofibers that have been shown to resist degradation in acidic or alkaline environments.[21,26,97] The size and unusual stability of these nanofibers under extreme solution conditions make these peptides promising materials for applications in nanotechnology. In particular, the possibility of fabricating conductive nanowires using self-assembled peptide nanostructures as templates is of special interest to the electronics industry. The "bottom-up" nanofabrication technique based on molecular self-assembly to

*This chapter is based on the paper "H. Yang, M. Pritzker, S.-Y. Fung, Y. Sheng, W. Wang and P. Chen, Anion Effect on the Self-Assembled Nanostructures of a Metal Ion Binding Peptide, *Langmuir* 2006 22(20) 8553-8562".

construct supermolecules from single molecules can overcome the various limitations of traditional 'top down' (an approach starting from large-scale operation) approaches, such as optical lithography.[56] These top-down methods have approached their physical limits of resolution due to constraints mainly arising from the wavelength of the optical sources and quantum mechanical effects.[222] In addition, increasing costs also impede the further scaling down of conventional silicon technology.[210] The search for alternative technologies for metallic nanowire and electronic device fabrication has stimulated a considerable amount of research interest.[29,35,72,223-227]

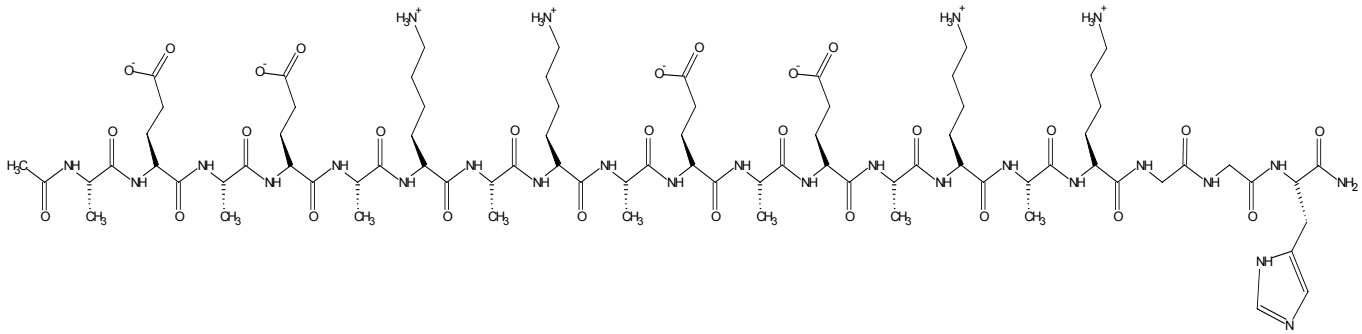

Figure 6.1 Schematic diagram of EAK16(II)GGH structure. The gray portion shows the functional GGH group

One important application of peptide self-assembled nanofibers is to act as templates for metallic nanowire fabrication.[29,35,228] Our current effort in this direction focuses on the production of nanowires from copper due to its widespread use in the electronics industry. Our strategy is to incorporate copper into the nanofibers via a metal binding site in a self-assembling peptide. EAK16-II, an ionic complementary peptide well-known for its ability to self-assemble into nanofibers, has been chosen to serve as the model peptide. It is modified by adding a functional Cu^{2+} binding group GGH[229] (G, glycine; H, histidine) to the C-terminus of EAK16-II. The molecular structure of this newly designed peptide, called EAK16(II)GGH, is shown in Figure 6.1. GGH has been chosen as the

metal binding group and located at the C-terminus for the following reasons: (1) it can provide nitrogen donors to coordinate with Cu^{2+} in a tetragonal geometry[230,231] and is not expected to significantly affect the self-assembly of EAK16-II into nanofibers due to its small size, and (2) GGH has been shown from quantum mechanical calculations to have a higher binding constant for Cu^{2+} than other tripeptides.[230] Thus, the designed peptide may bind with copper strongly and the metal-peptide complex may have high stability, an important factor for the later metallization of the peptide nanofiber.

During preliminary experiments, it became apparent that the type of Cu^{2+} salt present has a strong impact on the geometry of the peptide self-assembled nanostructures. This chapter describes the results of a detailed experimental study on the influence of SO_4^{2-}, Cl^- and NO_3^- anions on the molecular structure, self-assembled nanostructure and thermodynamic behavior of the newly designed peptide EAK16(II)GGH. The binding of EAK16(II)GGH to Cu^{2+} was characterized by Nuclear Magnetic Resonance (NMR) and UV-Vis Absorption spectroscopy. The peptide secondary structure was characterized by Fourier Transform Infrared spectroscopy (FTIR). The nanostructures of the peptide assemblies were observed using Atomic Force Microscopy (AFM). Since EAK16(II)GGH has an amphiphilic structure and surfactant-like properties similar to EAK16s,[21,26,27] with hydrophilic residues on one side and hydrophobic residues on the other side, the self-assembled nanostructure may also exhibit such amphiphilicity. Thus, the surface tensions of solutions containing EAK16(II)GGH and the copper salts were measured using the Axisymmetric Drop Shape Analysis-Profile (ADSA-P) technique. Surface tension can be used to assess the surface activity of peptide assemblies and kinetics of peptide adsorption at surfaces.

6.2 Materials and Methods

6.2.1 Materials

The self-assembling peptide EAK16(II)GGH ($C_{80}H_{134}N_{26}O_{28}$, molecular weight 1908 g/mol) has a sequence of AEAEAKAKAEAEAKAKGGH (see Figure 6.1) where A corresponds to alanine, E to glutamic acid, K to lysine, G to glycine and H to histidine. At neutral pH, A and G are neutral hydrophobic residues, whereas E is a negatively charged hydrophilic residue, K is positively charged and H may be partially charged since its normal pKa is about 6.0. The real pKa value of histidine in a specific peptide or protein can be changed by the formation of peptide bond,[232] terminal modification,[233] the location,[234,235] and the interaction with other amino acids.[234] The proportion of charged histidine groups can be expressed as $10^{(pKa - pH)}/[1+10^{(pKa - pH)}]$. This peptide was purchased from Invitrogen (Burlington, Canada) with a purity of >95% (purified by reverse-phase high-performance liquid chromatography). The N-terminus and C-terminus of the peptide were protected by acetyl and amino groups, respectively, to minimize end-to-end electrostatic attraction between peptides.[27]

Peptide solutions were freshly prepared in pure water (18.2 MΩ; Millipore Milli-Q system) and copper salt stock solutions (from 0.05 mM to 10.0 mM) at concentrations of 0.025 and 0.05 mg/ml (12.4 and 24.8 μM EAK16(II)GGH). In order to avoid interference from other anions, a buffer solution was not used to control pH. However, in the copper binding experiments, a minute amount of NaOH was used to adjust the solution pH to 6.0 to enable the binding of copper to peptide molecules and to stabilize the chemical shift of protons in NMR (see below). At a peptide concentration of 0.05 mg/ml, the pH measured in the presence of 1.0 mM copper salts without the addition of NaOH was about 5.9 regardless of the anion present, whereas the pH was 6.2 in the absence of the salt. The ionic strength of the solutions was not further adjusted by the addition of any other electrolyte to avoid

interference from other ions. All peptide solutions were stored at 4 °C before use. Copper sulfate, copper chloride, copper nitrate, sodium sulfate and sodium chloride (Sigma-Aldrich, Oakville, Canada) with purity of 99.9+ % were used in the experiments.

6.2.2 Methods

Nuclear Magnetic Resonance (NMR)

The ^{1}H NMR spectra were acquired at 25°C on a Bruker Avance DMX 600 MHz spectrometer equipped with a triple resonance xyz-gradient probe and processed using Felix 97.0 software (MSI, Inc.). The spectra were recorded using 90% H_2O/10% D_2O solutions, typically at a peptide concentration of 1.0 mM. The pH of the peptide solution was adjusted to 6.0 using small aliquots of 0.1 M NaOH prepared in 90% H_2O/10% D_2O solution. The choice of this pH was dictated by the solubility of Cu^{2+} (K_{sp} of $Cu(OH)_2$, 1.6×10^{-19}) and the capability of copper binding to histidine. The measured pH values were uncorrected for the isotope effect. In the metal ion binding study, small aliquots (0.25 mM) of $CuCl_2$ and $CuSO_4$ solution were added to the peptide solution, respectively. Correction for the volume change during copper titration was made during the analysis.

UV-Vis Absorption Spectroscopy

The absorption spectra were obtained on a UV-Vis spectrophotometer (Biochrom Ultraspec 4300 Pro, Cambridge, England) using a 1 cm path-length quartz cuvette. The copper ion titration was performed by adding small aliquots of $CuCl_2$ or $CuSO_4$ stock solution (70 mM) to 0.6 mg/ml (0.3 mM) EAK16(II)GGH solution. The final contents of copper ions for each titration ranged from 0.19 to 1.82 mM. The solution pH was adjusted to 6.0 by adding small amounts of 0.1 M NaOH, HCl (for experiments involving $CuCl_2$) or H_2SO_4 (for experiments involving $CuSO_4$). The spectra were

smoothed and deconvoluted after background correction using the PeakFit 4.12 software (Hearne Scientific Software LLC, Chicago, USA) to obtain the absorbance of bound copper ions at ~611 nm.

Fourier Transform Infrared Spectroscopy (FTIR)

FTIR spectra over the range from 1600-1700 cm^{-1} where the characteristic amide I band appears were obtained to determine the secondary structure of peptide in different copper salt solutions. Examination of this band enables distinction to be made between β-sheets and α-helices/random coils. The peptide (1.0 mM) or peptide/copper salt (1.0 mM) solutions (~100 μl, incubated for one week to allow secondary structures to form) were placed on a crystal slide of calcium fluoride (CaF_2) and dried at room temperature. The FTIR spectra of the thin films were obtained at a wavenumber resolution of 4 cm^{-1} with a Bio-Rad spectrometer (FTS3000MX, EXCALIBUR series, Hercules, CA). The baseline was subtracted from the observed absorption intensity and the resulting spectrum was normalized with respect to the maximum intensity.

Atomic Force Microscopy (AFM)

The nanostructures formed by self-assembly of the peptide in pure water and the copper salt solutions were characterized by AFM. Approximately 10 μl of sample solution was placed on the surface of a freshly cleaved mica sheet fixed to a steel AFM sample plate. The sample was then covered by a Petri-dish to avoid dust and allowed to settle for 10 minutes to allow the peptide to adhere onto the mica surface. It was then rinsed twice with ~50 μl of pure water to remove any unattached peptides and salt components before being air-dried for 3 hours. Imaging was performed at room temperature on a PicoScan™ AFM (Molecular Imaging, Phoenix, AZ) using the tapping mode. This mode was used in order to reduce sample surface distortion due to tip and sample interactions. All images were acquired using a 225 μm silicon single-crystal cantilever (NCL type, Molecular Imaging, Phoenix, AZ) with a typical tip radius of 10 nm and resonance frequency of ~170 kHz. A scanner with the

maximum scan size of 6 × 6 μm^2 was used. All AFM images were obtained at a resolution of 512 × 512 pixels on a scale of 2 μm × 2 μm. All the peptide fiber widths reported herein were corrected using the deconvolution method reported by Fung *et al.*[21] The actual fiber width W^* can be calculated from the equation $W^* = W - 2\sqrt{H(2R_c - H)}$, where W is the apparent fiber width from the AFM image, H is the height of the fiber and R_c (10 nm) is the AFM tip radius. The dimensions of at least 50 fibers were measured at each concentration of peptide and copper salts to obtain the average fiber widths and heights. Fiber lengths were determined using the point-and-click measurement tool available with the PicoScan software. When a fiber was curved, a series of lines was used to trace the fiber axis and then all the individual line segments were added to yield the fiber length. At least 100 fibers were measured for each solution condition (concentration of peptide and copper salts) to obtain the distribution of the fiber lengths. The frequencies of the fiber length at the following size ranges were determined to generate the distribution histogram: very short fibers (<300 nm), short fibers (300-500 nm), intermediate fibers (500-1000 nm) and long fibers (>1000 nm).

Surface Tension Measurement

The experimental set-up of the Axisymmetric Drop Shape Analysis-Profile (ADSA-P) technique to study the dynamic surface tension of EAK16(II)GGH in pure water and copper salt solutions was described in more detail in an earlier publication.[101] A pendant drop of the peptide solution was formed at the tip of a vertical Teflon needle (0.92 mm inner diameter) connected to a motor-driven micro-syringe (1 ml, release speed of 0.04 ml/s). The sample was placed in a temperature-controlled environmental chamber, saturated with water vapor to maintain consistent humidity. The entire system was placed on a vibration-free table. The images of the pendant drop were magnified by an optical microscope and then captured by a CCD camera before being transferred to a computer. The surface tensions of the samples with pure copper salts and containing peptides were measured for 2

and 3 hours, respectively. During each run, images were acquired at 0.5 s intervals for the first 70 s and then at 20 s intervals for the remaining time. Software was used to digitize the images and generate a profile of the pendant drop. A theoretical curve governed by the Laplace equation of capillarity was then fitted to the profile, generating the surface tension value as a fitting parameter.[218] The standard deviation of the surface tension values obtained was less than 0.2 mJ/m^2.

6.3 Results

6.3.1 Copper Binding Study

The effect of Cu^{2+} on the ^1H NMR spectrum of EAK16(II)GGH was studied to obtain evidence for its binding to the peptide. In the absence of Cu^{2+}, the signal for one of the aromatic protons of histidine appears at 7.10 ppm, as shown in Figure 6.2a. This chemical shift has been previously assigned to the H-δ^2 proton of histidine at pH ~6.0.[236] The other aromatic protons are difficult to identify as a result of their overlapping with the amide protons of the peptide. The addition of the paramagnetic ion Cu^{2+} ($CuCl_2$ or $CuSO_4$) to EAK16(II)GGH causes line broadening of the proton resonance in the amide regions. These regions include NH groups from the peptide backbone, histidine and lysine residues, and the NH_2 of C-terminus. The most affected signal belongs to the H-δ^2 proton of histidine (7.10 ppm). The addition of Cu^{2+} to the solution causes this resonance to broaden significantly (Figure 6.2b and c) and almost disappear. This line broadening is associated with protons close to the paramagnetic ion.[237,238] With such a low level of Cu^{2+} present (0.25 mM), the observation of significant broadening of the resonance of the δ proton of histidine provides evidence for the binding of Cu^{2+} to the histidine residue. In the meanwhile, the selective line broadening of the proton resonance in the amide regions may indicate that some amides in addition to histidine were also involved in the copper binding. The NMR spectra (Figure 6.2) do not vary depending on whether the anion Cl^- or SO_4^{2-} is present.

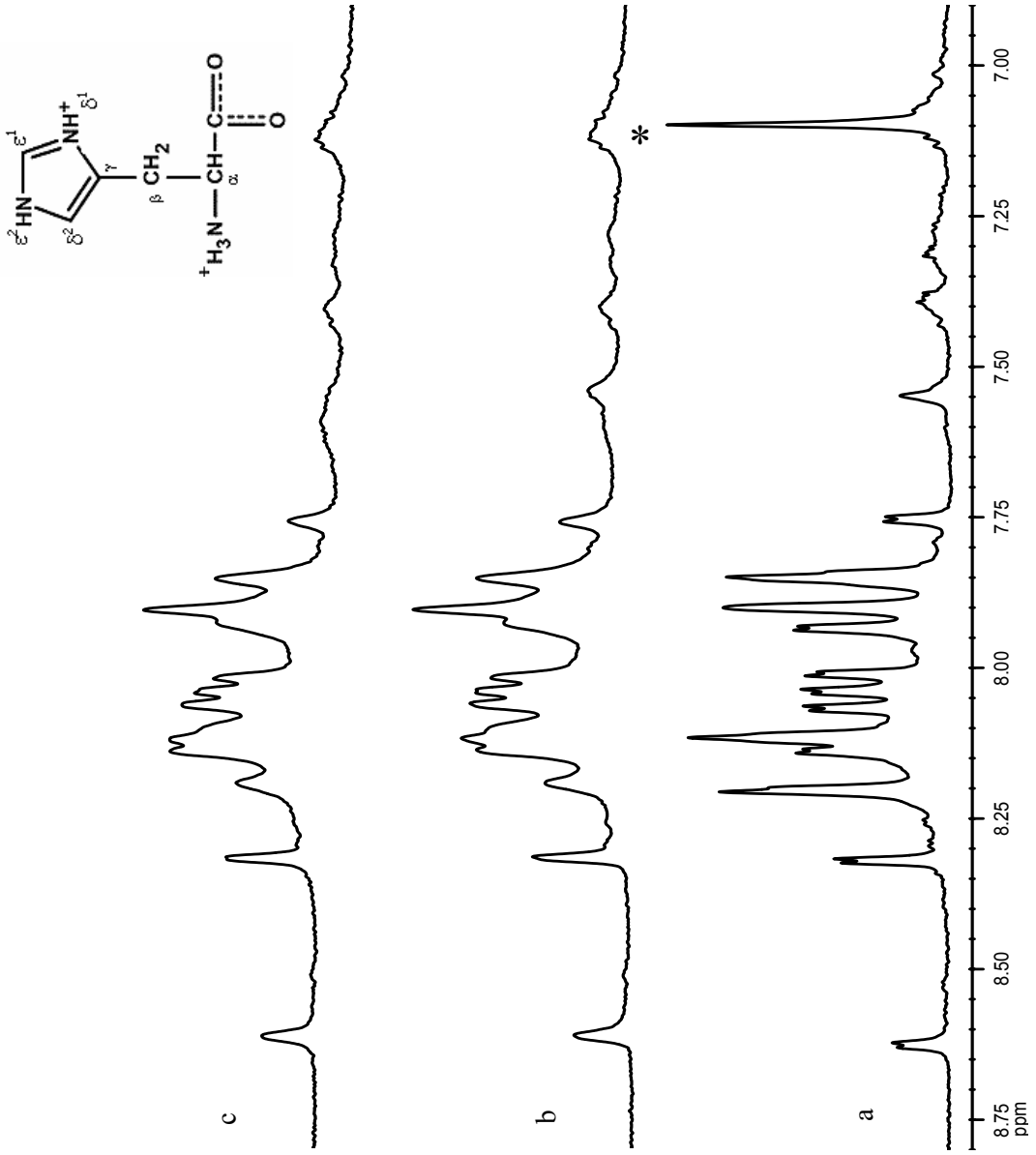

Figure 6.2 ^{1}H NMR spectra of 1.0 mM EAK16(II)GGH at pH 6.0. The lower spectrum (a) corresponds to EAK16(II)GGH, whereas the upper spectrum (b) corresponds to EAK16(II)GGH with 0.25 mM of $CuCl_2$ titrated in and (c) corresponds to EAK16(II)GGH with 0.25 mM of $CuSO_4$ titrated in. * denotes the signal for the H-δ^2 proton of histidine imidazole side chain. The inset is the structure of histidine.

The effect of anions on the amount of copper binding to EAK16(II)GGH was studied via UV-Vis absorption spectroscopy. As shown in Figure 6.3a, the addition of Cu^{2+} led to an increase in absorbance in the spectra between 500 nm to 1000 nm. In this region, the presence of copper led to an absorption band centered at 611 nm for the first 0.19 mM Cu^{2+} and a second feature centered near 800 nm wtih further increasing Cu^{2+} concentration. The latter band is similar to that observed in pure copper chloride solutions, indicating that it is associated with the free (unbound) copper in solution. Thus, the absorption band at ~611 nm is correlated to the absorption band of the copper-peptide complex. This observation provides further evidence of the binding of Cu^{2+} with the peptide EAK16(II)GGH. The plot of the deconvoluted absorption at 611 nm with increasing concentration of $CuCl_2$ and $CuSO_4$ (Figure 6.3b) shows a linear increase of the absorbance up to 0.37 mM of Cu^{2+} before reaching a plateau for both copper salts. The addition of excess Cu^{2+} did not result in a further increase in the absorbance. The presence of different anions (Cl^-, SO_4^{2-}) did not show a significant change in the absorbance of the peptide-copper complexes. This indicates the amount of copper bound to the peptide EAK16(II)GGH was not affected by the presence of different anions, at least to the resolution of the measurement.

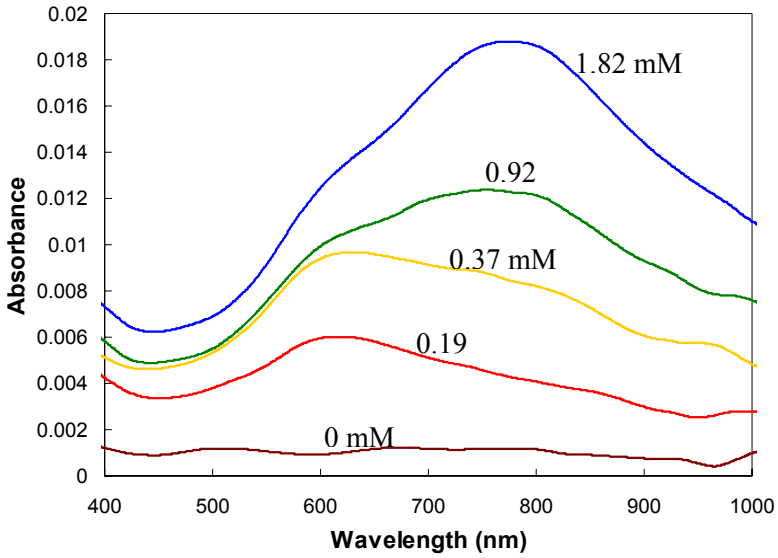

(a)

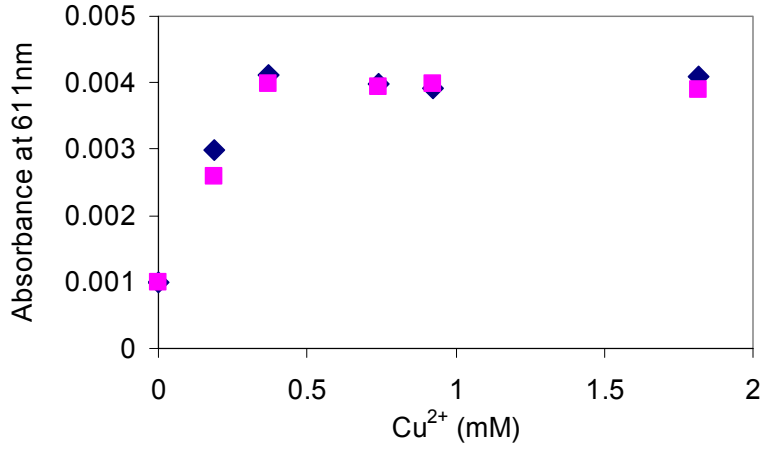

(b)

Figure 6.3 UV-Vis spectra resulting from Cu^{2+} titration of 0.6 mg/ml EAK16(II)GGH (0.3 mM) at pH 6.0. Absorbance spectra of EAK16(II)GGH titrated with increasing concentraions of $CuCl_2$ are shown in (a). A plot of the deconvoluted absorbance at 611 nm versus increasing concentrations of $CuCl_2$ (solid diamond) and $CuSO_4$ (solid square) are shown in (b).

6.3.2 Secondary Structure of EAK16(II)GGH

To study the effect of the different copper salts on the peptide conformation, FTIR spectroscopy was used since it can distinguish between β-sheets and α-helices/random coils within the amide I band (1600 to 1700 cm^{-1}) caused by C=O stretching. Figure 6.4 shows the FTIR spectra of the amide I band for EAK16(II)GGH samples obtained in the absence and presence of the copper salts. Two characteristic bands appear in these spectra. The peak at about 1626 cm^{-1} can be attributed to the formation of a β-sheet structure.[27,239] The assignment of the band at about 1655 cm^{-1} is complicated since absorbance in this region can arise from α-helix and random coil structures.[240] In the absence of copper salts, a prominent peak appears at 1655 cm^{-1}, revealing that α-helix/random coils form a major portion of the secondary structure. However, a distinct peak also occurs at 1626 cm^{-1} and indicates that β-sheets form as well. The addition of the copper salts causes significant changes to the spectra. In the presence of $CuCl_2$ and $Cu(NO_3)_2$, the absorbance at 1655 cm^{-1} diminishes whereas the 1626 cm^{-1} peak increases relative to that obtained in the salt-free solution. This clearly shows that the salts promote the formation of β-sheets over the other structures. The absorbance at 1655 cm^{-1} is slightly higher when $CuCl_2$ is present than when $Cu(NO_3)_2$ is added. As with the other measurements of this study, the behavior observed in the presence of $CuSO_4$ differs considerably from that of the other two salts. The absorbance signal for the α-helix/random coil structure disappears entirely and the peak characteristic of a β-sheet structure becomes sharper and shifts slightly toward lower wavenumbers. A shift of approximately 2 cm^{-1} of the β-sheet peak toward lower frequency relative to that observed in the other spectra may reflect an increase in the number of hydrogen bonds.[241] Based on the ratio of the 1626 cm^{-1} and 1655 cm^{-1} peak heights, the relative content of β-sheet to α-helix/random coil structures formed in the presence of the different anions can be estimated and follows the order $SO_4^{2-} > NO_3^- > Cl^-$. $CuSO_4$ is apparently more effective than the other two salts at promoting the formation of β-sheets to the exclusion of the other secondary structures.

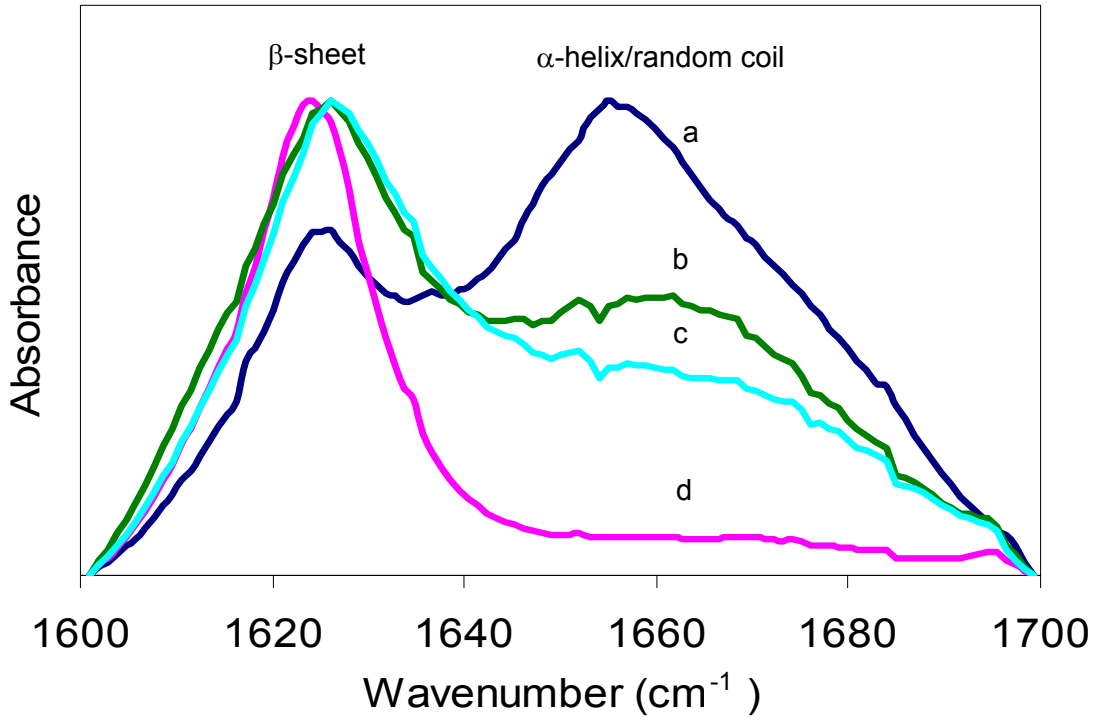

Figure 6.4 FTIR spectra of EAK16(II)GGH film formed with (a) no salt and in the presence of (b) $CuCl_2$, (c) $Cu(NO_3)_2$ and (d) $CuSO_4$

6.3.3 Effect of Anion on Nanostructures

Figure 6.5 (a, b, c and d) shows the AFM images of self-assembled nanostructures in solutions containing 0.025 mg/ml EAK16(II)GGH in the presence and absence of 1.0 mM copper salts. A significant difference in the morphology of the peptide nanostructures is observed depending on the solution composition. In pure water (Figure 6.5a), copper chloride (Figure 6.5c) and copper nitrate (Figure 6.5d) solutions, the peptide tends to form randomly dispersed short fibers and a few small aggregates, whereas elongated fibers are formed in copper sulfate solution (Figure 6.5b). This phenomenon is also observed at a higher peptide concentration of 0.05 mg/ml and over salt concentrations ranging from 0.05 to 10.0 mM (see below). The dimensions of the EAK16(II)GGH

nanofibers shown in the AFM images (Figure 6.5a-d) are summarized in Table 6.1. The peptide forms ribbon-like structures in pure water and copper salt solutions, as reflected in the fiber dimensions (the fiber width is much larger than the fiber height). No significant changes in the fiber width and height are found in the different solutions. The average fiber widths and heights vary from 40 to 50 nm and 0.5 to 1.0 nm, respectively (Table 6.1). Statistical analysis in Figure 6.5e shows that the percentage of fibers that lie in the very short range (< 300 nm) are 92%, 88% and 67% in pure water, 1.0 mM $CuCl_2$ and $Cu(NO_3)_2$ solutions, respectively. However, no fibers in this category are found in 1.0 mM $CuSO_4$ solution. Instead, 94% of fibers formed in this solution have a length longer than 1000 nm. The fiber lengths obtained in the presence of the three copper salts are affected by the anion in the following order: $SO_4^{2-} >> NO_3^- \geq Cl^-$.

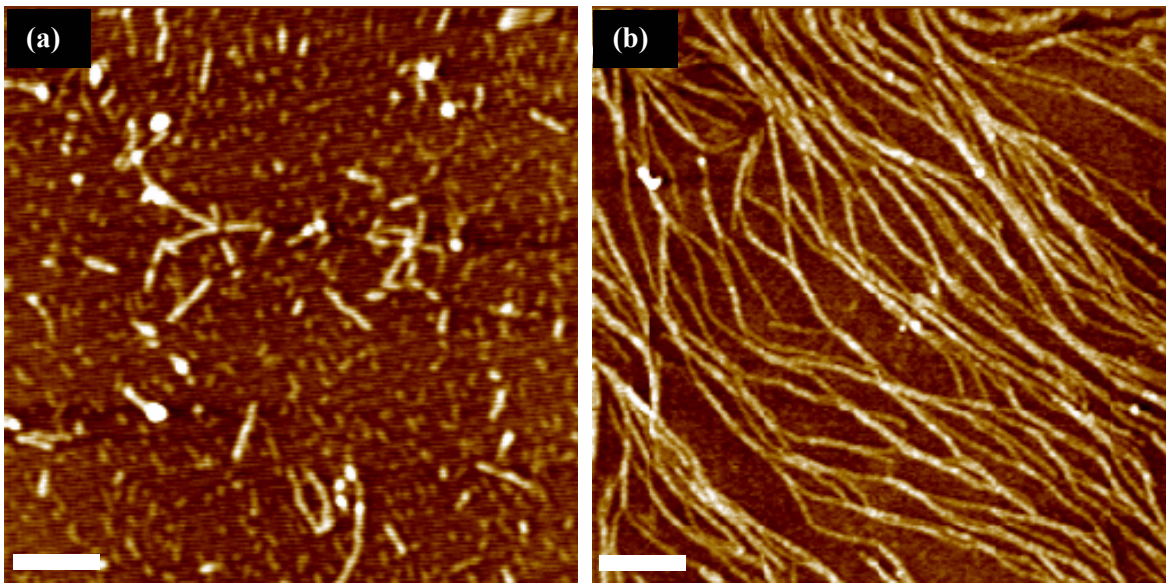

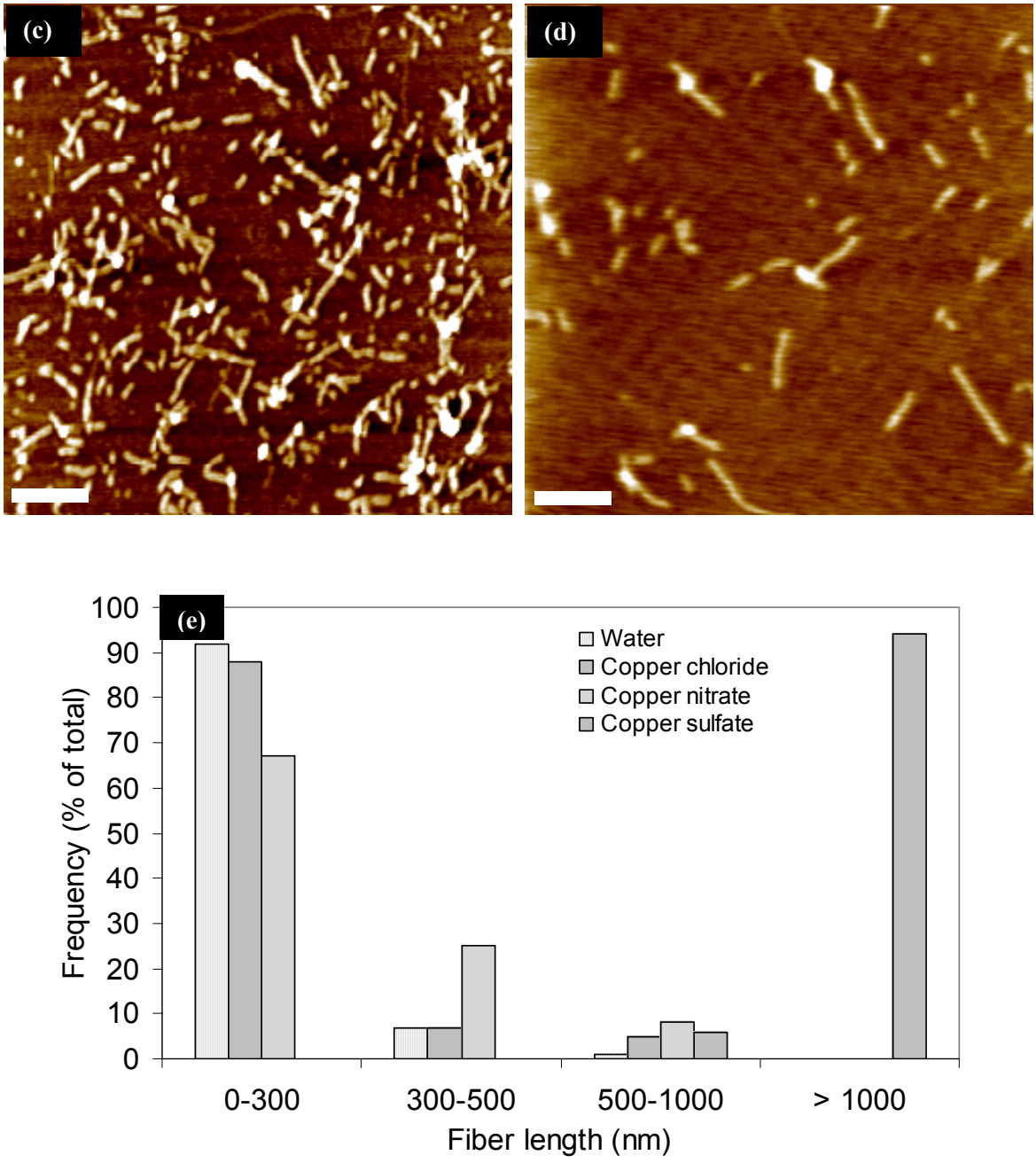

Figure 6.5 AFM images of nanostructures formed in 0.025 mg/ml EAK16(II)GGH solutions containing 1.0 mM salts after 4 h incubation time: (a) no salt, (b) $CuSO_4$, (c) $CuCl_2$, (d) $Cu(NO_3)_2$, and (e) histogram of fiber length analysis. The scale bar in each image corresponds to 300 nm.

To investigate if the observed anion effect applies to salts without copper, we conducted control experiments in which 0.025 mg/ml peptide was dissolved in 1.0 mM Na_2SO_4 and NaCl rather than the corresponding copper salts. As shown in Figure 6.6, EAK16(II)GGH formed short fiber network structures, not long fibers, in the presence of sodium salts (NaCl and Na_2SO_4). There is no significant change depending on the presence of the different anions. This observation showed that the presence of Cu^{2+} is important for the anion effect on the peptide self-assembled nanostructures.

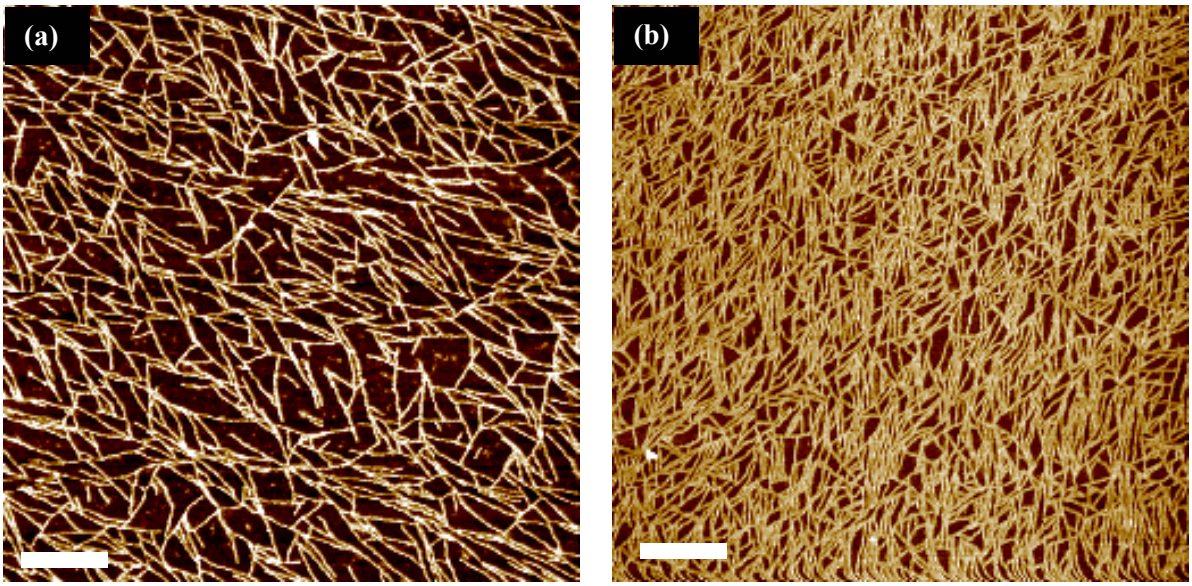

Figure 6.6 AFM images of nanostructures formed in 0.025 mg/ml EAK16(II)GGH with solutions containing 1.0 mM (a) Na_2SO_4 and (b) NaCl after 4h incubation time. Scale bar represents 300 nm

6.3.4 Effect of Salt Concentration on Nanostructures

Figure 6.7 presents the nanostructures obtained in 0.05 mg/ml EAK16(II)GGH solutions in the absence of a copper salt (Figure 6.7a) and at different $CuSO_4$ concentrations (Figure 6.7b-e). The peptide forms short fibers and a few small aggregates in pure water (Figure 6.7a), but longer fibers are observed in the presence of copper sulfate. The fiber length was found to depend on the

concentration of copper sulfate (Figure 6.7b-e). The dimensions of the peptide fibers are shown in Table 6.1. The average widths of the peptide fibers vary from 50 to 60 nm while the average heights vary from 0.5 to 1.0 nm, both independent of copper sulfate concentration. The statistical analysis (Figure 6.7f) shows that 80% of fibers formed in pure water are very short (<300 nm). In 0.05 mM $CuSO_4$ solution, only 12% of fibers are very short, but 82% of fibers have a length ranging from 300 to 1000 nm; few fibers (6%) are longer than 1000 nm. With an increase of copper sulfate concentration from 0.05 mM to 10.0 mM, the population of fibers with a length above 1000 nm increases from 6% to 94%. When the copper sulfate concentration is above 1.0 mM, the peptide forms long fibers almost exclusively.

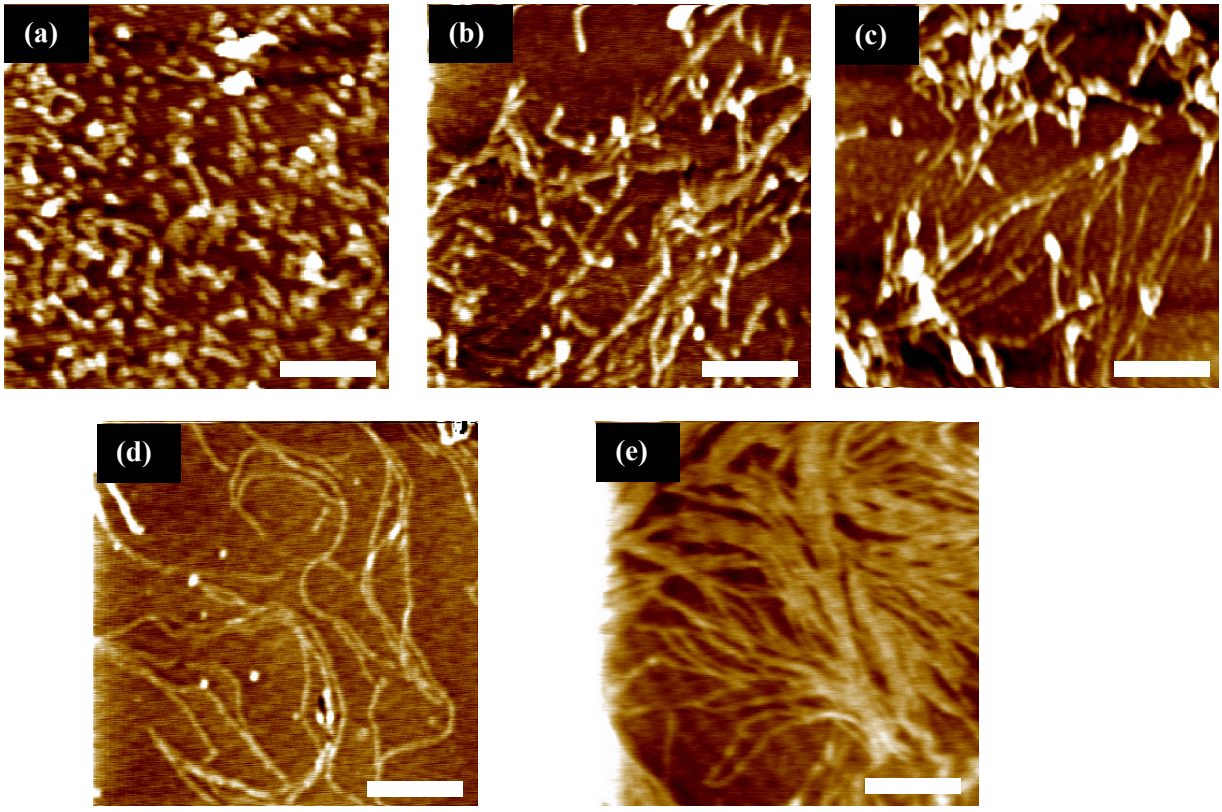

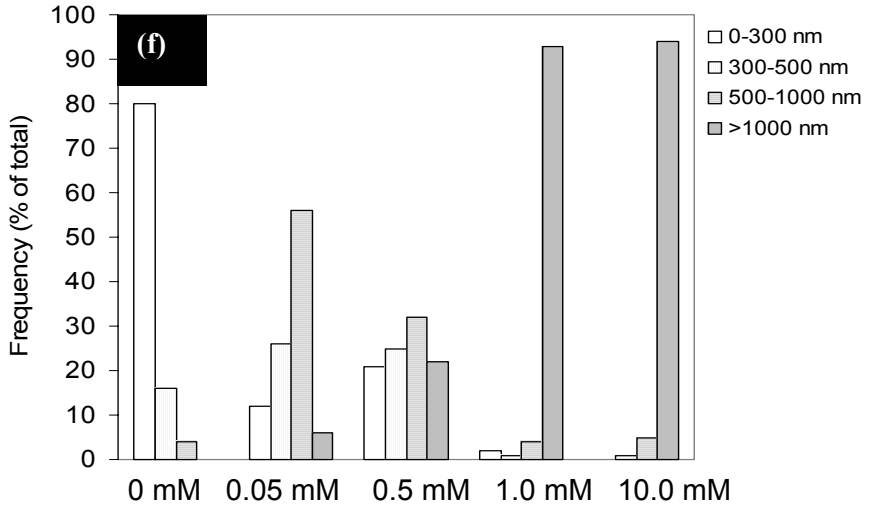

Figure 6.7 AFM images of nanostructures formed in 0.05 mg/ml EAK16(II)GGH containing different $CuSO_4$ concentrations after 4 h incubation time: (a) 0, (b) 0.05 mM, (c) 0.5 mM, (d) 1.0 mM, (e) 10.0 mM, and (f) histogram of fiber length analysis. The scale bar in each image corresponds to 500 nm.

The nanostructures found in 0.05 mg/ml EAK16(II)GGH solutions containing $CuCl_2$ (0.05 mM to 10.0 mM) consist predominately of very short fibers (Figure 6.8a-d). No long fibers (>1000 nm) are observed over the salt concentration range studied. The width and height of these fibers are independent of $CuCl_2$ concentration, as shown in Table 6.1. The fiber width and height are found to be ~60 nm and ~0.5-1.0 nm, respectively. The statistical analysis shows that ~80% of fibers have a length below 300 nm over the $CuCl_2$ concentration range of 0.05 mM to 10.0 mM (Figure 6.8e). Similar behavior is observed in $Cu(NO_3)_2$ solutions, with very short fibers being evident at both 0.05 mM and 10.0 mM concentrations (Figure 6.9a and b). The fiber width and height are found to be ~50 nm and ~0.5-1.0 nm, respectively (Table 6.1). Although the population of short fibers (300-500 nm)

slightly increases at a higher $Cu(NO_3)_2$ concentration of 10.0 mM, the predominant population of fiber length is still below 300 nm at concentrations of 0.05 mM (86%) and 10.0 mM (76%) (Figure 6.9c).

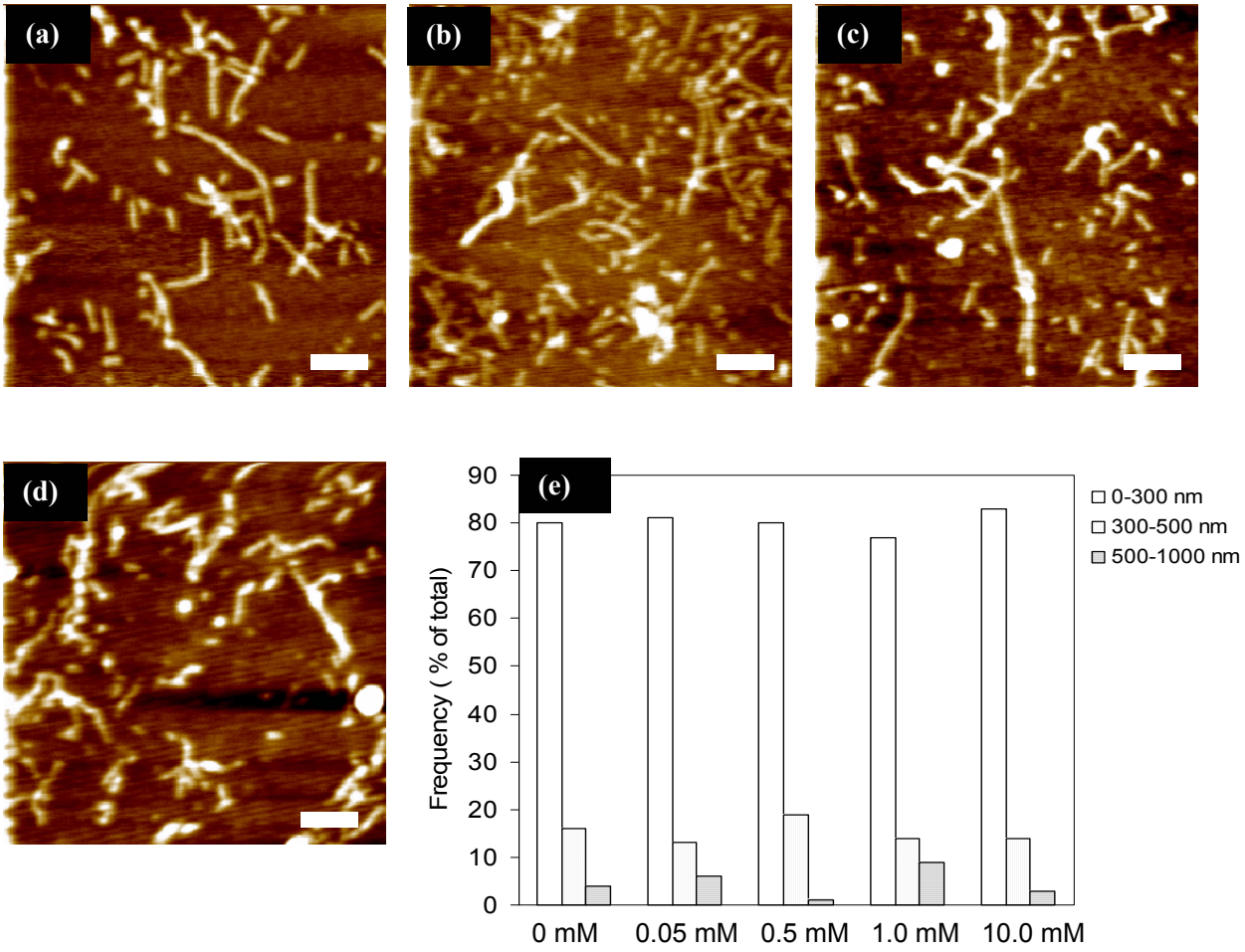

Figure 6.8 AFM images of nanostructures formed in 0.05 mg/ml EAK16(II)GGH containing different $CuCl_2$ concentrations after 4 h incubation time: (a) 0.05 mM, (b) 0.5 mM, (c) 1.0 mM, (d) 10.0 mM, and (e) histogram of fiber length analysis. The scale bar in each image corresponds to 300 nm.

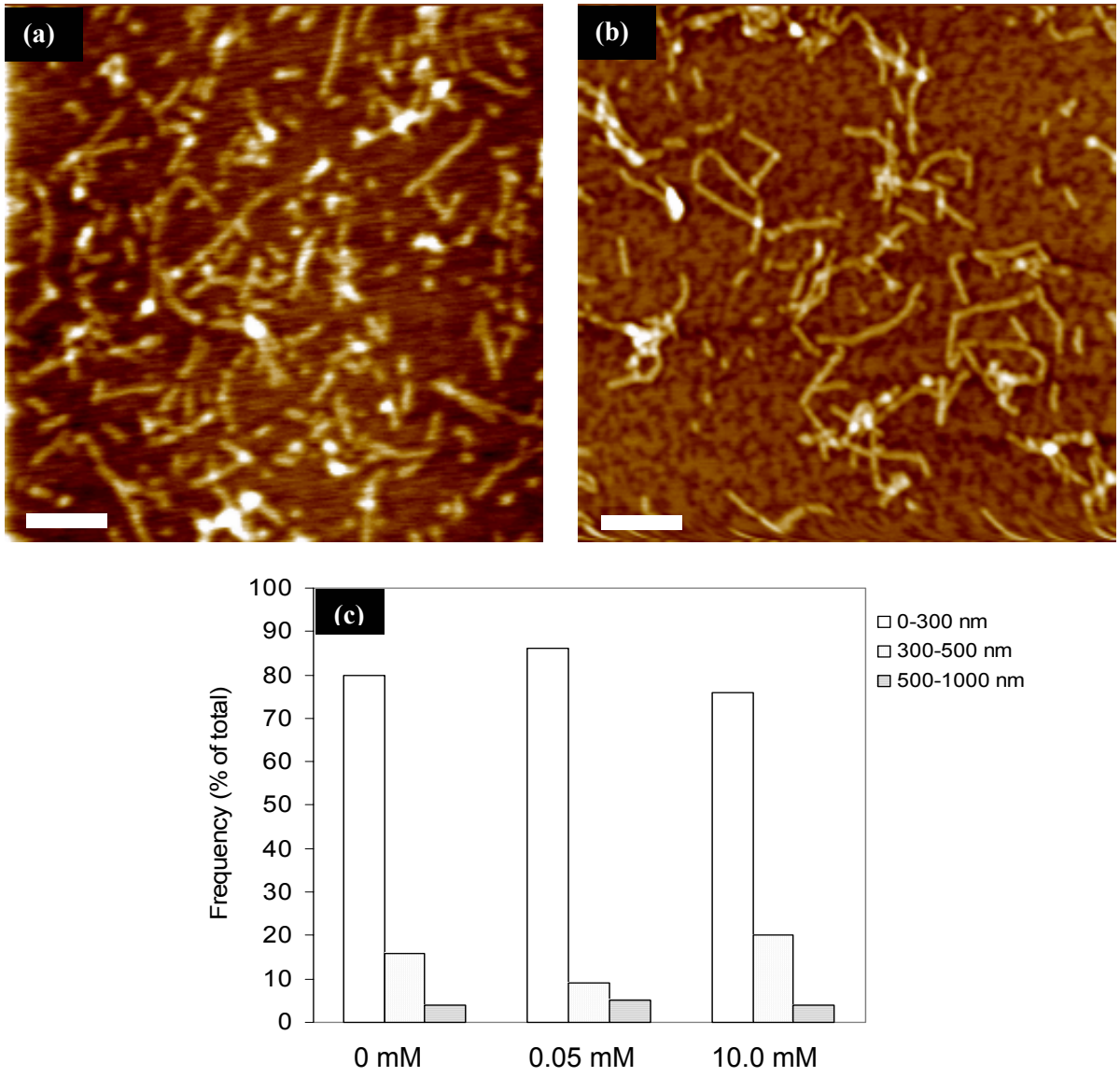

Figure 6.9 AFM images of nanostructures formed in 0.05 mg/ml EAK16(II)GGH containing different $Cu(NO_3)_2$ concentrations after 4 h incubation time: (a) 0.05 mM, (b) 10.0 mM, and (c) histogram of fiber length analysis. The scale bar in each image corresponds to 300 nm.

Table 6.1 The Width (W) and height (H) of EAK16(II)GGH self-assembled nanofibers at various conditions

Peptide (mg/ml)	Water		1.0 mM $CuSO_4$		1.0 mM $CuCl_2$		1.0 mM $Cu(NO_3)_2$	
0.025	W (nm)	H (nm)	W (nm)	H (nm)	W (nm)	H (nm)	W (nm)	H (nm)
	41.5±8.5	1.0±0.20	36.4±5.8	0.5±0.1	38.8±7.0	0.9±0.2	50.0±6.4	0.6±0.1
0.05	56.3±8.3	0.6±0.1						
	Salt (mM)		$CuSO_4$		$CuCl_2$		$Cu(NO_3)_2$	
			W (nm)	H (nm)	W (nm)	H (nm)	W (nm)	H (nm)
	0.05		63.8±14.3	0.6±0.2	59.8±9.3	0.6±0.1	51.5±11.4	0.6±0.1
	0.5		58.2±8.3	0.8±0.3	60.9±9.9	0.4±0.1	–	–
	1.0		51.7±9.4	0.5±0.2	68.1±12.2	0.5±0.1	–	–
	10.0		58.7±7.8	0.4±0.1	63.7±11.2	0.6±0.2	49.7±8.8	0.8±0.2

6.3.5 Effect of Anion on Surface Tensions of EAK16(II)GGH Solutions

Surface tension measurements can give information on the amphiphilicity of the peptide and the nature of its self-assembly in different copper salt solutions. The greater the peptide amphiphilicity, the greater is its activity at the air-liquid interface and the lower its surface tension. Figure 6.10 shows the variation of surface tension with time for 0.05 mg/ml EAK16(II)GGH in salt-free solution and in the presence of 1.0 mM copper salts. The surface tensions of the control samples, including pure water and 1.0 mM copper salt solutions, remain constant (~72 mJ/m^2) over 2 hours. For peptide solutions with and without copper salts, the surface tensions decrease rapidly at the outset before leveling off and slowly approaching equilibrium. The equilibrium surface tension values were calculated based on the average over the last ten points of data. The peptide has an equilibrium surface tension value of 64.1 mJ/m^2 in pure water. The presence of the copper salts causes the surface tension to decrease to a level that depends on the salt type. Once again, the behavior in $CuSO_4$

solution appears to stand out from that observed in the other two copper salt solutions. The equilibrium surface tensions of the peptide in $CuCl_2$ and $Cu(NO_3)_2$ solutions are 62.6 and 62.2 mJ/m^2, respectively, but only 57.6 mJ/m^2 in the presence of $CuSO_4$. These results indicate that the surface activity of peptide self-assemblies in different copper salt solutions depends on the anion type in the following order: $SO_4^{2-} > NO_3^- \geq Cl^-$. Although the equilibrium surface tension value of the peptide in the presence of $CuCl_2$ is only slightly higher than in the presence of $Cu(NO_3)_2$, this trend is consistently observed in repeated experiments.

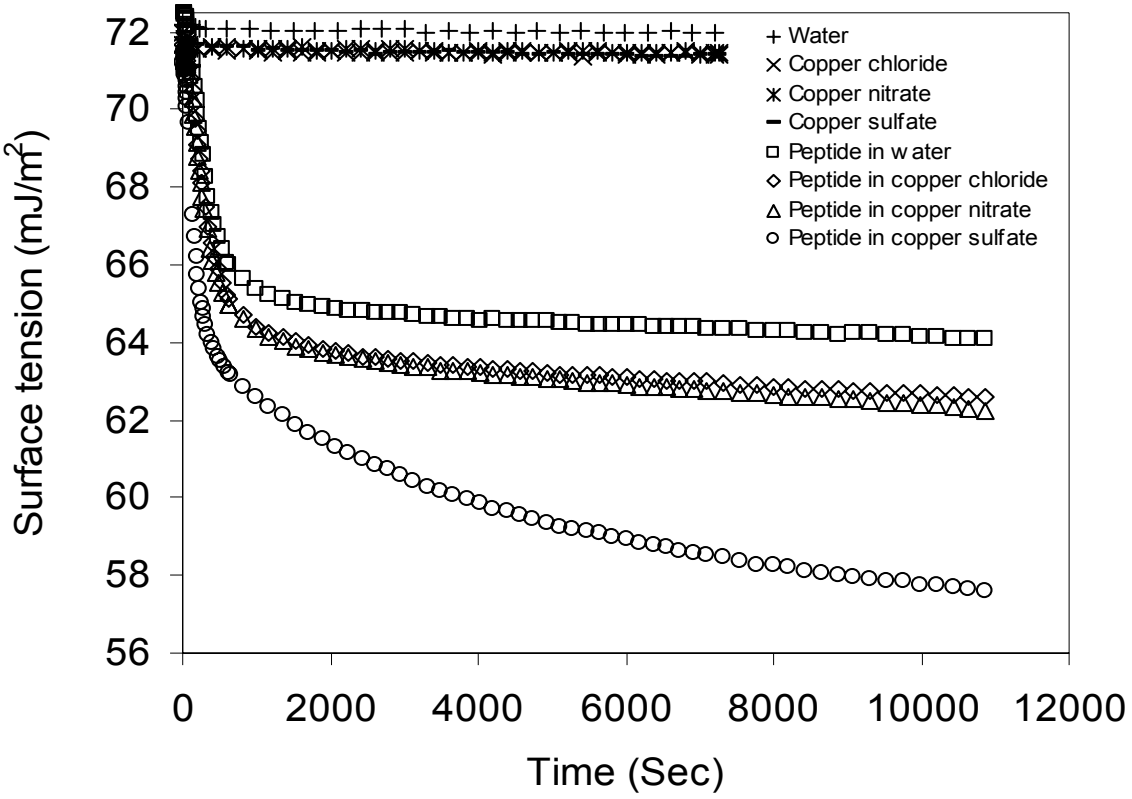

Figure 6.10 Dynamic surface tension of pure water, copper salts, and 0.05 mg/ml EAK16(II)GGH with and without copper salt solutions.

6.4 Discussion

6.4.1 Peptide Design and Secondary Structure in the Absence of Copper Salts

EAK16-II, the molecular motif for EAK16(II)GGH, is an ionic complementary peptide which has been well studied and shown to form a β-sheet structure in pure water.[27] It is expected that the secondary structure of EAK16-II is formed through hydrogen bonding and stabilized by hydrophobic and electrostatic interactions. However, with the addition of the short metal ion binding group GGH at the C-terminus, the peptide EAK16(II)GGH has been found to form a predominantly α-helix/random coil structure (Figure 6.4), suggesting that the GGH group located at the C-terminus affects the secondary structure of the peptide. One possible reason for this phenomenon is that the introduction of the GGH group reduces the ionic complementary character on the C-terminal side of the peptide. This makes it more difficult for the peptide to self-assemble into β-sheets than in the case of the more ionic complementary EAK16-II. Another contributing factor may be the presence of the glycine residue introduced by the modification of the peptide. Since the glycine residue is the shortest among all amino acids, its presence may increase the backbone flexibility of the peptide chain and disrupt the β-sheet secondary structure. It has been reported that the replacement of alanine by glycine can hinder the formation of β-sheets.[11] Although the modification causes a change in the secondary structure, it should be emphasized that the modified peptide can still self-assemble into nanofibers, only to a less extent.

6.4.2 Effect of Anion on the Secondary Structure of EAK16(II)GGH

The secondary structure of a peptide molecule in solution can be affected by the solution composition.[242-245] Our FTIR spectra show that the secondary structure of EAK16(II)GGH is affected by the presence of the copper salts containing different anions (Figure 6.4). In the presence of sulfate, the peptide predominantly forms β-sheets. However, in the presence of chloride and nitrate anions,

the peptide forms a mixture of α-helices/random coils and β-sheets. The observed anion effect on EAK16(II)GGH may be due to the different valence of anions. The divalent sulfate anion may serve as a bridge to link two peptide molecules by interacting with two positively charged lysine residues. Such an intermolecular interaction may bring the two peptide molecules together, promoting the formation of β-sheets. Monovalent anions (i.e., chloride and nitrate) cannot function as bridges and so their primary effect may be to shield the charges on peptide molecules electrostatically. This shielding may still facilitate β-sheet formation, but not to the extent with a "bridging agent" such as sulfate. Therefore, a mixed secondary structure was observed in copper chloride and copper nitrate solutions.

6.4.3 Effect of Anion on the Self-Assembled Nanostructure of EAK16(II)GGH

Our results show that the self-assembled nanostructure of EAK16(II)GGH in aqueous solution depends significantly on the particular anion present. Sulfate can induce long fiber formation, while chloride and nitrate cannot. This phenomenon is observed at different peptide concentrations (0.025 and 0.05 mg/ml) and over salt concentrations ranging from 0.05 to 10.0 mM (Figures 6.5, 6.7-6.9). Anions have been previously shown to increase or decrease the pKa of histidine by 0.1 to 0.3 pH unit depending on the location of histidine on a peptide chain and the type of anion present.[235] A change in the pKa value of histidine could affect the amount of copper binding to the peptide. However, our UV-Vis titration and nuclear magnetic resonance (NMR) results show that the type of anion does not affect the amount of copper binding to the peptide (Figures 6.2 and 6.3). This indicates that the observed anion effect may not be due to differences in the extent of copper binding.

The divalent SO_4^{2-} anion may bridge the peptide molecules through the electrostatic interaction with the positively charged residues from two peptide molecules similar to the role of divalent cations in DNA condensation.[108] Many multivalent cations have been found to be more efficient than monovalent cations in inducing the condensation and fiber formation of DNA and other synthetic

polyelectrolytes.[246,247] It has been reported that when the size of a divalent cation is much smaller than the space between two neighboring negatively charged residues along a polyelectrolyte chain, the primary effect of the divalent cation may not be to electrostatically interact with the charges from these two residues; instead, it is more likely for the cation to interact with one negative residue of one chain and one negative residue of another chain and bring about the onset of condensation.[248] A similar effect may explain the influence of sulfate on the positively charged residues of EAK16(II)GGH. The minimum spacing between two positive residues on EAK16(II)GGH is greater than 7.3 Å (estimated from Chemsketch software without optimization), which is considerably larger than the sulfate ionic radius of 2.9 Å.[249] Thus, it is not likely that the divalent anion can interact with the two neighboring lysine residues on a single peptide. Instead, it may electrostatically interact with one positive lysine residue of one peptide molecule and serve as a sticky point for a positive lysine residue of a second peptide molecule. In this way, sulfate facilitates the peptide molecules to interact with one another. Such intermolecular attraction might greatly favor β-sheet formation of EAK16(II)GGH (Figure 6.4). The extensive β-sheet formation may cause the peptide to form long fibers due to the growth in the direction perpendicular to the β strands or the interaction between β-sheets. On the other hand, monovalent chloride and nitrate anions may not have such a bridging capability and so the peptide secondary structure contains mixed α-helices/random coils and β-sheets in copper chloride and copper nitrate solutions. These mixed structures may prevent long fiber formation and cause the peptide to self-assemble into short fibers and small aggregates, similar to that observed in pure water. A very preliminary model of peptide self-assembly and fiber growth is proposed in Appendix C.

It should be noted that the binding of copper to the peptide may play an important role in the way that the anion affects the peptide nanostructures. The self-assembled EAK16(II)GGH nanostructures formed in sodium salt solutions were similar, regardless of the anion type present as

shown in Figure 6.6. This suggests a close relationship between the binding of Cu^{2+} to the peptide and the effect of anions on the self-assembled nanostructures. We investigated this question further by carrying out experiments to compare the effects of the different copper and sodium salts on the self-assembled nanostructures of EAK16-II, which does not contain a specific copper binding moiety (see Appendix B). Once again, the specific anion present had no effect on the self-assembled nanostructures. These results provide strong support that the copper binding to the peptide is pivotal to the effect of the different anions on EAK16(II)GGH nanostructures.

6.4.4 Surface Activity of Peptide Assemblies in Copper Salt Solutions

The change in the morphology of peptide self-assembled nanostructures due to the presence of the different anions was also studied from surface tension measurements. The peptide solution exhibits a lower surface tension in the presence of sulfate than that of the other two anions. Experiments conducted with the copper salt solutions in the absence of the peptide show that the surface tensions of different salts are very similar to each other and to that of pure water (~72.0 mJ/m^2). The different surface tensions shown in Figure 6.10 are therefore likely due to amphiphilicity changes of the peptide self-assemblies in the presence of the different anions. According to the order of surface tension values of the peptide in different copper salt solutions, the amphiphilicity of the peptide self-assemblies may decrease depending on anion type in the following order: $SO_4^{2-} > NO_3^- \geq Cl^-$. This order correlates well with the variation of the β-sheet content in the peptide secondary structure (Figure 6.4).

A characteristic feature of an EAK16(II)GGH molecule is that most of its hydrophobic (●) and hydrophilic (○) residues are arranged in an alternating pattern ●○●○●○●○●○●○●○●○●●○, except at the GGH end. As discussed previously, such an alternating pattern in a β-strand will result in a unique structure: hydrophilic residues on one side of the peptide chain and hydrophobic residues on the other

side.[250] Thus, β-sheets containing this unique structure are predominantly amphiphilic and tend to move to an air-water interface. The orientation of the β-sheets with the hydrophobic side facing the air and the hydrophilic side directed into the aqueous solution would result in a lower surface tension. On the other hand, since α-helix/random coil structures of EAK16(II)GGH do not have such a unique amphiphilic feature, they may not have the same surface activity as a β-sheet structure does. This last comparison may explain our finding that the order of the surface activity in different copper salts correlates well with the β-sheet content in the secondary structure of peptide self-assembled nanofibers (Figures 6.4 and 6.10).

6.5 Conclusions

EAK16(II)GGH peptide capable of binding with Cu^{2+} has been successfully designed by adding a GGH group to the C-terminus of the peptide EAK16-II. The binding of Cu^{2+} to the histidine group of the peptide has been confirmed by ^{1}H NMR and UV-Vis absorption spectroscopy. The effect of anions (SO_4^{2-}, Cl^- and NO_3^-) in solution on peptide self-assembly was investigated using AFM, surface tension measurement and FTIR spectroscopy. The experimental results suggest that the type of the anion has a significant effect on the EAK16(II)GGH secondary structure, self-assembled nanostructures and surface activity over a range of peptide and salt concentrations. The length of peptide nanofibers, the β-sheet content and the surface activity increase according to the type of the anion present in the following order: $SO_4^{2-} > NO_3^- \geq Cl^-$. The divalent SO_4^{2-} may serve as a bridge linking two peptide molecules resulting in long fiber formation.

Our study showed that the dimension of EAK16(II)GGH self-assembled nanostructures could be controlled by adding copper salts with different types of anions. Sulfate induces long fiber formation, whereas chloride and nitrate cause short fiber formation. This may be important for different applications in nanotechnology, especially metallic nanowire fabrication. By controlling the

dimension of a peptide template, desired dimensions of the fabricated nanowire may be obtained. Furthermore, the successful design of peptide EAK16(II)GGH with the combined properties of fiber formation and metal ion binding capability provides a simple way to create functional biological materials and provide a simple model for metal ion binding proteins such as prion and β-amyloid proteins.

Chapter 7
Original Contributions and Recommendations

7.1 Original Contributions to Research:

Surface-Assisted Peptide Assembly on Mica. In this thesis, the assembly of a model ionic-complementary peptide EAK16-II on hydrophilic mica and hydrophobic HOPG surfaces has been systematically studied. On the mica surface, the growth of peptide nanofibers was monitored in real-time via *in-situ* AFM and growth kinetics of single nanofibers was quantified. In pure water, the average nanofiber growth rate is 0.74 ± 0.40 nm/s. From DLS experiments, nanofiber growth was found to be a surface-assisted phenomenon: nanofibers that have virtually ceased growing in solution begin to grow again once they adsorb onto the surface. This surface-assisted nanofiber growth appears to follow a nucleation and growth mechanism, which involves (i) adsorption of nanofiber "seeds" or fiber clusters formed in stock solution to serve as nuclei and (ii) fiber elongation from the active ends of these nuclei. Such surface-assisted nanofiber growth can be controlled by adjusting the solution pH to regulate both nucleation and growth steps. The amount of nanofiber "seeds" that adsorb on mica decreases as the solution pH increases. Once nuclei have formed, the growth rate of nanofibers in different solutions follows the order: pure water > 1 mM HCl > 1mM NaOH > 10 mM HCl ≈10 mM NaOH ≈ 0. The surface-assisted EAK16-II assembly has many similar characteristics to amyloid fibrillization on surfaces and thereby provides a model to help understand and control surface-assisted fibrillization of disease-related peptides/proteins. In addition, the controllable nanofiber growth may be beneficial to the design and fabrication of functional, supramolecular structures on surfaces.

Surface-Assisted/Directed Peptide Assembly on HOPG. On a hydrophobic HOPG surface, EAK16-II was found to form well-ordered nanofiber patterns with preferential orientations at angles

of 60° or 120° to each other. This orientation resembles the crystallographic structure of the graphite surface. Nanofiber growth on HOPG is also surface-assisted and follows a nucleation and growth mechanism similar to that on mica. Interestingly, this surface-assisted peptide assembly can also be affected by adjusting the solution pH to regulate the adsorption of peptide molecules/nanofibers on HOPG, although the adsorption presumably occurs through hydrophobic interaction in contrast to electrostatic interaction on mica. It was found that the surface-assisted assembly occurs in pure water and basic solutions (1 and 10 mM NaOH), but not in an acidic environment (1 and 10 mM HCl), very different from that on mica. This phenomenon can be explained by the pH-dependent hydrophobicity of the peptides revealed by surface tension measurements. In acidic solutions, the peptide has a surface tension value very close to pure water (~72 mJ/m^2), indicating that the peptide is more hydrophilic and less likely to adsorb on hydrophobic HOPG surface. However, the peptide has lower surface tensions in pure water and basic solutions (<65 mJ/m^2), suggesting that it is more hydrophobic and likely to adsorb on HOPG.

Mechanical Force-Induced Peptide Assembly and Fabrication of Patterned Peptide Nanostructures on Surfaces. An interesting finding in EAK16-II assembly is the mechanical force-induced nanofiber growth by a tapping AFM tip on both mica and HOPG surfaces. The force applied by the AFM tip can be controlled by adjusting the scan area and the scan speed. This force-induced nanofiber growth occurs when the tip first cuts the adsorbed nanofibers into small segments that serve as seeds for new nanofiber growth. This finding allows one to locally grow nanofibers that densely cover desired regions of the surface. In addition, breakage of the peptide nanofibers using such a method combined with adjustment of the solution pH (in acidic solutions) provides a new AFM lithography method to fabricate patterned peptide nanostructures at desired locations on a surface. These patterned peptide nanofibers could serve as templates to immobilize proteins/enzymes, DNA and cells for biomolecular sensing and other biomedical applications.

Surface Modification of Hydrophilic and Hydrophobic Surfaces Using Peptide Assemblies. In order to apply ionic-complementary peptides for surface modification applications, the work was extended to study the wettability and stability of the peptide-modified mica and HOPG surfaces. After modification with EAK16-II, the water contact angle of a mica surface increases from <10° to 20.3 ± 2.9°. However, the hydrophobicity of the HOPG surface is significantly reduced as the water contact angle decreases from 71.2 ± 11.1° to 39.4 ± 4.3°. The EAK16-II-modified mica surface is stable in acidic solution but not in alkaline solution, while the modified HOPG surface is stable in both acidic and alkaline solutions for at least 10 hours. This work shows the potential of using ionic-complementary peptides to modify both hydrophobic and hydrophilic surfaces and function as possible new surface modifiers in addition to traditional thiol-gold technology.

The controllable peptide assembly on the surface has an exciting potential application in constructing biocompatible electrodes for biosensors. Preliminary results showed that the EAK16-II modified HOPG electrode can successfully immobilize the model GOx enzyme to fabricate enzymatic biosensors.

Ionic-Complementary Peptides for Metallic Nanowire Fabrication. Another potential application of EAK16-II assembly on surfaces is to fabricate one-dimensional metallic nanowires. This can be achieved by first giving metal ion binding capability to the peptide by adding a metal ion (Cu^{2+}) binding motif GGH to the C-terminus. This newly designed peptide EAK16(II)GGH was shown to bind with Cu^{2+} through the histidine group while maintaining its ability to self-assemble into nanofibers. Further studies of the effect of various electrolytes on the peptide assembly showed that anion type (SO_4^{2-}, Cl^- and NO_3^-) significantly affects the peptide secondary structure, self-assembled nanostructure and surface activity over a range of peptide and salt concentrations. The length of peptide nanofibers, β-sheet content and surface activity increase according to anion type in the following order: $SO_4^{2-} > NO_3^- \geq Cl^-$. This effect may be due to the fact that divalent SO_4^{2-} can serve as

a bridge linking two peptide molecules, facilitating β-sheet formation and leading to formation of long fibers. The control of nanofiber length by adding copper salts with different anions may enable better control of the fabrication of metallic nanowires with desired dimensions. Furthermore, this successful peptide design could serve as a simple model to study metal ion binding proteins such as prions and β-amyloid proteins.

7.2 Recommendations

Recommended future studies regarding the fundamental understanding and the potential applications of peptide assembly on surfaces include the following:

1. Other types of surfaces in addition to negatively charged mica and hydrophobic HOPG should be studied to determine if the surface effect on peptide assembly investigated in this study is a general phenomenon and to develop other surface modification applications. Example surfaces include gold, silicon and GaAs in order to examine if ionic-complementary peptides can assemble and modify semiconducting and metallic surfaces. Different surface lattices may direct peptide assembly into various patterned nanostructures. In addition, the formation of biocompatible coatings on a semiconductor surface may aid in the development of novel implants and (bio)sensors.

2. Effects of salts (including salt types and ionic strength) and organic solvents on peptide assembly in solution and on surfaces are important topics to provide further understanding and control of peptide nanostructure formation. The solvent selection should consider the (i) peptide solubility in the solvent and (ii) affinity of the solvent to the surfaces.

3. Determination of the detailed kinetics of ionic-complementary peptide assembly is still a large hurdle due to the complexity of self-assembling systems. A primary difficulty is to accurately measure the concentration of peptide monomers and assemblies in solution. This is further complicated by the fact that the peptide powders, in their as-purchased form, already contain some

peptide assemblies formed during synthesis. To overcome such a challenge, one should develop a strategy to separate peptide aggregates from the monomers to obtain the monomeric peptide concentration or study the assembly kinetics from pure peptide monomers. Filtration with a small pore size filter or ultracentrifugation may serve this purpose. Another approach combined with could be to modify the peptide sequence (e.g., replacing Ala to Trp) to give detectable signals (e.g., UV absorption or fluorescence) that can be used to measure the peptide concentration. The kinetic model could be adapted from knowledge of the well-studied amyloid fibril growth or supramolecular polymerization.[251,252]

4. In addition to the mechanical force-induced peptide assembly on surfaces investigated in this study, the effect of mechanical force on peptide assembly in solution is another interesting topic. One approach is to monitor the assembly kinetics under conditions of well-controlled mechanical stirring. This work has already been initiated in our group. Studies on the detailed characterization and comparison of the assemble nanostructures with/without mechanical stirring are underway.

5. Although not discussed in the main body of the thesis, the potential application of ionic-complementary peptides in molecular (bio)sensing has been preliminarily studied, using EAK16-II as the model peptide to modify the graphite electrode for immobilizing GOx enzyme (see Appendix A). Questions concerning the detection limit, selectivity, interferences, long-term reliability and storage stability of the fabricated biosensor should be further addressed. Furthermore, optimization of biosensor fabrication process should be done to enhance the biosensor performance. This approach can be applied to develop other enzyme biosensors in situations where ionic-complementary peptides are advantageous to other surface modifiers. In addition, since the fabricated glucose biosensor functions similarly to an anode in a biofuel cell, ionic-complementary peptides may have application to this field as well.

6. The designed peptide EAK16(II)GGH has shown promise for metallic nanowire fabrication with its ability to bind with metal ions and form controllable one-dimensional nanostructures. The next step would be to reduce the bound metal ions to produce metallic nanowires either by chemical reduction or electrochemical reduction. This should be followed by characterization and further optimization of the electronic properties of the metallic nanowires so formed.

Appendix

A Potential Application of the Ionic-Complementary Peptide in (Bio)Molecular Sensing

Understanding and controlling surface-assisted peptide assembly is beneficial for the design and construction of many biocompatible devices, such as immunosensors[253] and enzyme biosensors.[254] Such devices often require surface modification to immobilize biomolecules on various conducting matrices. The surface modifiers should contain reactive groups to immobilize biomolecules, enhance the stability and maintain the activity of the immobilized proteins/enzymes and promote electron transfer from the proteins/enzymes to the electrode (for amperometric sensors). Self-assembling peptides could be an ideal material for these purposes. We have utilized EAK16-II assembled nanostructures to modify an electronically conductive highly ordered pyrolytic graphite (HOPG) electrode. An amperometric enzyme biosensor was successfully fabricated using this EAK16-II modified electrode by immobilizing a model enzyme of glucose oxidase (GOx) to the carboxylate groups on EAK16-II. The immobilized GOx exhibits good catalytic activity upon the addition of glucose. Further detailed studies of peptide-modified electrodes as biosensors will be discussed in following sections.

A.1 Preparation of Enzyme Electrode

100 μl 0.5 mg/ml EAK16-II stock solution was injected onto the freshly cleaved HOPG electrode (1.44 cm^2) and immobilized for overnight, in order to fabricate EAK16-II-modified electrode. This EAK16-II-modified electrode was washed three times with pure water to remove the unattached EAK16-II. The carboxylic groups of EAK16-II on the electrode were then activated by 200 ml 50 mM phosphate buffer (pH 5.5) containing 2 mM EDC and 5 mM NHS for 1 h at room temperature. In this step, EDC converts the carboxyl group into a reactive intermediate, which is susceptible to attack

by amines, and amide bonds then form between the enzyme molecules and glutamic acids. After the activation, the electrodes were rinsed with phosphate buffer three times and immediately placed with 200 ml 50 mM phosphate buffer (pH 5.5) containing 1 mg/ml GOx (EC 1.1.3.4 type X-S, from *Aspergillus niger*, purchased from Sigma) overnight at 4 °C. The enzyme electrode was then rinsed with phosphate buffer (pH 7.0) and used immediately. Figure A1 shows this activation reaction process.

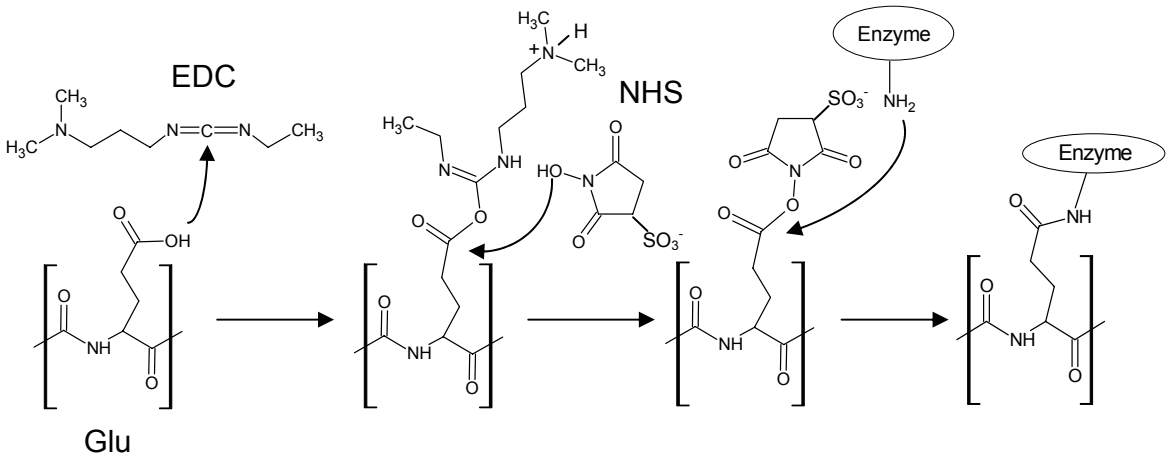

Figure A1. The covalent attachment of an enzyme GOx to the glutamic acid residue of EAK16-II using 1-ethyl-3-(3-dimethylaminopropyl) carbodiimide (EDC) and n-hydroxysuccinimide (NHS).[255]

A.2 Electrochemical Measurements

Cyclic voltammetry was carried out in a conventional three-electrode configuration, with GOx-immobilized-EAK-modified HOPG electrode (GOx/EAK/HOPG, geometric area of 1.44 cm^2) as the working electrode, a platinum wire as the auxiliary electrode, and Ag/AgCl (3M NaCl) as reference electrode. The electrolyte was 100 mM phosphate buffer containing 2 mM ferrocenecarboxylic acid (FCA) and various concentrations of glucose ranging from 0 to 20 mM (diluted from stock solution

prepared at least 24 h prior to use for mutarotation to occur). The acitivity of immobilized GOx was tested by measuring the current response to glucose.

A.3 Electrochemical Characterization of EAK16-II-Modified HOPG Electrode

Figure A2 shows the cyclic voltammograms (CV) of 1.0 mM $K_3Fe(CN)_6$ on the bare HOPG and EAK/HOPG electrodes at a scan speed of 2 mV/s. The CVs of bare HOPG and EAK16-II-modified HOPG show the similar well-behaved response characteristic of the ferricyanide-ferrocyanide redox couple, indicating that the presence of EAK16-II nanofiber coatings does not block the electron transfer significantly at a scan speed of 2 mV/s.

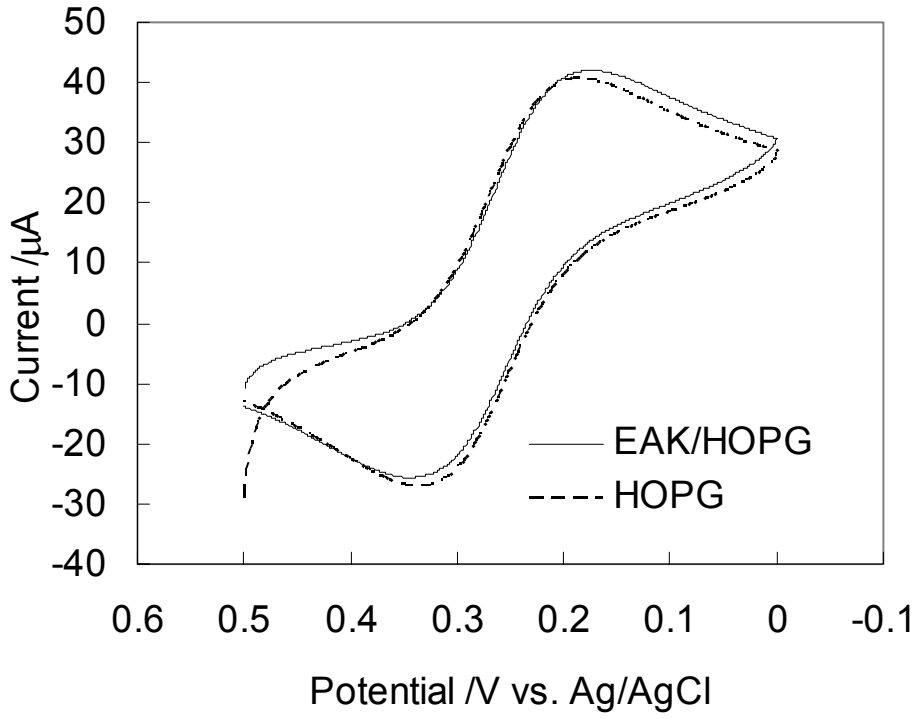

Figure A2. Cyclic voltammograms of 1.0 mM $K_3Fe(CN)_6$ on bare HOPG (dashed line) and EAK16-II nanofiber modified HOPG surface (solid line). Scan rate = 2 mV/s, electrode area = 1.44 cm^2.

A.4 Electrocatalytic oxidation of glucose

Figure A3 shows the CVs of a GOx-immobilized EAK/HOPG electrode in 100 mM potassium phosphate buffer (pH 7.0) containing 0.2 mM ferrocenecarboxylic acid (FCA, mediator)[256] in the absence and presence of 10 mM glucose. In the absence of glucose, the characteristic and well-behaved redox response of FCA is observed (Figure A3, dotted line). In the presence of glucose, an electrocatalytic anodic current is observed (Figure A3, solid line), indicating that GOx molecules are immobilized on the surface and maintain their activity.[257]

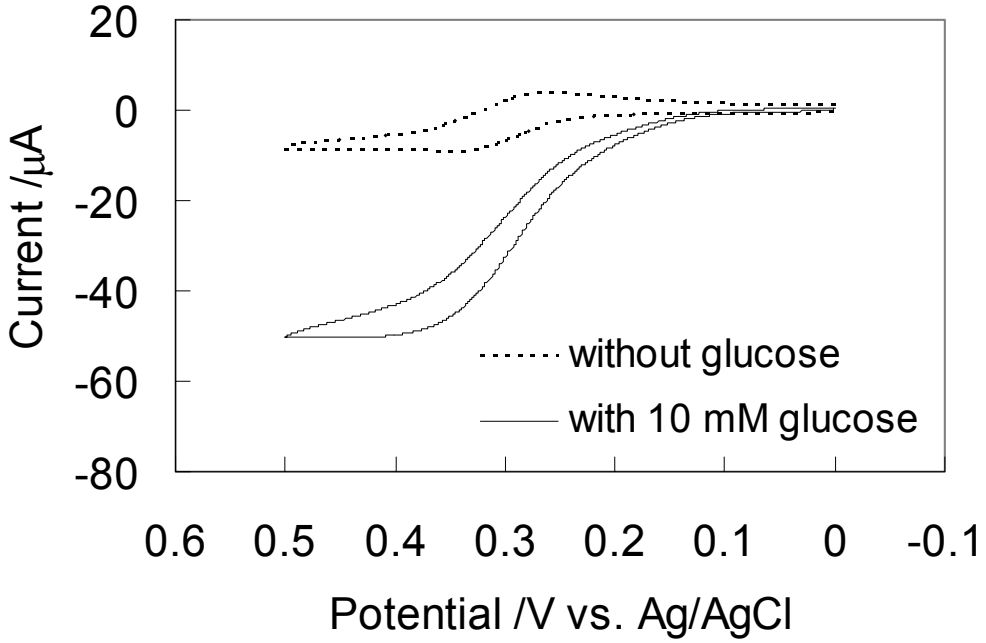

Figure A3. Cyclic voltammograms of a GOx-immobilized EAK/HOPG electrode in 100 mM potassium phosphate buffer (pH 7.0) containing 0.2 mM FCA before (dotted line) and after (solid line) the addition of 10 mM glucose. Scan rate = 2 mV/s, electrode area = 1.44 cm^2.

B Effect of Copper and Sodium Salts on the Self-Assembled Nanostructures of EAK16-II

EAK16-II solutions were prepared at concentrations of 0.02 mg/ml (12 μM) or 0.05 mg/ml (29 μM) with 1.0 mM various copper and sodium salts. All peptide solutions were stored at 4 °C for 4 hrs before use.

The peptide EAK16-II does not contain the specific copper binding group GGH. In the presence of the different copper salts, there is no significant difference in the peptide nanostructures, as shown in Figure B1a-c. In the presence of sodium salts (NaCl and Na_2SO_4), EAK16-II formed similar fiber network structures (Figures B1d and e). Comparing with the copper salt effect on the peptide EAK16(II)GGH, this shows that the presence of a copper binding motif and copper ions are important for the anion effect on the peptide self-assembled nanostructures.

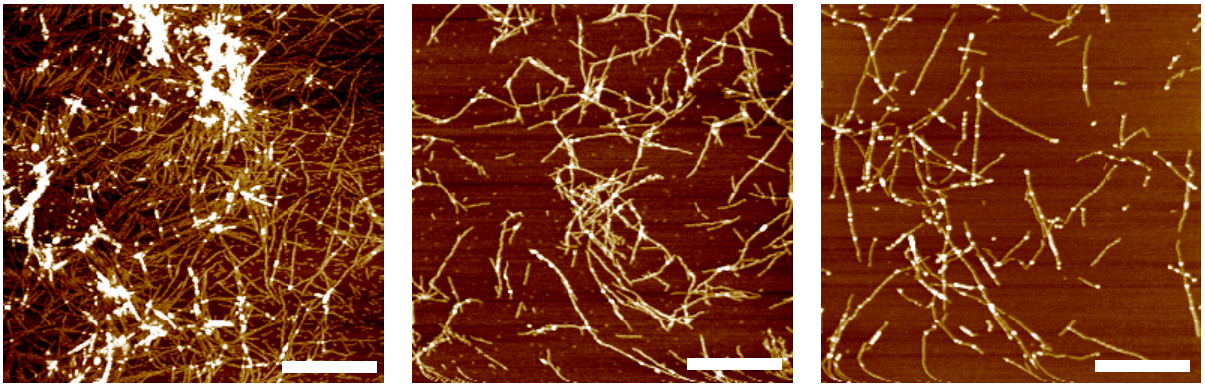

(a) (b) (c)

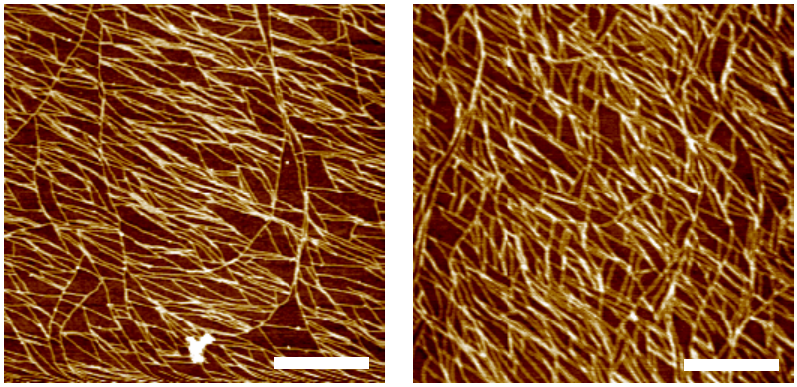

(d) (e)

Figure B1 AFM images of 0.02 mg/ml EAK16-II with 1.0 mM of the copper salts $CuSO_4$ (a), $CuCl_2$ (b), $Cu(NO_3)_2$ (c) and 0.05 mg/ml EAK16-II in 1.0 mM Na_2SO_4 (d) and 1.0 mM NaCl (e) after 4 h incubation time. Scale bar represents 500 nm.

C Proposed Self-Assembly Model of EAK16(II)GGH in Copper Salt Solutions

From the experimental results, a preliminary self-assembly model of EAK16(II)GGH in copper salt solutions was proposed in Figure C1. The two adjacent peptide molecules could be linked by a divalent SO_4^{2-} interacting with two lysine residues, which enhances the β-sheet formation through hydrogen bonding between two peptide backbones (Figure C1a and b). The red dotted lines indicate the hydrogen bonding between two adjacent peptide backbones. The β-sheets could be either parallel or anti-parallel. In these arrangements, the hydrophilic residues (E and K) are on one side of the β-sheet while the hydrophobic residues (A) are on the other side. In this case, two β-sheets could stack together either through electrostatic interaction or hydrophobic interaction, although the latter would be more likely to occur in the aqueous environment, as shown in Figure C1c. In this model, it is speculated that the peptide strands lie perpendicular to the long axis of the fiber (fiber growth direction). In the presence of the various copper salts, divalent SO_4^{2-} tends to induce long fiber formation while monovalent Cl^- and NO_3^- promote short fiber formation (Figure C1d). It should be emphasized that the proposed model of peptide self-assembly is very preliminary and there is little

evidence to support this model at current stage. Future experiments, such as solid-state NMR and x-ray fiber diffraction and so on, need to be done to verify the model.

(a)

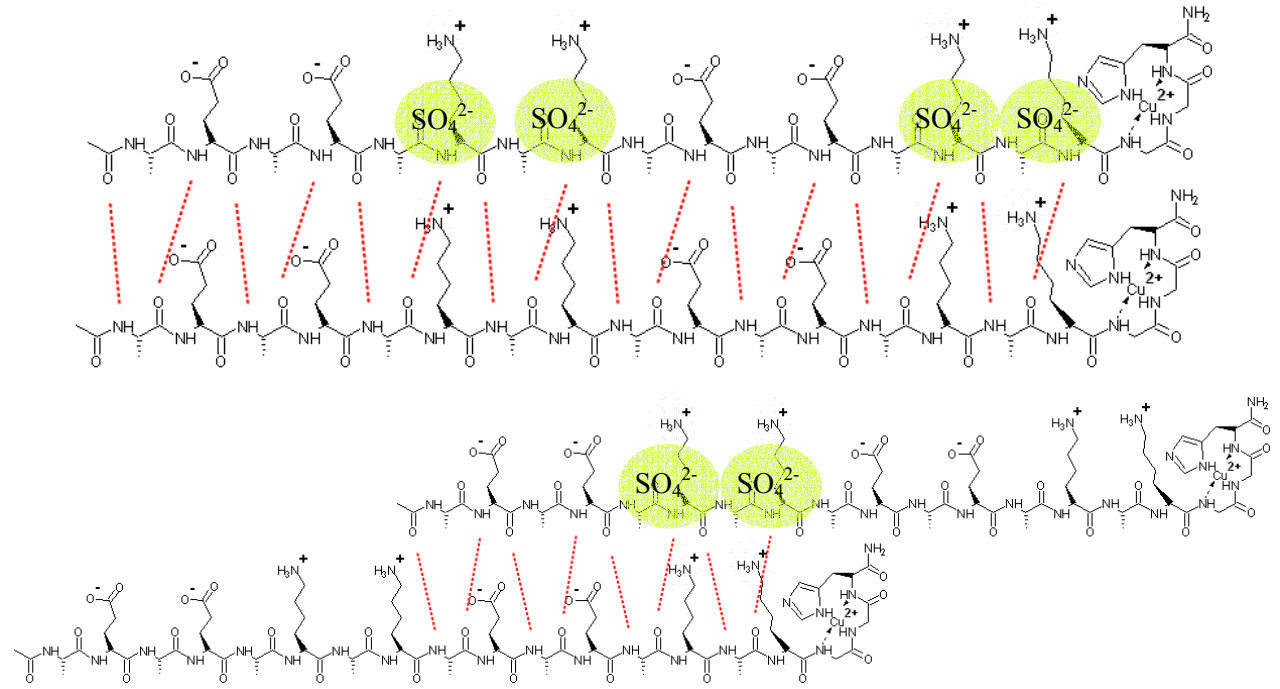

(b)

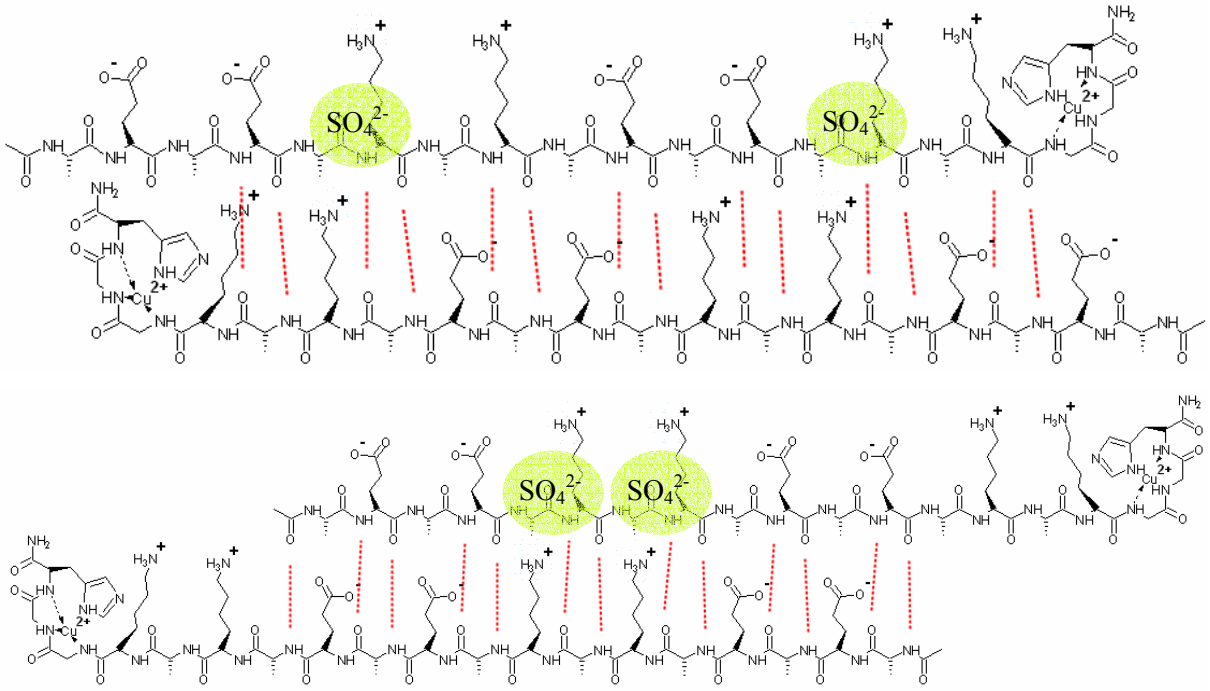

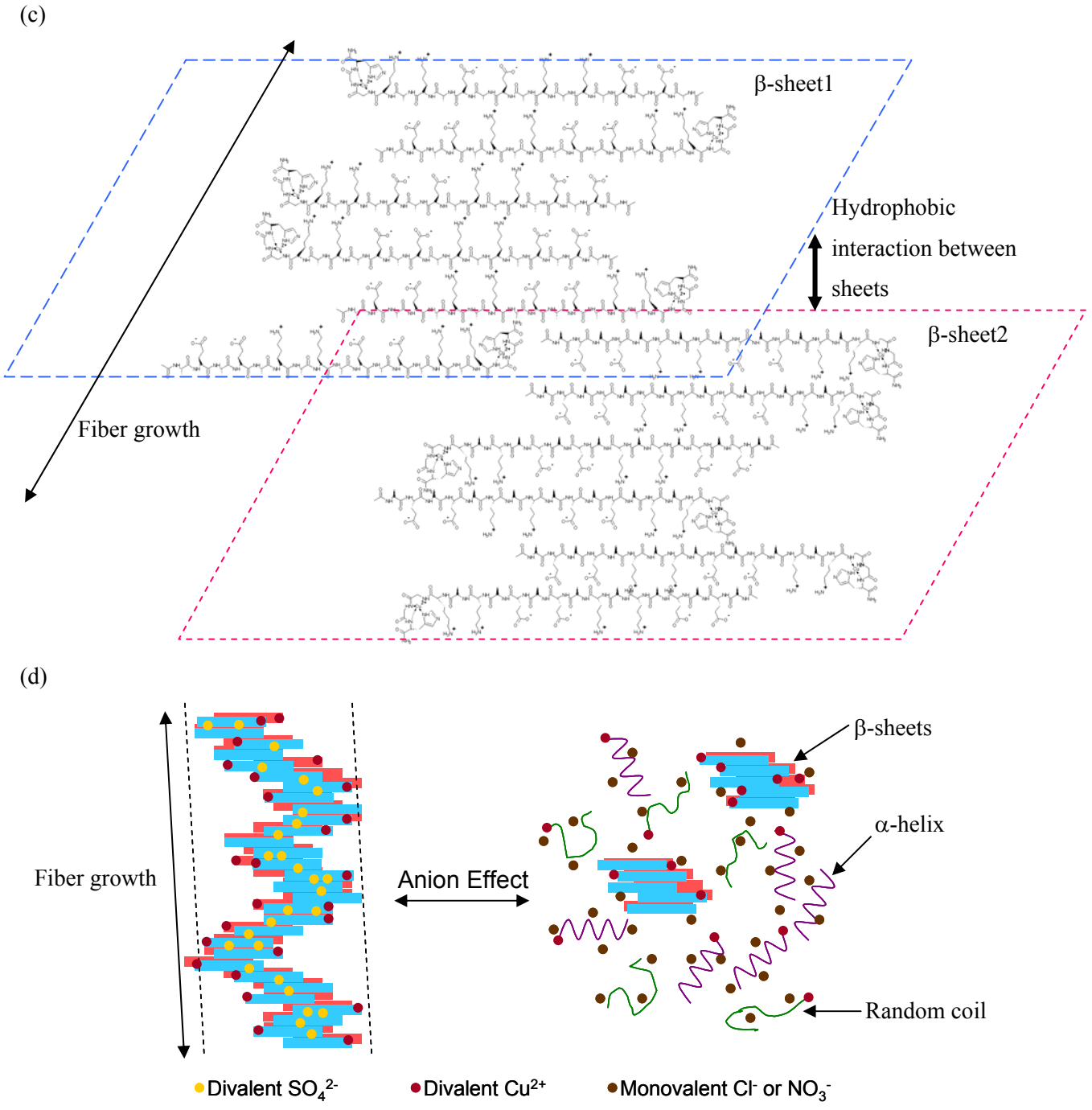

Figure C1 Proposed model of EAK16(II)GGH self-assembly

Reference List

1. Zhang, S. in *Encyclopedia of materials: science and technology*; Buschow, K. H. J.; Cahn, R. W.; Hemings, M. C.; Ilschner, B.; Kramer, E. J.; Mahajan, S., Eds.; Elsevier: Oxford, 2001; p 5822.

2. Service, R. F. *Science* **2001,** *294*, 2442-2443.

3. Aizenberg, J.; Black, A. J.; Whitesides, G. M. *Nature* **1999,** *398*, 495-498.

4. Service, R. F. *Science* **2002,** *295*, 2398-2399.

5. Schmidt, O. G.; Eberl, K. *Nature* **2001,** *410*, 168.

6. Whitesides, G. M.; Mathias, J. P.; Seto, C. T. *Science* **1991,** *254*, 1312-1319.

7. Hartgerink, J. D.; Beniash, E.; Stupp, S. I. *Proc. Natl. Acad. Sci. USA* **2002,** *99*, 5133-5138.

8. Zhang, S. *Nat. Biotech.* **2003,** *21*, 1171-1178.

9. Stefani, M.; Dobson, C. M. *J. Mol. Med.* **2003,** *81*, 678-699.

10. Murphy, R. M. *Annu. Rev. Biomed. Eng.* **2002,** *4*, 155-174.

11. Petty, S. A.; Adalsteinsson, T.; Decatur, S. M. *Biochemistry* **2005,** *44*, 4720-4726.

12. Depace, A. H.; Weissman, J. S. *Nat. Struct. Biol.* **2002,** *9*, 389-396.

13. Li, Y.; Tseng, Y. D.; Kwon, S. Y.; d'Espaux, L.; Bunch, J. S.; McEuen, P. L.; Luo, D. *Nat. Mater.* **2004,** *3*, 38-42.

14. Um, S. H.; Lee, J. B.; Park, N.; Kwon, S. Y.; Umbach, C. C.; Luo, D. *Nat. Mater.* **2006,** *5*, 797-801.

15. Mao, C.; Sun, W.; Seeman, N. C. *J. Am. Chem. Soc.* **1999,** *121*, 5437-5443.

16. Ding, B.; Sha, R.; Seeman, N. C. *J. Am. Chem. Soc.* **2004,** *126*, 10230-10231.

17. Liu, D.; Wang, M.; Deng, Z.; Walulu, R.; Mao, C. *J. Am. Chem. Soc.* **2004,** *126*, 2324-2325.

18. Yurke, B.; Turberfield, A. J.; Mills Jr, A. P.; Simmel, F. C.; Neumann, J. L. *Nature* **2000,** *406*, 605-608.

19. Simmel, F.; Yurke, V. *Phys. Rev. E* **2001,** *63*, 041913: 1-5.

20. Li, H.; Park, S. H.; Reif, J. H.; LaBean, T. H.; Yan, H. *J. Am. Chem. Soc.* **2004,** *126*, 418-419.

21. Fung, S. Y.; Keyes, C.; Duhamel, J.; Chen, P. *Biophys. J.* **2003,** *85*, 537-548.

22. Yang, H.; Pritzker, M.; Fung, S. Y.; Sheng, Y.; Wang, W.; Chen, P. *Langmuir* **2006,** *22*, 8553-8562.

23. Haldar, D.; Banerjee, A.; Drew, M. G. B.; Das, A. K.; Banerjee, A. *Chem. Commun.* **2003,** 1406-1407.

24. Matsui, H.; Gologan, B.; Douberly Jr, G. E. *Eur. Phys. J. D* **2001,** *16*, 403-406.

25. Santoso, S.; Hwang, W.; Hartman, H.; Zhang, S. *Nano Lett.* **2002,** *2*, 687-691.

26. Hong, Y.; Legge, R. L.; Zhang, S.; Chen, P. *Biomacromolecules* **2003,** *4*, 1433-1442.

27. Jun, S.; Hong, Y.; Immamura, H.; Ha, B.-Y.; Bechhoefer, J.; Chen, P. *Biophys. J.* **2004,** *87*, 1249-1259.

28. Djalali, R.; Chen, Y.; Matsui, H. *J. Am. Chem. Soc.* **2003,** *125*, 5873-5879.

29. Reches, M.; Gazit, E. *Science* **2003,** *300*, 625-627.

30. Moulton, H. M.; Hase, M. C.; Smith, K. M.; Iversen, P. L. *Antisense Nucleic Acid Drug Dev.* **2003,** *13*, 31-43.

31. Kubo, T.; Fujii, M. *Nucleic Acid Symposium Series* **1999,** 167-168.

32. Fung, S. Y.; Yang, H.; Chen, P. *Colloids Surf. B: Biointerfaces* **2006,** *55*, 200-211.

33. Tseng, Y. L.; Liu, J.-J.; Hong, R.-L. *Mol Pharmacol* **2002,** *62*, 864-872.

34. Rasmussen, U. B.; Schreiber, V.; Schultz, H.; Mischler, F.; Schughart, K. *Cancer Gene Therapy* **2002,** *9*, 606-612.

35. Scheibel, T.; Parthasaarathy, R.; Sawicki, G.; Lin, X.-M.; Jaeger, H.; Lindquist, S. L. *Proc. Natl. Acad. Sci. USA* **2003,** *100*, 4527-4532.

36. Kisiday, J.; Jin, M.; Kurz, B.; Hung, H.; Semino, C.; Zhang, S.; Grodzinsky, A. J. *Proc. Natl. Acad. Sci. USA* **2002,** *99*, 9996-10001.

37. Semino, C.; Merok, J. R.; Crane, G. G.; Panagiotakos, G.; Zhang, S. *Differentiation* **2003,** *71*, 262-270.

38. Verdier, Y.; Zarandi, M.; Penke, B. *J. Peptide Sci.* **2004,** *10*, 229-248.

39. Yip, C. M.; McLaurin, J. *Biophys. J.* **2001,** *80*, 1359-1371.

40. Hoyer, W.; Cherny, D.; Subramaniam, V.; Jovin, T. M. *J. Mol. Biol.* **2004,** *340*, 127-139.

41. Brown, C. L.; Aksay, I. A.; Saville, D. A.; Hecht, M. H. *J. Am. Chem. Soc.* **2002,** *124*, 6846-6848.

42. Yang, G.; Woodhouse, K. A.; Yip, C. M. *J. Am. Chem. Soc.* **2002,** *124*, 10648-10649.

43. Kowalewski, T.; Holtzman, D. M. *Proc. Natl. Acad. Sci. USA* **1999,** *96*, 3688-3693.

44. Wouters, D.; Schubert, U. S. *Angew. Chem. Int. Ed.* **2004,** *43*, 2480-2495.

45. Paquim, A. C.; Oretskaya, T. S.; Brett, A. M. O. *Electrochim. Acta* **2006,** *51*, 5037-5045.

46. Wei, Y.; Tong, W.; Wise, C.; Wei, X.; Armbrust, K.; Zimmt, M. *J. Am. Chem. Soc.* **2006,** *128*, 13362-13363.

47. Lim, H. S.; Han, J. T.; Kwak, D.; Jin, M.; Cho, K. *J. Am. Chem. Soc.* **2006,** *128*, 14458-14459.

48. Yemini, M.; Reches, M.; Gazit, E.; Rishpon, J. *Anal. Chem.* **2005,** *77*, 5155-5159.

49. Yemini, M.; Reches, M.; Rishpon, J.; Gazit, E. *Nano Lett.* **2005,** *5*, 183-186.

50. Zhang, S.; Lockshin, C.; Cook, R.; Rich, A. *Biopolymers* **1994,** *34*, 663-672.

51. Hong, Y.; Lau, L. S.; Legge, R. L.; Chen, P. *J. Adhesion* **2004,** *80*, 913-931.

52. Hong, Y.; Pritzker, M. D.; Legge, R. L.; Chen, P. *Colloids Surf. B: Biointerfaces* **2005,** *46*, 152-161.

53. Santoso, S.; Zhang, S. in *Encyclopedia of Nanoscience and Nanotechnology*; Nalwa, H. S., Ed.; American Scientific Publishers: Stevenson Ranch, CA, 2003.

54. Santoso, S. S.; Vauthey, S.; Zhang, S. *Curr. Opin. Coll. Inter. Sci.* **2002,** *7*, 262-266.

55. Zhang, S. *Biotechnol. Adv.* **2002,** *20*, 321-339.

56. Zhang, S.; Marini, D. M.; Hwang, W.; Santoso, S. *Curr. Opin. Chem. Biol.* **2002,** *6*, 865-871.

57. Benzinger, T. L. S.; Gregory, D. M.; Burkoth, T. S.; Miller-Auer, H.; Lynn, D. G.; Botto, R. E.; Meredith, S. C. *Biochemistry* **2000,** *39*, 3491-3499.

58. Tcherkasskaya, O.; Sanders, W.; Chynwat, V.; Davidson, E. A.; Orser, C. S. *J. Biomol. Struct. & Dynamics* **2003,** *21*, 353-365.

59. Ray, S.; Das, A. K.; Drew, M. G.; Banerjee, A. *Chem. Commun.* **2006,** *40*, 4230-4232.

60. Aggeli, A.; Nyrkova, I. A.; Bell, M.; Harding, R.; Carrick, L.; McLeish, T. C. B.; Semenov, A. N.; Boden, N. *Proc. Natl. Acad. Sci. USA* **2001,** *98*, 11857-11862.

61. Aggeli, A.; Bell, M.; Carrick, L. M.; Fishwick, C. W. G.; Harding, R.; Mawer, P. J.; Radford, S. E.; Strong, A. E.; Boden, N. *J. Am. Chem. Soc.* **2003,** *125*, 9619-9628.

62. Vauthey, S.; Santoso, S.; Gong, H.; Watson, N.; Zhang, S. *Proc. Natl. Acad. Sci. USA* **2002,** *99*, 5355-5360.

63. Paramonov, S. E.; Jun, H.-W.; Hartgerink, J. D. *Biomacromolecules* **2006,** *7*, 24-26.

64. Hartgerink, J. D.; Beniash, E.; Stupp, S. I. *Science* **2001,** *294*, 1684-1688.

65. Niece, K. L.; Hartgerink, J. D.; Donners, J. J. J. M.; Stupp, S. I. *J. Am. Chem. Soc.* **2003,** *125*, 7146-7147.

66. Service, R. F. *Science* **2001,** *294*, 1635-1637.

67. Matsui, H.; Pan, S.; Gologan, B.; Jonas, S. H. *J. Phys. Chem. B* **2000,** *104*, 9576-9579.

68. Kogiso, M.; Ohnishi, S.; Yase, K.; Masuda, M.; Shimizu, T. *Langmuir* **1998,** *14*, 4978-4986.

69. Matsui, H.; Gologan, B. *J. Phys. Chem. B* **2000,** *104*, 1183-3386.

70. Yu, L.; Banerjee, I. A.; Shima, M.; Rajan, K.; Matsui, H. *Adv. Mater.* **2004,** *16*, 709-712.

71. Banerjee, I. A.; Yu, L.; Matsui, H. *Proc. Natl. Acad. Sci. USA* **2003,** *100*, 14678-14682.

72. Djalali, R.; Chen, Y.; Matsui, H. *J. Am. Chem. Soc.* **2002,** *124*, 13660-13661.

73. Yu, L.; Banerjee, I. A.; Matsui, H. *J. Mater. Chem.* **2004,** *14*, 739-743.

74. Whaley, S. R.; English, D. S.; Hu, E. L.; Barbara, P. F.; Belcher, A. M. *Nature* **2000,** *405*, 665-668.

75. Ghadiri, M. R.; Granja, J. R.; Milligan, R. A.; McRee, D. E.; Khazanovich, N. *Nature* **1993,** *366*, 324.

76. Hartgerink, J. D.; Granja, J. R.; Milligan, R. A.; Ghadiri, M. R. *J. Am. Chem. Soc.* **1996,** *118*, 43-50.

77. Buriak, J. M.; Ghadiri, M. R. *Mater. Sci. Eng. C* **1997,** *4*, 207-212.

78. Fernandez-Lopez, S.; Kim, H.-S.; Chol, E. C.; Delgado, M.; Granja, J. R.; Khasanov, A.; Kraehenbuehl, K.; Long, G.; Weinberger, D. A.; Wilcoxen, K. M.; Ghadiri, M. R. *Nature* **2001,** *412*, 452-455.

79. Ghadiri, M. R.; Granja, J. R.; Milligan, R. A.; McRee, D. E.; Khazanovich, N. *Nature* **1993,** *366*, 324-327.

80. Horne, W. S.; Stout, C. D.; Ghadiri, M. R. *J. Am. Chem. Soc.* **2003,** *125*, 9372-9376.

81. Amorin, M.; Castedo, L.; Granja, J. R. *J. Am. Chem. Soc.* **2003,** *125*, 2844-2845.

82. Nagai, A.; Nagai, Y.; Qu, H.; Zhang, S. *J. Nanosci. Nanotechnol.* **2007,** *7*, 2246-2252.

83. Jayakumar, R.; Murugesan, M.; Ahmed, M. R. *Bioorg. Med. Chem. Lett.* **2000,** *10*, 1547-1550.

84. von Maltzahn, G.; Vauthey, S.; Santoso, S.; Zhang, S. *Langmuir* **2003,** *19*, 4332-4337.

85. Zhang, S.; Lockshin, C.; Herbert, A.; Winter, E.; Rich, A. *EMBO. J.* **1992,** *11*, 3787-3796.

86. Zhang, S.; Holmes, T.; Lockshin, C.; Rich, A. *Proc. Natl. Acad. Sci. USA* **1993,** *90*, 3334-3338.

87. Ellis-Behnke, R. G.; Liang, Y.-X.; Tay, D. K. C.; Shneider, G. E.; Zhang, S.; Wu, W.; So, K.-F. *Nanomedcine: Nanotech. Biol. Med.* **2006,** *2*, 207-215.

88. Caplan, M. R.; Schwartzfarb, E. M.; Zhang, S.; Kamm, R. D.; Lauffenburger, D. A. *Biomaterias* **2002,** *23*, 219-227.

89. Chen, P. *Colloids Surf. A* **2005,** *261*, 3-24.

90. de la Paz, M. L.; Goldie, K.; Zurdo, J.; Lacroix, E.; Dobson, C. M.; Hoenger, A.; Serrano, L. *Proc. Natl. Acad. Sci. USA* **2002,** *99*, 16052-46057.

91. Zhang, S.; Gelain, F.; Zhao, X. *Seminars in Cancer Biology* **2005,** *15*, 413-420.

92. Goeden-Wood, N. L.; Keasling, J. D.; Muller, S. J. *Macromolecules* **2003,** *36*, 2932-2938.

93. Zhang, S.; Altman, M. *React. Funct. Polym.* **1999,** *41*, 91-102.

94. Zhang, S.; Rich, A. *Proc. Natl. Acad. Sci. USA* **1997,** *94*, 23-28.

95. Collier, J. H.; Hu, B.-H.; Ruberti, J. W.; Zhang, J.; Shum, P.; Thompson, D. H.; Messersmith, P. B. *J. Am. Chem. Soc.* **2001,** *123*, 9463-9464.

96. Holmes, T. C.; de Lacalle, S.; Su, X.; Liu, G.; Rich, A.; Zhang, S. *Proc. Natl. Acad. Sci. USA* **2000,** *97*, 6728-6733.

97. Zhang, S.; Holmes, T.; DiPersio, C. M.; Hynes, R. O.; Su, X.; Rich, A. *Biomaterials* **1995,** *16*, 1385-1393.

98. Hong, Y.; Legge, R. L.; Zhang, S.; Chen, P. *Biomacromolecules* **2003,** *4*, 1433-1442.

99. Caplan, M. R.; Schwartzfarb, E. M.; Zhang, S.; Kamm, R. D.; Lauffenburger, D. A. *Biomaterials* **2002,** *23*, 219-227.

100. Caplan, M. R.; Moore, P. N.; Zhang, S.; Kamm, R. D.; Lauffenburger, D. A. *Biomacromolecules* **2000,** *1*, 627-631.

101. Chen, P.; Lahooti, S.; Policova, Z.; Cabrerizo-Vilchez, M. A.; Neumann, A. W. *Colloids Surf. B: Biointerfaces* **1996,** *6*, 279-289.

102. Makievski, A. V.; Fainerman, V. B.; Bree, M.; Wustneck, R.; Kragel, J.; Miller, R. *J. Phys. Chem. B* **1998,** *102*, 417-425.

103. Fainerman, V. B.; Lucassen-Reynders, E. H.; Miller, R. *Colloids Surf. A: Physicochemical and Engineering Aspects* **1998,** *143*, 141-165.

104. Soreghan, B.; Kosmoski, J.; Glabe, C. *J. Biol. Chem.* **1994,** *269*, 28551-28554.

105. Lomakin, A.; Chung, D. S.; Benedek, G. B.; Kirschner, D. A.; Teplow, D. B. *Proc. Natl. Acad. Sci. USA* **1996,** *93*, 1125-1129.

106. Arakawa, T.; Timasheff, S. N. *Biochemistry* **1984,** *23*, 5912-5923.

107. Nandi, P. K.; Robinson, D. R. *J. Am. Chem. Soc.* **1972,** *94*, 1299-1308.

108. Dahlgren, P. R.; Lyubechenko, Y. L. *Biochemistry* **2002,** *41*, 11372-11378.

109. Marini, D. M.; Hwang, W.; Lauffenburger, D. A.; Zhang, S.; Kamm, R. D. *Nano Lett.* **2002,** *2*, 295-299.

110. Banerjee, I. A.; Yu, L.; Matsui, H. *Proc. Natl. Acad. Sci. USA* **2003,** *100*, 14678-14682.

111. Yu, L.; Banerjee, I. A.; Matsui, H. *J. Am. Chem. Soc.* **2003,** *125*, 14837-14840.

112. Yu, L.; Banerjee, I. A.; Shima, M.; Rajan, K.; Matsui, H. *Adv. Mater.* **2004,** *16*, 709-712.

113. Porrata, P.; Goun, E.; Matsui, H. *Chem. Mater.* **2002,** *14*, 4378-4381.

114. Sotiropoulou, S.; Chaniotakis, N. A. *Anal. Bioanal. Chem.* **2003,** *375*, 103-105.

115. He, P.; Dai, L. in *BioMEMS and Biomedical Nanotechnology Volume I Biological and Biomedical Nanotechnology*; Ferrari, M.; Lee, A. P.; Lee, L. J., Eds.; Springer US: 2006; p 171.

116. Stromer, T.; Serpell, L. C. *Microsc. Res. Tech.* **2005,** *67*, 210-217.

117. Tycko, R. *Curr. Opin. Struct. Biol.* **2004,** *14*, 96-103.

118. Harper, J. D.; Lansbury Jr, P. T. *Annu. Rev. Biochem.* **1997,** *66*, 385-407.

119. Rochet, J.-C.; Lansbury Jr, P. T. *Curr. Opin. Struct. Biol.* **2000,** *10*, 60-68.

120. Kelly, J. W. *Curr. Opin. Struct. Biol.* **1998,** *8*, 101-106.

121. Gazit, E. *FEBS J.* **2005,** *272*, 5971-5978.

122. Fraser, P. E.; Nguyen, J. T.; Surewicz, W. K.; Kirschner, D. A. *Biophys. J.* **1991,** *60*, 1190-1201.

123. Mihara, H.; Takahashi, Y. *Curr. Opin. Struct. Biol.* **1997,** *7*, 501-508.

124. Takahashi, Y.; Ueno, A.; Mihara, H. *Bioorg. Med. Chem.* **1999,** *7*, 177-185.

125. Takahashi, Y.; Ueno, A.; Mihara, H. *ChemBioChem* **2001,** *1*, 75-79.

126. Takahashi, Y.; Yamashita, T.; Ueno, A.; Mihara, H. *Tetrahedron* **2000,** *56*, 7011-7018.

127. Takahashi, Y.; Ueno, A.; Mihara, H. *Chem. Eur. J.* **1998,** *4*, 2475-2484.

128. Takahashi, Y.; Ueno, A.; Mihara, H. *ChemBioChem* **2002,** *3*, 637-642.

129. Altman, M.; Lee, P.; Rich, A.; Zhang, S. *Protein Sci.* **2000,** *9*, 1095-1105.

130. Blackley, H. K. L.; Sanders, G. H. W.; Davies, M. C.; Roberts, C. J.; Tendler, S. J. B.; Wilkinson, M. J. *J. Mol. Biol.* **2000,** *298*, 883-840.

131. Smith, L. A.; Ma, P. X. *Colloid. Surf. B: Biointerfaces* **2004,** *39*, 125-131.

132. Fung, S. Y.; Hong, Y.; Dhadwar, S. S.; Zhao, X.; Chen, P. in *Handbook of Nanostructured Biomaterials and Their Applications in Nanobiotechnology*; Nalwa, H. S., Ed.; American Scientific Publishers: Stevenson Ranch, CA USA, 2004.

133. Lutolf, M. P.; Hubbell, J. A. *Nat. Biotech.* **2005,** *23*, 47-55.

134. Beniash, E.; Hartgerink, J. D.; Storrie, H.; Stendahl, J. C.; Stupp, S. I. *Acta Biomaterialia* **2005,** *1*, 387-397.

135. Bonzani, I. C.; George, J. H.; Stevens, M. M. *Curr. Opin. Chem. Biol.* **2006,** *10*, 568-575.

136. Davis, M. E.; Michael Motion, J. P.; Narmoneva, D. A.; Takahashi, T.; Hakuno, D.; Kamm, R. D.; Zhang, S.; Lee, R. T. *Circulation* **2005,** *111*, 442-450.

137. Zhang, S.; Gelain, F.; Zhao, X. *Seminars in Cancer Biology* **2005,** *15*, 413-420.

138. Semino, C. E.; Kasahara, J.; Hayashi, Y.; Zhang, S. *Tissue Eng.* **2004,** *10*, 643-655.

139. Leon, E. J.; Verma, N.; Zhang, S.; Lauffenburger, D. A.; Kamm, R. D. *J. Biomater. Sci. Polymer Edn.* **1998,** *9*, 297-312.

140. Gelain, F.; Bottai, D.; Vescovi, A.; Zhang, S. *PLoS One* **2006,** *1*, e119-11.

141. Horii, A.; Wang, X.; Gelain, F.; Zhang, S. *PLoS One* **2007,** *2*, e190-9.

142. Kopecek, J. *European journal of Pharmaceutical Sciences* **2003,** *20*, 1-16.

143. Hawiger, J. *Curr. Opin. Chem. Biol.* **1999,** *3*, 89-94.

144. Schwartz, J. J.; Zhang, S. *Curr. Opin. Mol. Ther.* **2000,** *2*, 162-167.

145. Aina, O. H.; Sroka, T. C.; Chen, M.-L.; Lam, K. S. *Biopolymers* **2002,** *66*, 184-199.

146. Langer, R. *Nature* **1998,** *392*, 5-10.

147. Keyes-Baig, C.; Duhamel, J.; Fung, S. Y.; Bezaire, J.; Chen, P. *J. Am. Chem. Soc.* **2004,** *126*, 7522-7532.

148. Wang, M.; Law, M.; Duhamel, J.; Chen, P. *Biophys. J.* **2007,** *93*, 2477-2490.

149. Davis, M. E.; Hsieh, P. C. H.; Takahashi, T.; Song, Q.; Zhang, S.; Kamm, R. D.; Grodzinsky, A. J.; Anversa, P.; Lee, R. T. *Proc. Natl. Acad. Sci. USA* **2006,** *103*, 8155-8160.

150. Tirrell, M.; Kokkoli, E.; Biesalski, M. *Surf. Sci.* **2002,** *500*, 61-83.

151. Lowe, C. R. *Curr. Opin. Struct. Biol.* **2000,** *10*, 428-434.

152. Malmsten, M. *Biopolymers at Interfaces;* 2nd ed.; Marcel Dekker, Inc.: New York, 2003.

153. Wee, A. T. S. *Encyclopedia of nanosci. and Nanotech.* **2006,** *9*, 641-652.

154. Klymchenko, A.; Furukawa, S.; Mullen, K.; Auweraer, M. V. d.; Feyter, S. D. *Nano Lett.* **2007,** *7*, 791-795.

155. Nakanishi, T.; Miyashita, N.; Michinobu, T.; Wakayama, Y.; Tsuruoka, T.; Ariga, K.; Kurth, D. G. *J. Am. Chem. Soc.* **2006,** *128*, 6328-6329.

156. Severin, N.; Okhapkin, I. M.; Khokhlov, A. R.; Rabe, J. P. *Nano Lett.* **2006,** *6*, 1018-1022.

157. Datar, A.; Oitker, R.; Zang, L. *Chem. Commun.* **2006,** 1649-1651.

158. Zhang, F.; Du, H.-N.; Zhang, Z.-X.; Ji, L.-N.; Li, H.-T.; Tang, L.; Wang, H.-B.; Fan, C.-H.; Xu, H.-J.; Zhang, Y.; Hu, J.; Hu, H.-Y.; He, J.-H. *Angew. Chem. Int. Ed.* **2006,** *45*, 3611-3613.

159. Ban, T.; Hoshino, M.; Takahashi, S.; Hamada, D.; Hasegawa, K.; Naiki, H.; Goto, Y. *J. Mol. Biol.* **2004,** *344*, 757-767.

160. Zhu, M.; Souillac, P. O.; Ionescu-Zanetti, C.; Carter, S. A.; Fink, A. L. *J. Biol. Chem.* **2002,** *277*, 50914-50922.

161. Necula, M.; Chirita, C. N.; Kuret, J. *J. Biol. Chem.* **2003,** *278*, 46674-46680.

162. Yoo, P. J.; Nam, K. T.; Qi, J.; Lee, S.; Park, J.; Belcher, A. M. *Nat. Mater.* **2006,** *5*, 234-240.

163. Nam, K. T.; Kim, D.-W.; Yoo, P. J.; Chiang, C.-Y.; Meethong, N.; Hammond, P. T.; Chiang, Y.-M.; Belcher, A. M. *Science* **2006,** *312*, 885-888.

164. Santos, N. C.; Castanho, M. A. R. B. *Biophys. Chem.* **2004,** *107*, 133-149.

165. Nishimura, S.; Scales, P. J.; Tateyama, H.; Tsunematsu, K.; Healy, T. W. *Langmuir* **1995,** *11*, 291-295.

166. Sato, T.; Ruch, R. *Stabilization of Colloidal Dispersions by Polymer Adsorption;* Marcel Dekker, Inc.: New York, 1980.

167. Blank, M. *Colloids Surf.* **1989,** *42*, 355-364.

168. Provencher, S. W. *Comput. Phys. Commun.* **1982,** *27*, 213.

169. Adamson, A. W.; Gast, A. P. *Physical chemistry of surfaces;* 6 ed.; John Wiley & Sons: New York, 1997.

170. Evans, D. F.; Wennerstrom, H. *The Colloidal Domain: Where Physics, Chemistry, Biology, and Technology Meet;* VCH Publishers, Inc.: New York, 1994.

171. Scheibel, T.; Parthasarathy, R.; Sawicki, G.; Lin, X.-M.; Jaeger, H.; Lindquist, S. L. *Proc. Natl. Acad. Sci. USA* **2003,** *100*, 4527-4532.

172. Nayak, R. R.; Roy, S.; Dey, J. *Polymer* **2005,** *46*, 12401-12409.

173. Zhao, X.; Dai, J.; Zhang, S. *Mat. Res. Soc. Symp. Proc.* **2004,** *820*, O1.1.1-O1.1.11.

174. Voet, D.; Voet, J. G.; Pratt, C. W. *Fundamentals of Biochemistry;* 2nd ed.; Johh Wiley & Sons, Inc: 2006.

175. Marini, D. M.; Hwang, W.; Lauffenburger, D. A.; Zhang, S.; Kamm, R. D. *Nano Lett.* **2002,** *2*, 295-299.

176. Aggeli, A.; Fytas, G.; Vlassopoulos, D.; McLeish, T. C. B.; Mawer, P. J.; Boden, N. *Biomacromolecules* **2001,** *2*, 378-388.

177. Georgalis, Y.; Starikov, E. B.; Hollenbach, B.; Lurz, R.; Scherzinger, E.; Saenger, W.; Lehrach, H.; Wanker, E. E. *Proc. Natl. Acad. Sci. USA* **1998,** *95*, 6118-6121.

178. Walsh, D. M.; Hartley, D. M.; Kusumoto, Y.; Fezoui, Y.; Condron, M. M.; Lomakin, A.; Benedek, G. B.; Selkoe, D. J.; Teplow, D. B. *J. Biol. Chem.* **1999,** *274*, 25945-25952.

179. Wood, S. J.; Wypych, J.; Steavenson, S.; Louis, J.-C.; Citron, M.; Biere, A. L. *J. Biol. Chem.* **1999,** *274*, 19509-19512.

180. Scherzinger, E.; Sittler, A.; Schweiger, K.; Heiser, V.; Lurz, R.; Hasenbank, R.; Bates, G. P.; Lehrach, H.; Wanker, E. E. *Proc. Natl. Acad. Sci. USA* **1999,** *96*, 4604-4609.

181. Kayed, R.; Bernhagen, J.; Greenfield, N.; Sweimeh, K.; Brunner, H.; Voelter, W.; Kapurniotu, A. *J. Mol. Biol.* **1999,** *287*, 781-796.

182. Friedhoff, P.; von Bergen, M.; Mandelkow, E.-M.; Davies, P.; Mandelkow, E. *Proc. Natl. Acad. Sci. USA* **1998,** *95*, 15712-15717.

183. Rhoades, E.; Agarwal, J.; Gafni, A. *Biochim. Biophys. Acta* **2000,** *1476*, 230-238.

184. Kim, Y.-S.; Randolph, T. W.; Stevens, F. J.; Carpenter, J. F. *J. Biol. Chem.* **2002,** *277*, 27240-27246.

185. Librizzi, F.; Rischel, C. *Protein Sci.* **2005,** *14*, 3129-3134.

186. Goldsbury, C.; Kistler, J.; Aebi, U.; Arvinte, T.; Cooper, G. J. S. *J. Mol. Biol.* **1999,** *285*, 33-39.

187. Scheibel, T.; Kowal, A. S.; Bloom, J. D.; Lindquist, S. L. *Curr. Biol.* **2001,** *11*, 366-369.

188. Lahann, J.; Klee, D.; Pluester, W.; Hoecker, H. *Biomaterials* **2001,** *22*, 817-826.

189. Chinn, J. A.; Sauter, J. A.; Phillips, R. E.; Kao, W. J.; Anderson, J. M.; Hanson, S. R.; Ashton, T. R. *J. Biomed. Mater. Res.* **1998,** *39*, 130-140.

190. Wisniewski, N.; Reichert, M. *Colloid. Surf. B: Biointerfaces* **2000,** *18*, 197-219.

191. Clare, T. L.; Clare, B. H.; Nichols, B. M.; Abbott, N. L.; Hamers, R. J. *Langmuir* **2005,** *21*, 6344-6355.

192. Sawant, R. M.; Hurley, J. P.; Salmaso, S.; Kale, A.; Tolcheva, E.; Levchenko, T. S.; Torchilin, V. P. *Bioconjugate Chem.* **2006,** *17*, 943-949.

193. Zhang, Y.; Zhang, J. *J. Colloid Interface Sci.* **2005,** *283*, 352-357.

194. Toublan, F. J.-J.; Boppart, S.; Suslick, K. S. *J. Am. Chem. Soc.* **2006,** *128*, 3472-3473.

195. Pallandre, A.; Lambert, B.; Attia, R. I.; Jonas, A. M.; Viovy, J.-L. *Electrophoresis* **2006,** *27*, 584-610.

196. Mansur, H. S.; Orefice, R. L.; Vasconcelos, W. L.; Lobato, Z. P.; Machado, L. J. C. *J. Mater. Sci. : Mater. Med.* **2005,** *16*, 333-340.

197. Schamberger, P. C.; Gardella Jr, J. A. *Colloid. Surf. B: Biointerfaces* **1994,** *2*, 209-223.

198. Larsen, C. C.; Kligman, F.; Kottke-Marchant, K.; Marchant, R. E. *Biomaterials* **2006,** *27*, 4846-4855.

199. Patel, S.; Thakar, R. G.; Wong, J.; McLeod, S. D.; Li, S. *Biomaterials* **2006,** *27*, 2890-2897.

200. Heller, D. A.; Garga, V.; Helleher, K. J.; Lee, T.-C.; Mahbubani, S.; Sigworth, L. A.; Lee, T. R.; Rea, M. A. *Biomaterials* **2005,** *26*, 883-889.

201. Semino, C. E.; Merok, J. R.; Crane, G. G.; Panagiotakos, G.; Zhang, S. *Differentiation* **2003,** *71*, 262-270.

202. Ellis-Behnke, R. G.; Liang, Y.-X.; You, S.-W.; Tay, D. K. C.; Zhang, S.; So, K.-F.; Schneider, G. E. *Proc. Natl. Acad. Sci. USA* **2006,** *103*, 5054-5059.

203. Zhang, S.; Yan, L.; Altman, M.; Lassle, M.; Nugent, H.; Frankel, F.; Lauffenburger, D. A.; Whitesides, G. M.; Rich, A. *Biomaterials* **1999,** *20*, 1213-1220.

204. Shervedani, R. K.; Mehrjardi, A. H.; Zamiri, N. *Bioelectrochemistry* **2006,** *69*, 201-208.

205. Zhang, S.; Wang, N.; Yu, H.; Niu, Y.; Sun, C. *Bioelectrochemistry* **2005,** *67*, 15-22.

206. Long, J.; Chen, P. *Langmuir* **2001,** *17*, 2965-2972.

207. Voet, D.; Voet, J. G. *Biochemistry;* 3 ed.; John Wiley & Sons, Inc.: Hoboken, USA, 2004.

208. Gettens, R. T. T.; Bai, Z.; Gilbert, J. L. *J. Biomed. Mater. Res.* **2005,** *72*, 246-257.

209. Walter, E. C.; Ng, K.; Zach, M. P.; Penner, R. M.; Favier, F. *Microelectronic Engeering* **2002,** *61-62*, 555-561.

210. He, H.; Tao, N. J. in *Encyclopedia of Nanosci. Nanotech.*; Nalwa, H. S., Ed.; American Scientific Publishers: Stevenson Ranch, CA, 2004; Vol. 2, p 755.

211. Falini, G.; Fermani, S.; Conforti, G.; Ripamonti, A. *Acta Cryst.* **2002,** *D58*, 1649-1652.

212. Moulton, S. E.; Barisci, J. N.; Bath, A.; Stella, R.; Wallace, G. G. *J. Colloid Interface Sci.* **2003,** *261*, 312-319.

213. Ying, P.; Viana, A. S.; Abrantes, L. M.; Jin, G. *J. Colloid Interface Sci.* **2004,** *279*, 95-99.

214. Nyffenegger, R. M.; Penner, R. M. *Chem. Rev.* **1997,** *97*, 1195-1230.

215. Kramer, S.; Fuierer, R. R.; Gorman, C. B. *Chem. Rev.* **2003,** *103*, 4367-4418.

216. Hickenboth, C. R.; Moore, J. S.; White, S. R.; Sottos, N. R.; Baudry, J.; Wilson, S. R. *Nature* **2007,** *446*, 423-427.

217. Duwez, A.-S.; Cuenot, S.; Jerome, C.; Gabriel, S.; Jerome, R.; Rapino, S.; Zerbetto, F. *Nat. Nanotech.* **2006,** *1*, 122-125.

218. Rotenberg, Y.; Boruvka, L.; Neumann, A. W. *J. Colloid Interface Sci.* **1983,** *93*, 169-183.

219. Stathopulos, P. B.; Scholz, G. A.; Hwang, Y.-M.; Rumfeldt, J. A. O.; Lepock, J. R.; Meiering, E. M. *Protein Sci* **2004,** *13*, 3017-3027.

220. Hawkins, C. L.; Davies, M. J. *Biochim. Biophys. Acta* **2001,** *1504*, 196-219.

221. Aggeli, A.; Boden, N.; Zhang, S. *Mol. Med. Today* **1999,** *5*, 512-513.

222. Stoltenberg, R. M.; Woolley, A. T. *Biomed. Microdev.* **2004,** *6*, 105-111.

223. Knez, M.; Bittner, A. M.; Boes, F.; Wege, C.; Jeske, H.; Mai, E.; Kern, K. *Nano Lett.* **2003,** *3*, 1079-1082.

224. Valizadeh, S.; George, J. M.; Leisner, P.; Hultman, L. *Electrochim. Acta* **2001,** *47*, 865-874.

225. Lee, S.-W.; Mao, C.; Flynn, C. E.; Belcher, A. M. *Science* **2002,** *296*, 892-895.

226. Cheng, C.; Gonela, R. K.; Gu, Q.; Haynie, D. T. *Nano Lett.* **2005,** *5*, 175-178.

227. Braun, E.; Eichen, Y.; Sivan, U.; Ben-Yoseph, G. *Nature* **1998,** *391*, 775-778.

228. Djalali, R.; Chen, Y.; Matsui, H. *Polymeric Materials: Sci. & Eng.* **2003,** *88*, 29-30.

229. Yang, W.; Jaramillo, D.; Gooding, J. J.; Hibbert, D. B.; Zhang, R.; Willett, G. D.; Fisher, K. *Chem. Commun.* **2001,** 1982-1983.

230. Yang, W.; Chow, E.; Willett, G. D.; Hibbert, D. B.; Gooding, J. J. *Analyst* **2003,** *128*, 712-718.

231. Sanna, D.; Agoston, C. G.; Sovago, I.; icera, G. *Polyhedron* **2001,** *20*, 937-947.

232. Nozaki, Y.; Tanford, C. *Methods Enzymol* **1967,** *11*, 715-734.

233. Tanokura, M. *Biochim. Biophys. Acta* **1983,** *742*, 576-585.

234. Singer, A. U.; Forman-Kay, J. D. *Protein Sci* **1997,** *6*, 1910-1919.

235. Lee, K. K.; Fitch, C. A.; Lecomte, J. T. J.; Garcia-Moreno, B. *Biochemistry* **2002,** *41*, 5656-5667.

236. Gaggelli, E.; Bernardi, F.; Molteni, E.; Pogni, R.; Valensin, D.; Valensin, G.; Remelli, M.; Luczkowski, M.; Kozlowski, H. *J. Am. Chem. Soc.* **2005,** *127*, 996-1006.

237. Tanaka, T.; Mizuno, T.; Fukui, S.; Hiroaki, H.; Oku, J.; Kanaori, K.; Tajima, K.; Shirakawa, M. *J. Am. Chem. Soc.* **2004,** *126*, 14023-14028.

238. Jones, C. E.; Abdelraheim, S. R.; Brown, D. R.; Viles, J. H. *J. Biol. Chem.* **2004,** *279*, 32018-32027.

239. Casal, H. L.; Kohler, U.; Mantsch, H. H. *Biochim. Biophys. Acta* **1988,** *957*, 11-20.

240. Lin, S.-Y.; Chu, H.-L. *Int. J. Biol. Macromol.* **2003,** *32*, 173-177.

241. Gustiananda, M.; Haris, P. I.; Milburn, P. J.; Gready, J. E. *FEBS Lett.* **2002,** *512*, 38-42.

242. Zhong, L.; Johnson, W. C. *Proc. Natl. Acad. Sci. USA* **1992,** *89*, 4462-4465.

243. Mutter, M.; Hersperger, R. *Angew. Chem. Int. Ed. Engl.* **1990,** *29*, 185-187.

244. Mutter, M.; Gassmann, R.; Buttkus, U.; Altmann, K.-H. *Angew. Chem. Int. Ed. Engl.* **1991,** *30*, 1514-1516.

245. Waterhous, V. D.; Johnson, W. C. *Biochem.* **1994,** *33*, 2121-2128.

246. Sun, X.-G.; Cao, E.-H.; Zhang, X.-Y.; Liu, D.; Bai, C. *Inorg. Chem. Commun.* **2002,** *5*, 181-186.

247. Korolev, N.; Lyubartsev, A. P.; Rupprecht, A.; Nordenskiold, L. *Biophys. J.* **1999,** *77*, 2736-2749.

248. Butler, J. C.; Angelini, T.; Tang, J. X.; Wong, G. C. L. *Phys. Rev. Lett.* **2003,** *91*, 28301.

249. Nightingale Jr., E. R. *J. Phys. Chem.* **1959,** *63*, 1381-1387.

250. Xu, G.; Wang, W.; Groves, J. T.; Hecht, M. H. *Proc. Natl. Acad. Soc.* **2001,** *98*, 3652-3657.

251. Pallitto, M. M.; Murphy, R. M. *Biophys. J.* **2001,** *81*, 1805-1822.

252. Zhao, D.; Moore, J. S. *Org. Biomol. Chem.* **2003,** *1*, 3471-3491.

253. Adanyi, N.; Varadi, M.; Kim, N.; Szendro, I. *Curr. Appl. Phys.* **2006,** *6*, 279-286.

254. Mena, M. L.; Carralero, V.; Gonzalez-Cortes, A.; Yanez-Sedeno, P.; Pingarron, J. M. *Electroanalysis* **2005,** *17*, 2155.

255. Gooding, J. J.; Hibbert, D. B. *TrAC-Trends Anal. Chem.* **1999,** *18*, 525-533.

256. Chaubey, A.; Malhotra, B. D. *Biosens. Bioelectron.* **2002,** *17*, 441-456.

257. Zhang, S.; Wang, N.; Yu, H.; Niu, Y.; Sun, C. *Bioelectrochemistry* **2005,** *67*, 15-22.